

Light Scatter in Eye and Its Impact on Vision

Onurcan SAHIN

January 2018

Thesis submitted in partial fulfilment of the requirements for the degree of

Doctor of Philosophy

Light Scatter in Eye and Its Effect on Vision

Submitted January 29th, 2018

Supervised by;

Siganos Charalambos	Assist. Prof. of Ophthalmology, Department of Medicine, University of Crete
Ioannis Pallikaris	Prof. of Ophthalmology, Department of Medicine, University of Crete
Miltiadis Tsilimbaris	Prof. of Ophthalmology, Department of Medicine, University of Crete

Members of the Examination Committee;

Ioannis Pallikaris	Prof. in Ophthalmology, Department of Medicine, University of Crete
Miltiadis Tsilimbaris	Prof. in Ophthalmology, Department of Medicine, University of Crete
Michalis Taroudakis	Professor of Mathematics, Department of Mathematics and Applied Mathematics, University of Crete
Aristidis Tsatsakis	Professor of Toxicology, Department of Medicine, University of Crete
Efstathios Detorakis	Assistant Professor of Ophthalmology, Department of Medicine, University of Crete
Siganos Charalambos	Assist. Prof. in Ophthalmology, Department of Medicine, University of Crete
Dimitrios Papazoglou	Assistant Professor of Physics, Department of Materials Science and Technology, University of Crete

ABSTRACT

Introduction The vision is the most fundamental and the most complex sense in the evolution progress. Although, the complete process of the visual function has not been fully understood, there are several essential factors take part in the vision. The optics of the eye, the retina, and the visual cortex should be considered as a complete structure while evaluating the visual performance. The interaction between the light and the structures of the eye determine the quality of the retinal image which is the key factor for the visual performance.

Two different interaction mechanisms of the light and the eye exists. The first mechanism is the optical interactions, which is detailed as optical properties of the eye and the second mechanism is detailed as the material properties of the eye. It is very important to understand and distinguish the difference between these two mechanisms. In order to have the good vision or in other words good retinal image quality, having the best refraction is as important as having transparent optics and clear optical way.

Amount of the irregularities or defects induce straylight in the eye. Although, effects of intraocular scattering exist for ages and observed in the clinical practice, the knowledge and understanding of the intraocular scattering is not as good as the understanding of the refraction or aberrations. We believe that a complete analysis of visual performance will only be completed with analyzing the intraocular straylight.

In this thesis, a novel optical device for measuring forward intraocular scattering with double pass method is developed and results are shown. The relevant chapters focus on several studies which worked on measuring, quantifying and understanding of the straylight phenomenon.

Methods The proof of concept, repeatability, functionality of the device was tested with either in test or clinical conditions. The first study on the proof and concept and

constancy evaluations were performed on an artificial eye and previously documented lenses. The straylight difference were evaluated of the artificial eye between different hard contact lenses which induce different amount of straylight.

The second study was performed with an artificial eye for determining the effect of defocus on the measurements. The measurements were collected by changing the position of the retina which was corresponding inducing myopia or hyperopia. Additionally, the repeatability and the effect of axial alignment of the pupil camera was tested by taking consecutive measurements from the different axial positions from a healthy eye of a subject.

In the third study, the scattering difference between healthy subjects and the effect of different diffusing filters which induce straylight were measured. Measurements with and without lenses and were evaluated.

The final studies were performed under clinical conditions with healthy subjects and cataract patients. Optical and psychophysical measurements were performed as well as the LOCS III grading in these studies. Correlation between two methods of measuring intraocular scattering and LOCS III grading system were evaluated.

Results Outcomes of these study showed the system is capable of detecting the amount straylight between different scatterers. The results also showed that the system is capable of detecting different amounts of straylight on human eyes and the system is immune for measuring patients with refractive error which is smaller than the 5D. The measurements of the optical and psychophysical measurements showed %80,3 and %84,4 ($p<0,01$) correlation. Furthermore, the psychophysical measurement and optical measurement showed 0,17 and 0,16 statistical significant difference ($P<0,001$). In addition, Bland-Altman analysis also confirmed that the bias was significant. The analysis of optical measurements between different groups of cataract gradings revealed significant differences between all groups ($P<0,004$).

Conclusion Development of this novel device, which is described in this thesis, gives advancement for the clinical routine beyond the aberrations and reflections. Besides the subjective methods of grading cataract, this method gives fast, relevant, sensitive and significant information for the effects of the forward scattering. This device could be a step forward in the clinical routine and helps clinicians for the objective evolution of the material properties of the eye.

ΠΕΡΙΛΗΨΗ

Εισαγωγή Στη διαδικασία της εξέλιξης η όραση ίσως αποτελεί την πιο θεμελιώδη και ταυτόχρονα την πιο σύνθετη ανθρώπινη αίσθηση. Παρόλο που ο συνολικός τρόπος λειτουργία της όρασης δεν έχει πλήρως κατανοηθεί, υπάρχουν κάποιοι σημαντικοί παράγοντες οι οποίοι συμβάλουν σε αυτή. Τα οπτικά του αφθαλμού, ο αμφιβληστροειδής ο οπτικός φλοιός και οι ανώτερες εγκεφαλικές λειτουργίες της όρασης θα πρέπει να αντιμετωπίζονται ως μια ενιαία δομή κατά την αξιολόγηση της όρασης. Η αλληλεπίδραση της φωτεινής ακτινοβολίας με τις δομές του οφθαλμού είναι που καθορίζει την ποιότητα του οπτικού ειδώλου στον αμφιβληστροειδή, και παίζει καθοριστικό ρόλο στην απόδοση της όρασης.

Υπάρχουν δυο διακριτοί μηχανισμοί αλληλεπίδρασης της φωτεινής ακτινοβολίας και του οφθαλμού. Ο πρώτος μηχανισμός είναι η οπτική αλληλεπίδραση και η οποία αναφέρετε ως οι οπτικές ιδιότητες του οφθαλμού, και ο δεύτερος είναι η αλληλεπίδραση του φωτός με το υλικό κατασκευής του οφθαλμού στο οποίο αναφερόμαστε σαν ιδιότητες του υλικού του οφθαλμού. Είναι σημαντική η κατανόηση της διαφορετικής συνισφοράς των δύο αυτών μηχανισμών στην όραση. Για την καλή απόδοση του οπτικού συστήματος ή αλλιώς η δημιουργία ευκρινούς αμφιβληστροειδικού ειδώλου είναι εξίσου σημαντικό τόσο η βέλτιστη διάθλαση όσο και η καλή διαφάνεια των οπτικών μέσων στη διαδρομή μέχρι τον αμφιβληστροειδή.

Το πλύθος των ανωμαλιών ή ατελειών στη δομή του οφθαλμού είχαν ως αποτέλεσμα την επαγωγή σκέδασης στον οφθαλμό. Παρόλο που η ενδοφθάλμια σκέδαση παρατηρείται συστηματικά για αρκετά χρόνια κατά την κλινική εφαρμογή, η γνώση και η κατανόηση της ως προς την επίδραση της στην όραση δεν είναι τόσο καλή όσο η κατανόηση της διάθλασης και των εκτροπών. Επομένως η πλήρης μελέτη της όρασης θα είναι εφικτή με την κατανόηση της ενδοφθάλμιας σκέδασης.

Σκοπός της παρούσας διατριβής είναι ανάπτυξη οπτικής συσκευής για την μέτρηση της εμπρόσθιας ενδοφθάλμιας σκέδασης με τη μέθοδο της διπλής διέλευσης, παράλληλα παρατίθενται και τα αποτελέσματα των μετρήσεων. Τα επιμέρους κεφάλαια εστιάζουν σε διάφορες μελέτες για τη μέτρηση, την ποσοτικοποίηση και την κατανόηση του φαινομένου της σκέδασης.

Μέθοδοι Η επιβεβαίωση της αρχής της έννοιας για την συσκευής, η επαναληψιμότητα, και η λειτουργία της έχουν εξεταστεί τόσο μέσω πειραματικών διατάξεων όσο και σε κλινικές συνθήκες. Τα πρώτα πειράματα πραγματοποιήθηκαν με την χρήση τεχνητού οφθαλμού και συστήματος φακών των οποίων οι οπτικές ιδιότητες είχαν οριστεί από προηγούμενες μελέτες. Η διαφορά στην σκέδαση για τον τεχνητό οφθαλμό αξιολογήθηκε από διαφορετικούς σκληρούς φακούς επαφής οι οποίοι εισήγαγαν διαφορετικό ποσό σκέδασης.

Η δεύτερη μελέτη πραγματοποιήθηκε επίσης με τεχνητό οφθαλμό και σε αυτήν καθορίστηκε η επίδραση του διαθλαστικού σφάλματος στις μετρήσεις. Η συλλογή των μετρήσεων έγινε με την μετακίνηση του αμφιβληστροειδή αυξάνοντας την μυωπία ή την υπερμετροπία. Επιπλέον έχει εξεταστεί η επαναληψιμότητα και η επίδραση της αξονικής ευθυγράμμισης της κόρης της κάμερας με διαδοχικές μετρήσεις από διαφορετικές αξονικές θέσεις υγιών οφθαλμών.

Στην τρίτη μελέτη αξιολογήθηκε η διαφορά στην σκέδαση μεταξύ υγιών οφθαλμών και της επίδρασης που είχε στην όρασή τους, με την προσθήκη διαφορετικών φίλτρων διάχυσης τα οποία αύξαναν την σκέδαση. Η αξιολόγηση έγινε με χρήση φακών αλλά και χωρίς.

Οι τελικές μελέτες πραγματοποιήθηκαν σε κλινικές συνθήκες με τη συμμετοχή υγιών οφθαλμών αλλά και καταρρακτικούς οφθαλμών. Σε αυτές τις μελέτες έχουν πραγματοποιηθεί οπτικές και ψυχοφυσικές μετρήσεις καθώς επίσης και η μέθοδος βαθμονόμησης LOCS III. Επιπλέον έγινε αξιολόγηση της συσχέτισης μεταξύ των δυο μεθόδων μέτρησης της ενδοφθάλμιας σκέδασης και της μεθόδου βαθμονόμησης LOCS III.

Αποτελέσματα Τα αποτελέσματα αυτής της μελέτης έδειξαν ότι το σύστημα που αναπτύχθηκε είναι ικανό να εντοπίζει την ποσότητα της σκέδασης μεταξύ διαφορετικών σκεδαστών. Επίσης έδειξαν την ικανότητά του να εντοπίζει και να ποσοτικοποιεί την σκέδαση στον ανθρώπινο οφθαλμό ενώ είναι οι μετρήσεις δεν επηρεάζονται από διαθλαστικά σφάλματα μικρότερα από 5D. Οι οπτικές και ψυχοφυσικές μετρήσεις από τις δύο κλινικές μελέτες έδειξαν συσχέτιση 80.3% και 84.4% ($p < 0.01$) αντίστοιχα. Επίσης οι ψυχοφυσικές και οι οπτικές μετρήσεις έδειξαν 0.17 και 0.16 στατιστικά σημαντική διαφορά ($P < 0.001$). Επιπλέον ανάλυση Bland-Altman επιβεβαίωσε ότι η απόκλιση ήταν στατιστικά σημαντική. Η ανάλυση των μετρήσεων μεταξύ των διαφορετικών ομάδων καταρρακτικών ασθενών έδειξαν στατιστικά σημαντική διαφορά μεταξύ όλων των ομάδων ($< P 0.004$).

Συμπεράσματα Η ανάπτυξη της καινοτόμου αυτής συσκευής, η οποία περιγράφεται στην παρούσα διατριβή, αποτελεί εξέλιξη για την κλινική εφαρμογή πέραν από τη εκτροπές και τις ανακλάσεις. Εκτός από τις υποκειμενικές μεθόδους βαθμονόμησης του καταρράκτη, η μέθοδος που περιγράφεται εδώ παρέχει γρήγορη, ευαίσθητη και σημαντική πληροφορία για την δράση της εμπροσθοσκέδασης. Η συσκευή αυτή θα μπορούσε να είναι το επόμενο βήμα στην κλινική εφαρμογή μια αντικειμενική μέθοδος μέτρησης των υλικών ιδιοτήτων του οφθαλμού.

Babam'a

ACKNOWLEDGEMENTS

It has been an amazing 3 years journey. There are so many people and factors that made possible to achieve the success of this thesis.

I remember my very the first day in the lab. I remember that Haris had a colored printout of the PSF distribution from a well-known scatter paper and there was a red pin on the 8th degree. While pointing that red pin, he said; “I want to measure here at the end of this project”. After spending days, months, years for this purpose, I am glad to be able to say that we did it! We succeeded! It was such a unique and fulfilling experience working with Harileos Ginis. I can not thank enough not only the guidance and the support as my supervisor but also for the good memories and the friendship we developed throughout years.

Within three years I find opportunity to be a part of several projects. In these different projects, I worked with several professions including the medical personnel, nurses and the doctors. Without their patience and support neither this thesis nor other projects would be succeeded. For this reason, I would also like to thank Prof. Tsilimbaris for his guidance, generosity, support and kindness.

All this journey started with an opportunity offered in a meeting at 2011. It was the first time that I met with Prof. Pallikaris. I do not have any words for describing how grateful I am for this opportunity to work in Crete and the trust that professor put on us. Our time with professor either in Crete and Turkey formed a family relationship as well as the professional relationship between us. Beside the technical, medical knowledge; I learned so much with the time that I worked with Prof. Pallikaris. He was like an open source and his knowledge guided me through any problem that I faced with. Once more I would like to thank Prof. Pallikaris for giving me the opportunity to become a better scientist and a better man.

I would also like thank members of my thesis defense committee Prof. Taroudakis, Prof. Tsatsakis, Prof. Detorakis, Prof. Charalambos and Prof. Papazoglu for their support and valuable comments.

In this journey, I had a privilege of becoming a member of the E.U. project called OPAL. This training network was a wonderful experience for improving ourselves. Without this support, our valuable works could not be existed.

Family: “A basic social unit consisting of parents and their children, considered as a group, whether dwelling together or not” or “any group of persons closely related by blood, as parents, children, uncles, aunts, and cousins”. Different than dictionary, family has much broader definition for me. When I moved Heraklion, I knew nobody and I was a total stranger. But there are some people that we shared so many good memories and eventually we become brothers and sisters from different mothers and fathers. We become a family!

For this reason, I would like to thank to;

My family at the university; Trisevgieni, Pavlina, Iro, Xrisa, Thasos, Georgios (Kontadakis), Petros, Manos, Eirini (Kokolaki), Aris, Sotiris, Stavros (Smirlis), Vasilis (Nikiforidis),

And my big Cretan family; Alex (Mantaras), Manolis (Garefalakis), Valeria, Katerina, Stavros (Lambrakis), Mariella, Sifis, Georgios (Stefanakis), Lefteris (Andriotis), Xara, Vasilis (Dermitzakis), Nikos (Sfakianakis), Aggeliki, Nikitas, Eirini (Chrysikou), Nina, Michalis (Marinakis),

My brothers, Gergeos (Metaksakis), Kostas (Solakakis), Kostas (Sifakis),

My dear Thalia,

My dear Ioannis (Kouvidis),

My family at Athens; Erhan, Elena, Zeynep and Davetas family,

I am so lucky to know you and it was a privilege to share all these beautiful memories we had.

And my dear Alexandros (Pennos), Loukia and Nikos. We were together since the first time I stepped in the lab and I hope we will be together till our last breath.

Finally, some words for my family back in Istanbul. Dostlukların, mesafelerin ve özlemlerin üstesinden bu kadar kolay gelebileceğine inanamazdım. Desteklerini ve dualarını üzerimden eksik etmeyen canım ailem, belki en büyük teşekkürü sizlere borçluyum. Dünyanın her neresine gidersem gideyim sizleri hep yüreğimde taşıyacağım ve aramızdaki bu bağ karşılaştığım tüm zorlukların üzerinden gelebilmem için ihtiyacım olan en önemli şey. İyi ki varsınız ve sizleri çok seviyorum.

With the deepest love from my hearth; thank you all.

Onurcan.

TABLE OF CONTENTS

ABSTRACT	V
ΠΕΡΙΛΗΨΗ	IX
ACKNOWLEDGEMENTS	XIV
TABLE OF CONTENTS	XVII
LIST OF FIGURES	XIX
LIST OF TABLES	XXI
LIST OF ABBREVIATIONS	XXIII
1 INTRODUCTION	1
2 THE ANATOMY OF THE EYE	3
2.1 THE EYEBALL	3
2.2 THE TEAR FILM	5
2.3 THE CONJUNCTIVA:	5
2.4 THE SCLERA AND EPISCLERA:.....	5
2.5 THE CORNEA	6
2.6 THE AQUEOUS HUMOUR.....	8
2.7 THE IRIS	8
2.8 THE CILIARY BODY.....	9
2.9 THE LENS.....	10
2.10 THE VITREOUS.....	12
2.11 THE RETINA	12
3 THE INTERACTION OF THE LIGHT AND THE EYE	15
3.1 THE OPTICAL PROPERTIES OF THE EYE	15
3.1.1 <i>The Refraction</i>	15
3.1.2 <i>Diffraction</i>	17
3.1.3 <i>Aberrations</i>	18
Chromatic Aberrations	19
Monochromatic Aberrations	19
The Hartmann-Shack Aberrometer	20
Ray Tracing Aberrometer.....	21
3.1.4 <i>The Point Spread Function</i>	22
3.2 MATERIAL PROPERTIES OF THE EYE	23
4 INTRAOCULAR SCATTERING & STRAYLIGHT	27
4.1 PSYCHOPHYSICAL MEASUREMENT OF THE STRAYLIGHT	29
4.2 OPTICAL MEASUREMENT OF THE STRAYLIGHT	31
4.2.1 <i>Optical Quality Analysis System (OQAS) II - DP Optical System for Measuring Cataracts</i>	32
4.2.2 <i>DP Optical Method for Reconstructing the Wide-Angle PSF of the Human Eye</i>	34
5 FAST OPTICAL MEASUREMENTS OF THE STRAYLIGHT	39
5.1 INSTRUMENT SPECIFICATIONS	40
5.1.1 <i>The Hardware</i>	41
5.1.2 <i>The Software</i>	44
5.1.3 <i>The Analysis</i>	45
5.2 THE PROOF OF CONCEPT AND PUBLICATIONS.....	47

5.2.1	<i>Study I - Artificial Eye And Lenses With Microspheres.....</i>	48
5.2.2	<i>Study II – Effect of the Defocus on the Artificial Eye and the Pilot Measurements of an Human Eye</i>	49
5.2.3	<i>Study III – Healthy Human Eyes And Diffusers</i>	50
5.2.4	<i>Study IV - Optical And Psychophysical Measurements Comparison Clinical Study I.....</i>	51
5.2.5	<i>Study IV - Optical And Psychophysical Measurements Comparison Clinical Study II.....</i>	53
6	CONCLUSION	57
7	BIBLIOGRAPHY	61
8	APPENDIX.....	67
A1	System 1 st Generation	67
A1.1	Hardware.....	68
A1.1.1	Light Source.....	68
A1.1.2	Optics	70
A1.1.3	Photomultiplier	72
A1.1.4	NI DAQ-6009 Data Acquisition Card.....	72
A1.2	Electronics	73
A1.2.1	Power Box	73
A1.2.2	Control Board	73
A1.2.3	Limiter Circuits	74
A1.2.4	PIC Microprocessor	75
A1.3	Software	75
A1.3.1	Labview	76
A1.3.2	Matlab.....	76
A2	System 2 nd Generation	79
A2.1	Hardware.....	79
A2.1.1	Light Source.....	79
A2.1.2	Optics	80
A2.2	Electronics	81
A3	System 3 rd Generation (Sigma).....	83
A3.1	Hardware.....	83
A3.1.1	Optics	83
A3.2	Electronics	84
A4	Final Codes	85
A4.1	Matlab	85
A4.1.1	GUI Screens	85
A4.1.2	Code of Main Gui.....	88
A4.1.3	Code of Measurement GUI.....	89
A4.1.4	Code of Calibration Gui	91
A4.1.5	Code of Database GUI	94

LIST OF FIGURES

FIGURE 1 THE SCHEMATIC DIAGRAM OF THE HUMAN EYE [2]	4
FIGURE 2 THE LAYERS OF THE IRIS [3], [6].....	9
FIGURE 3 THE COMPUTER-ANIMATED MODELING OF HUMAN ACCOMMODATION OF GOLDBERG [7]	10
FIGURE 4 THE LENS STRUCTURES[3], [8].....	11
FIGURE 5 CELL TYPES AND HISTOLOGIC LAYERS IN HUMAN RETINA [3], [9].....	12
FIGURE 6 GAUSS' EYE MODEL	16
FIGURE 7 LISTING'S REDUCED EYE MODEL.....	16
FIGURE 8 THE AXES AND THE ANGLES OF THE EYE	17
FIGURE 9 AIRY DISK PATTERN AND PROFILE.....	18
FIGURE 10 THE LCA (LEFT) AND TCA (RIGHT)	19
FIGURE 11 ABERRATIONS REPRESENTED AS ZERNIKE FUNCTIONS.....	20
FIGURE 12 THE SCHEMATIC OF HARTMANN-SHACK ABERROMETER	21
FIGURE 13 SCHEMATIC OF RAY TRACING ABERROMETER	21
FIGURE 14 THE POINT SPREAD FUNCTION ON OPTICAL SYSTEMS AND HUMAN EYE	22
FIGURE 15 REPRESENTATIVE IMAGES OF THE DIFFERENT CORNEAL LAYERS BEFORE (LEFT) AND AFTER (RIGHT) REFRACTIVE SURGERY AS SEEN IN IN VIVO CONFOCAL MICROSCOPY. [26]	24
FIGURE 16 THE SOURCES OF INTRAOCULAR SCATTERING[29]	27
FIGURE 17 THE EFFECT OF THE STRAYLIGHT	28
FIGURE 18 TEST SCREEN OF PSYCHOPHYSICAL STRAYLIGHT METER (C-QUANT) [28]	29
FIGURE 19 LOG(S) VALUES AS A FUNCTION OF AGE FOR A POPULATION OF EUROPEAN DRIVERS [29], [35]	31
FIGURE 20 SCHEMATIC REPRESENTATION OF DP SYSTEM FOR OPTICAL MEASUREMENT OF THE STRAYLIGHT[38]	32
FIGURE 21 EXAMPLE OF THE SELECTION OF THE ZONE IN THE DOUBLE-PASS IMAGE USED TO DEFINE THE OBJECTIVE SCATTER INDEX (OSI)[38].....	33
FIGURE 22 THE OSI VALUES WITH RESPECT TO GRADING GROUPS (LEFT) AND THE AVERAGE OSI VALUES WITH RESPECT TO GRADING GROUPS (RIGHT)[38].....	33
FIGURE 23 OPTICAL SETUP FOR RECONSTRUCTION THE WIDE-ANGLE PSF OF THE HUMAN EYE[39].....	34
FIGURE 24 UNIFORM DISK WHICH IS PROJECTED TO RETINA AND THE DIMENSIONS WHICH ARE USED FOR CALCULATION OF THE PSF[39]	35
FIGURE 25 EXPERIMENTAL DATA ACQUIRED FROM TWO HEALTHY SUBJECTS [39]	36
FIGURE 26 EXPERIMENTAL DATA BETWEEN ARTIFICIAL EYE, TWO HEALTHY SUBJECTS AND ADDITIONAL SCATTERERS [39] 36	36
FIGURE 27 SCHEMATIC OF THE OPTICAL SETUP	41
FIGURE 28 THE LIGHT SOURCE	41
FIGURE 29 THE SEPARATION OF THE ILLUMINATION AND IMAGING PATH VIA DIAPHRAGM 1 AND 2 ON THE PUPIL PLANE 42	42
FIGURE 30 ACTUAL IMAGE OF THE PROJECTED LED SOURCE ON THE FUNDUS.	42
FIGURE 31 THE USE OF THE PUPIL CAMERAS FOR ALIGNMENT.....	43
FIGURE 32 THE EFFECT OF THE SCATTER ON MEASURING THE CENTRAL PART OF THE FUNDUS IMAGE	44
FIGURE 33 THE ANALOG SIGNAL (UP) AND THE SIGNAL AFTER FFT IS APPLIED (DOWN).....	45
FIGURE 34 ARTIFICIAL EYE (LEFT) THE ARTIFICIAL EYE (MIDDLE) AND SPECIAL LENS WITH MICROSPHERES (RIGHT)....	48
FIGURE 35 STRAYLIGHT MEASUREMENTS OF ARTIFICIAL EYE AND LENSES WITH MICROSPHERES FOR DIFFERENT ANGLES..	49
FIGURE 36 THE DEFOCUS CURVE (LEFT) AND STRAYLIGHT MEASUREMENTS OF AN HEALTH EYE WITH DIFFERENT ALIGNMENTS (RIGHT)	50
FIGURE 37 STRAYLIGHT MEASUREMENT WITH HUMAN EYES AND DIFFUSING FILTERS.....	51
FIGURE 38 OUTCOMES OF THE OPTICAL AND PSYCHOPHYSICAL MEASUREMENTS OF THE STUDY.....	52
FIGURE 39 CORRELATION BETWEEN PSYCHOPHYSICAL AND OPTICAL MEASUREMENTS (LEFT) AND STRAYLIGHT MEASUREMENTS WITH LOCS III GRADINGS OF CATARACT (RIGHT).....	52
FIGURE 40 CORRELATION GRAPH OF OPTICAL AND PSYCHOPHYSICAL MEASUREMENTS.....	54
FIGURE 41 BLAND-ALTMAN PLOT.....	55
FIGURE 42 STRAYLIGHT PARAMETER VALUES WITHIN DIFFERENT CATARACT GROUPS AND HEALTHY SUBJECTS.....	55
FIGURE 43 ADVANTAGES AND DISADVANTAGES OF PREVIOUS SYSTEMS FOR MEASURING INTRAOCULAR SCATTERING AND SIGMA.....	57
FIGURE 44 THE DEVELOPED COMPACT SYSTEM FOR OPTICAL MEASUREMENTS OF FORWARD SCATTERING.....	60
FIGURE 45 MEASUREMENT PROCESS	67

FIGURE 46 ANALYZING PROCESS	68
FIGURE 47 USED LEDs AND DIMENSIONS (MM/INCH)	69
FIGURE 48 RINGS.....	69
FIGURE 49 ZONES OF THE LIGHT SOURCE OF THE FIRST GENERATION	70
FIGURE 50 OPTICAL SYSTEM	70
FIGURE 51 OPTICAL SYSTEM ZEMAX SIMULATION	71
FIGURE 52 DIAPHRAGMS.....	71
FIGURE 53 MIRROR.....	72
FIGURE 54 PHOTOMULTIPLIER TUBE	72
FIGURE 55 DATAQ-6009 DATA ACQUISITION CARD	73
FIGURE 56 CONTROL BOARD (FUSE CIRCUIT)	74
FIGURE 57 LIMITER CIRCUIT	74
FIGURE 58 WORKING FLOW OF PIC MICROPROCESSOR.....	75
FIGURE 59 LABVIEW GUI	76
FIGURE 60 SIGNAL DETECTION OUTPUT	76
FIGURE 61 FFT RESULTS OUTPUT	77
FIGURE 62 CLINICAL SETUP FOR PSYCHOPHYSICAL AND OPTICAL MEASUREMENTS OF INTRAOCULAR STRAYLIGHT	79
FIGURE 63 THE LIGHT SOURCE OF THE 2 ND GENERATION SYSTEM	79
FIGURE 64 SCHEMATIC OF THE OPTICAL OF THE 2 ND GENERATION SYSTEM.....	80
FIGURE 65 OPTICAL SETUP OF THE 2 ND GENERATION SYSTEM(LEFT)F AND THE FLYING MIRROR (RIGHT).....	80
FIGURE 66 ILLUMINATION (LEFT) AND MEASUREMENT PATHS (RIGHT)	80
FIGURE 67 ELECTRONIC BOX OF THE 2 ND GENERATION SYSTEM	81
FIGURE 68 THE DEVELOPED COMPACT SYSTEM FOR OPTICAL MEASUREMENTS OF FORWARD SCATTERING.....	83
FIGURE 69 OPTICS OF THE SIGMA	83
FIGURE 70 HARDWARE BOX OF THE SIGMA	84
FIGURE 71 MAIN GUI OF THE SIGMA	85
FIGURE 72 MEASUREMENT GUI OF THE SIGMA	85
FIGURE 73 PSF CALCULATION GUI OF THE SIGMA	86
FIGURE 74 DATABASE GUI OF THE SIGMA	86
FIGURE 75 CALIBRATION GUI OF THE SIGMA	87

LIST OF TABLES

TABLE 1 THE AVERAGE OSI VALUES WITH RESPECT TO GRADING GROUPS.....	33
TABLE 2 ADVANTAGES AND DISADVANTAGES OF PREVIOUS SYSTEMS FOR MEASURING INTRAOCULAR SCATTERING	40
TABLE 3 AGE DISTRIBUTION OF THE HEALTHY SUBJECTS AND THE CATARACT PATIENTS	53
TABLE 4 NUMBER OF LEDs ON RINGS.....	69
TABLE 5 DETAILED INFORMATION OF EACH ZONE IN LIGHT SOURCE	69

LIST OF ABBREVIATIONS

AC:	ANTERIOR CHAMBER
ARVO	ASSOCIATION FOR RESEARCH IN VISION AND OPHTHALMOLOGY
AS:	ANTERIOR SEGMENT
BCVA	BEST CORRECTED VISUAL ACUITY
CIE	COMMISSION INTERNATIONALE DE L'ÉCLAIRAGE
CS:	CONTRAST SENSITIVITY
D:	DIOPTERS
DP	DOUBLE PASS
GUI	GRAPHICAL USER INTERFACE
IOL:	INTRA OCULAR LENS
IOVS	INVESTIGATIVE OPHTHALMOLOGY & VISUAL SCIENCE
LCA	LONGITUDINAL CHROMATIC ABERRATION
LCM	LIQUID CRYSTAL MODULATOR
OQAS	OPTICAL QUALITY ANALYSIS SYSTEM
OSI	OBJECTIVE SCATTER INDEX
PC:	POSTERIOR CHAMBER
PS:	POSTERIOR SEGMENT
PSF	POINT SPREAD FUNCTION
S	STRAYLIGHT PARAMETER
SP	SINGLE PASS
TCA	TRANSVERSE CHROMATIC ABERRATIONS
UCVA:	UNCORRECTED VISUAL ACUITY
VA:	VISUAL ACUITY
VP:	VISUAL PERFORMANCE

1 INTRODUCTION

Adaptation and the natural selection are the critical factors for the survival in nature. Useful systems have been preserved, and inefficient were abandoned or improved during evolution. Thus, necessity and effectiveness of any system were tested for any species. Several complex information systems have been developed such as; hearing, tasting, touching. However, the vision is the most fundamental and the most complex sense in the evolution progress. Depending on this progress, many different eye or eye-like structures are formed in nature. For example, while the most complex visual systems in animals process a tremendous amount of information, the primitive eye like structures detects only the existence of the light. Although, the complete process of the visual function has not been fully understood there are several essential factors take part in the vision. The optics of the eye, the retina, and the visual cortex should be considered as a complete structure while evaluating the visual performance (VP).

Visual acuity (VA) and contrast sensitivity (CS) tests are common metrics for evaluating visual performance. The performance of an eye without any correction is described with uncorrected visual acuity (UCVA), and the performance of an eye with optical correction is described with best corrected visual acuity (BCVA). The decrease of either UCVA and BCVA could depend on several reasons such as bad refraction, bad optics, retinal problems, neural problems, straylight, etc. There are various methods for evaluating the impairment in VA assessments such as refractometers, aberrometers, contrast sensitivity tests, etc.

This thesis focuses on the straylight and its effect on vision with a new objective technique for measuring this phenomenon while describing the anatomy, optical and material properties of the eye. Besides, there is a lack of knowledge and understanding the effect of

straylight and glare in the ophthalmic practices. Since the early 90s there are several groups, laboratories and companies focus and work on the measurement and evaluation of the intraocular straylight. The novel techniques and advanced technologies are developed by their studies.

In this thesis, we introduce a novel optical device, prototyped at the University of Crete. It is so called “Sigma” and capable of having optical measurements of the intraocular starlight. We performed various studies and tested Sigma under several conditions such as studies with artificial eyes, healthy eyes with filters, healthy eyes as a control group with cataract patients, correlation and comparison studies with the psychophysical method. The optical model and setup, hardware, software components formed the complete system are studied. Data acquisition techniques and signal conditioning processes are detailed in the relevant chapter. The results have been discussed with details.

2 THE ANATOMY OF THE EYE

The eye is the organ, which detects the reflected light from objects, converts this information to electrical signals and delivers this to visual cortex through the optic nerve. This chapter gives information on the anatomy and the structures of the eye.

2.1 THE EYEBALL

Formation of an image in the brain requires highly complex processes and structures. The eye is the first the organ in the visual process. The eyeball, which can also be called as the globe, is not a perfect sphere. The eyeball has two maximum points, which are called as the anterior and the posterior pole as well as the middle plane within them is called as the equator.

The dimensions of an adult human globe are approximately 23 – 25 mm in diameter anteroposteriorly, 23 mm vertically and 23,5 mm horizontally [1]. Eyes with hyperopia tend to be shorter, and eyes with myopia tend to be longer. The eye can be divided into two structures to investigate. The first structure is called as the anterior segment (AS) and the second structure is called as the posterior segment (PS). The anterior segment contains structures such as the cornea, the iris, the crystalline lens and empty rooms called the anterior and posterior chamber.

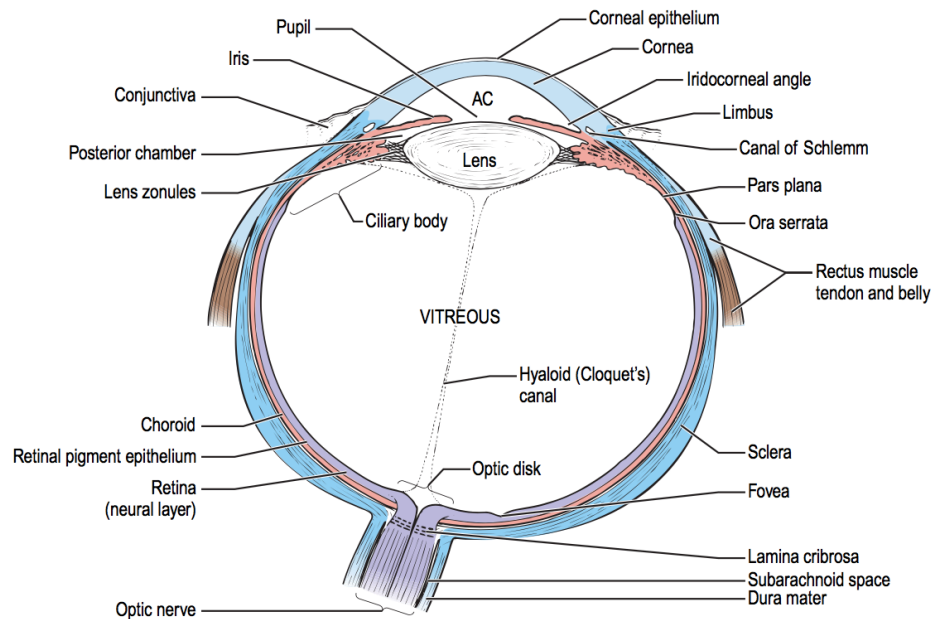


Figure 1 The schematic diagram of the human eye [2]

The anterior and the posterior chamber is divided by iris. The anterior chamber is the space, which is filled with the aqueous, between the posterior cornea and the anterior part of the iris. The anterior chamber (AC) has 2,5 to 3 mm of depth and contains 0,25 ml of aqueous humour. The posterior chamber (PC) is the space, which is filled with 0.06 ml of the aqueous, between the posterior part of the iris and the anterior part of the lens.

The second structure of the eye, which is the largest space in the eye, is called as the posterior segment (PS). The PS also contains 5 – 6 ml of a gel-like material, which is called as vitreous body. Furthermore, the PS also contains structures such as retina, choroid and optic disk [3].

The tunics are the three concentric layers, which form and protect the eye. The outlying layer is anteriorly the cornea, which is clear, and posteriorly is the sclera, which is opaque. This layer provides protection for the eye by the consisting hard tissues inside. The Uvea is the middle layer, and it contains blood vessels for nutrition. The Choroid, the ciliary body, and the iris are the structures of the Uvea. The most inner layer is called as the retina which contains neural cells. The retina has an important area which is called the fovea. The fovea is

specialized for detecting the focused light, converting and delivering the information to the visual cortex for processing in the brain [2].

2.2 THE TEAR FILM

The tear film has several protective and functional responsibilities for the cornea and the conjunctiva. The tear film forms a protective oily layer on the cornea, which removes away debris, and noxious irritants. Thus, the tear film and the blinking reflex prevent an unstable environment, which is suitable for bacteria to grow. Furthermore, the tear film works as an oxygen supply for the corneal epithelium and keeps the cornea and conjunctiva moist [1].

The tear film has three layers. The anterior layer of the tear film contains lipid substance. The middle layer is the aqueous layer and mucus layer forms the posterior layer. These three different layers provide a stable tear film structure, which also keeps evaporation of the aqueous component of the tear film on the cornea.

The tear film loses most of the aqueous and mucus layers by the blinking reflex. Afterwards, the remaining mucus layer regenerates itself [2].

2.3 THE CONJUNCTIVA:

The structure between the anterior surface of the sclera and posterior surface of the eyelids is called as the conjunctiva. The conjunctiva also forms a junction between the eyelids, and epithelium of the cornea [4].

The conjunctiva has two critical functions; the first is producing the mucus layer the tear film and the second providing the support for protecting the eye from infections [2].

2.4 THE SCLERA AND EPISCLERA:

The sclera is the dense and white protective layer of the eye, which mostly contains collagens. The sclera forms from the cornea to the optic nerve [4]. The thickness of sclera

can vary from 300 microns to 1 mm while it shall be measured 400 to 500 microns on the equator [3].

The episclera is the thin elastic layer, that forms around anterior sclera, which creates low friction environment for the movements of the eyeball. Additionally, the blood vessels of the episclera provides the nutrition for the eye.

2.5 THE CORNEA

The Cornea is a transparent tissue, which is inserted into sclera at the limbus. The cornea is responsible for %70 of the refraction [5]. The surface of the cornea forms a positive lens of approximately 43 diopters (D) [3]. Additionally, because of its location, the cornea also serves as a protective barrier to trauma and infections [2]. The anterior cornea is elliptical with the vertical diameter of 10.6 mm and the horizontal diameter of 11.7 mm, whereas the posterior surface is circular and measures a diameter of 11.7 mm [5]. The posterior surface of the cornea is more curved than the anterior. This form creates thickness difference between center and periphery. The average central thickness of a healthy adult is approximately 530 microns, whereas the thickness at the periphery is about 660 microns [2], [5]. Therefore, the cornea flattens in the periphery. However, this non-symmetrical flattening is more extensive nasally and superiorly than temporally and inferiorly [3]. The vessels of the limbus, the aqueous and the tears are the nutrition sources of the cornea. Additionally, the oxygen from the atmosphere supplies the superficial cornea.

The cornea consists of five layers which are the epithelium, Bowman's Layer, stroma, Descemet's membrane and endothelium.

The Epithelium has five to seven layers of cells and it is approximately 50-60 microns thick [2]. The anterior surface of the epithelium helps to stabilize the pre-corneal tear film. The posterior surface anchors to the Bowman's Layer.

The Bowman's is a rigid layer which was formed by different collagen fibrils (I, III, V and VI) with various diameters ranging 20-30 nm. The anterior surface is well delineated and it is separated from the epithelium by the thin basal lamina, while the posterior boundary merges with the stroma [2]. Furthermore, it is unable to regenerate and, if injured, heals by scarring [5].

The Stroma, which is also known as substantia propria, is thick (90% of the cornea thickness) dense, irregular, connective tissue. About 200 layers of collagen lamellae, ground substance and collagen-producing keratocytes form the Stroma. Uniform fibrils which are formed by various collagen types (I, III, V, VI, and VII) connect the stroma to the epithelium. Furthermore, the transparency is determined by the uniformity and regularity of those fibrils.

The Descemet's Membrane, which is also known as posterior limiting lamina, consists of a fetal anterior banded zone and posterior non-banded zone. The thickness is 8-12 nm, and it increases with age. The Descemet Membrane is rich in type IV collagen and provides the historical record of the syntactic function of the endothelium [3]. Similar to the Bowman's Layer, the Descemet Membrane is unable to regenerate.

A single layer of hexagonal cells, which are characterized histologically epithelial phenotype, forms the endothelium. The maintenance of the hydration of the corneal is the important duty of the endothelium together with the aqueous humour. Furthermore, these two structures are also responsible for transportation of ions. Therefore, the health of the endothelium is essential for the transparency and deturgescence of the cornea. There are approximately 500k cells are present, at a density of about 3000 cells/mm² [2]. The endothelium does not regenerate, and endothelial cells decrease with age. The cell loss is compensated by enagement and migration of neighboring cells.

2.6 THE AQUEOUS HUMOUR

The Aqueous Humour is a transparent fluid (with refractive index 1,336) that fills the anterior (0,25 ml) and posterior (0,06 ml) chamber which has several essential functions in the eye. The aqueous is responsible for providing nutrition and oxygen and drainage of the metabolic waste of the structures of the AC, such as the lens, cornea and trabecular meshwork. Furthermore, the aqueous maintain the appropriate intraocular pressure. The aqueous is formed at a rate of 2-3 $\mu\text{l}/\text{min}$ [3] and flows from posterior chamber into the anterior chamber through the pupil. The composition of aqueous humour in anterior and posterior chambers differs because of metabolic change. The concentration of bicarbonate (HCO_3) is higher posteriorly and chlorine (Cl) is higher anteriorly [1].

The aqueous outflow is sustained by two ways; trabecular (conventional) and uveoscleral (unconventional). The main drainage (%90) of the aqueous humour is throughout the trabecular meshwork. The aqueous humour flows freely from the trabecular meshwork to the Schlemm's canal. The second mechanism of the aqueous drainage is the uveoscleral outflow. The rest of the outflow (%10) is drained with this mechanism by aqueous passing across the ciliary body into the suprachoroidal space and is drained by the venous circulation in the ciliary body, choroid, and sclera [1].

2.7 THE IRIS

The Iris is the most anterior extension of the uveal tract and it is pigmented, contractile disk (approximately 12mm), which is similar to the diaphragm of the camera. The iris is the border between the anterior and posterior chamber. The pupil is a circular opening which is located inferonasally on the iris and it connects the anterior and posterior chamber. The extension and contraction ability of the iris allows the pupil to changing its size varying 1 to 8 mm in diameter. When the iris is contracted (mydriasis) it is pulled into numerous ridges

and folds. On the other hand when the iris is extended (miosis) the anterior surface appears to be smoother.

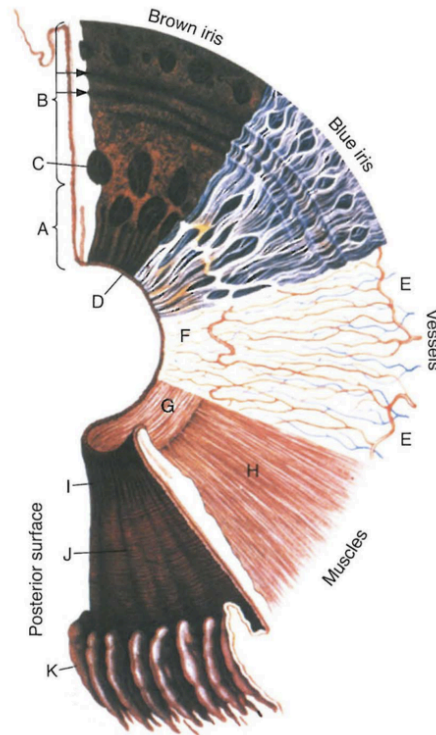


Figure 2 The layers of the iris [3], [6]

Under low light conditions, fear or excitement as contraction of the dilator pupillae muscle the iris dilate (mydriasis). When the Iris is under high illuminated conditions or while sleeping the iris contracts (miosis) as the contraction of sphincter pupillae muscle [2].

The iris (stroma) composed of pigmented cells and for any color its structure is similar. The difference is existence and amount of pigmentation. Lightly pigmented stromas are the blue irides and densely pigmented stromas, which absorbs more light, are the brown irides.

Anterior border layer, stroma, dilator pupillae muscle and posterior pigment epithelium are the four layers of the iris from anterior to posterior.

2.8 THE CILIARY BODY

Ciliary Body is the triangular shaped structure between the anterior and posterior segments. The ciliary body consists of two parts and has a width between 5 to 6 mm. The first part is

the pars plana which is avascular, smooth and pigmented zone. The second part is pars plicata, which is richly vascularized and consists of ciliary processes which the zonular fibers of the lens are attached [3].

The ciliary body has several principal functions; Accommodation, production of aqueous humour, lens zonules, vitreal glycosaminoglycans and vitreal collagen.

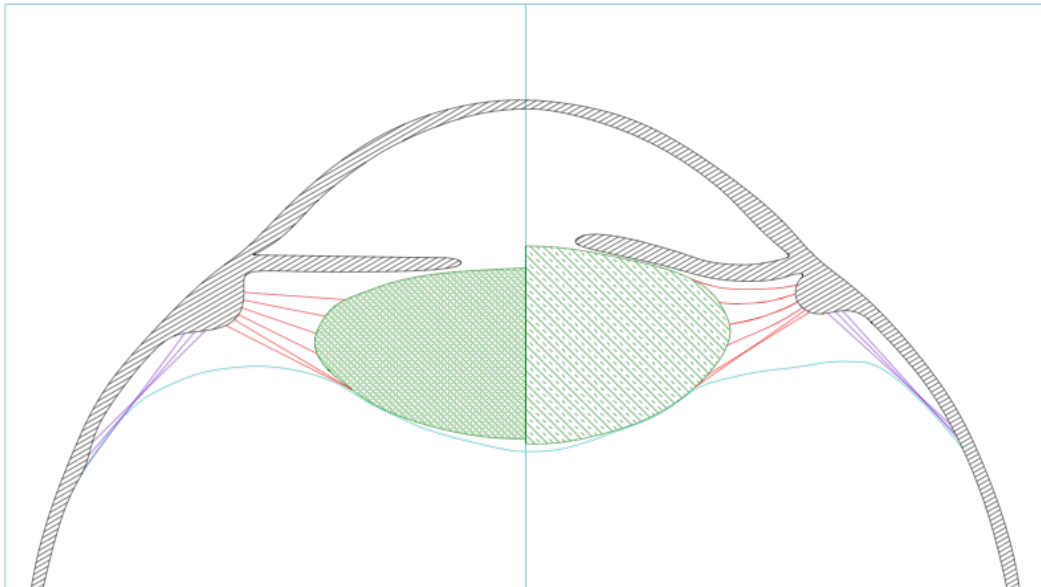


Figure 3 The computer-animated modeling of human accommodation of Goldberg [7]

The ciliary muscle is located in the anterior part of the ciliary body and it is the conjunction with the zonules of the lens. The contraction of the ciliary muscle controls the accommodation by changing the refractive power of the lens. Goldberg presented a new study with the advancement of computer animations and modeling [7]. The outcomes of the study revealed and created a better understanding of mechanisms of accommodation.

2.9 THE LENS

The lens is transparent and avascular structure, which is also the second biconvex refractive structure (the first cornea), focuses the light on the retina. The lens is placed in the capsule, which is behind the iris. The lens contributes 20D of 60D, which is the total human focusing power. Furthermore, the lens can change its shape with the effect of ciliary body and

zonules. At age eight the power is 14D. The effect of accommodation is lost with aging. Until the age of 28 years the accommodative power decreased to approximately 9D and continue decreasing to 1-2 D by 60 years [2]–[4].

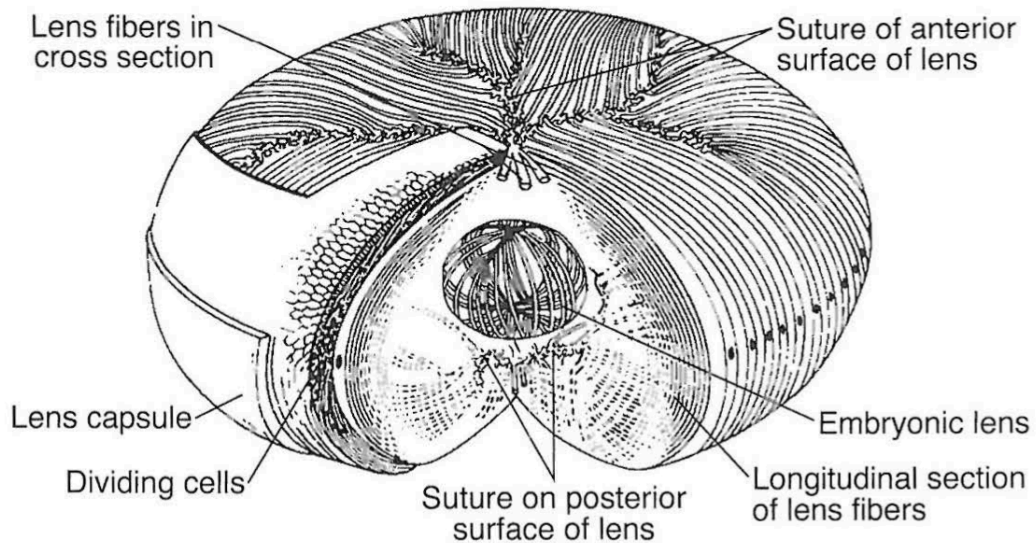


Figure 4 The lens structures[3], [8]

The anterior curvature is 10 ± 3 mm and the posterior curvature is 6 ± 2 mm. The maximum points of both curvatures are called as the anterior and the posterior poles. An adult lens measures 10mm in diameter and 4mm axially. The lens tends to grow with age and become rounder especially after the age 20 [2].

The lens consists of 3 structures; capsule, epithelium, and fibers.

The lens capsule, which is also called as basal lamina, envelops the lens. The capsule is produced by the lens epithelium. The thickness of the capsule varies. It measures 12 ± 3 microns at the anterior pole and 23 ± 5 microns at the posterior pole. The capsule has elastic characteristics, which causes rounder shape for the lens with no zonular tension. The capsule places an important role in the cataract surgeries. A circular opening is created (capsulorhexis) in the anterior capsule and the lens is broken by either with ultrasound waves or laser through this opening and then the new artificial lens (IOL) is placed in the capsule.

2.10 THE VITREOUS

The vitreous is a transparent gel-like structure, which fills the posterior segment. The vitreous is located between posterior lens and retina and its approximate volume is approximately 4 ml. Vitreous is composed of water, protein, and hyaluronan. The vitreous is not homogeneous although it is transparent. Due to the existence of hyaluronic acid the vitreous shows viscoelastic characteristics. The vitreous is an excellent shock absorber, which protects the highly fragile retina. Additionally, the vitreous supports the lens capsule during accommodation. With the aging, the vitreous loses viscoelastic characteristic and becomes more liquid.

2.11 THE RETINA

The retina is the innermost layer of the eyeball, and it is located between the vitreous and choroid. Retina, which is also called fundus, consists of 10 layers and it is responsible for converting the light to neural signals. Fundus contains three cell types; photoreceptors, bipolar cells and ganglion cells.

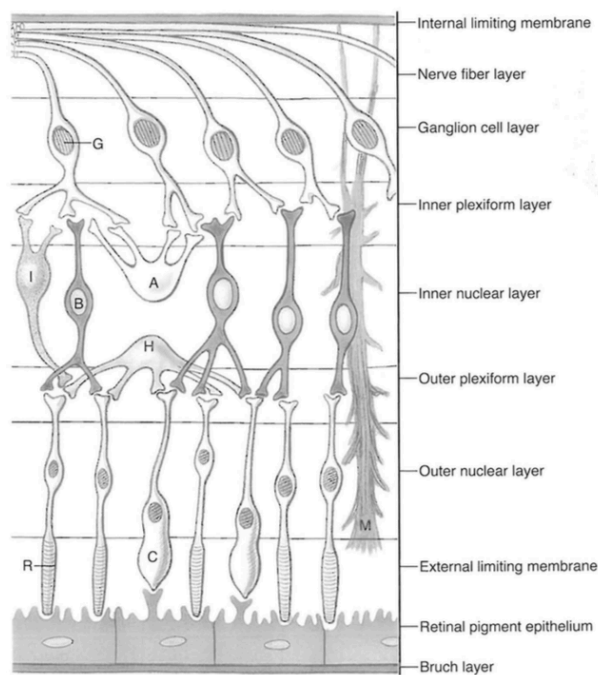


Figure 5 Cell types and histologic layers in human retina [3], [9]

The photoreceptors are specialized cells, which contains photo-pigments for absorbing the light. The rods and cones are the different types of the photoreceptors. Cones are mostly active in the highly illuminated conditions and responsible for color vision and the rods are more active under low illuminated conditions. The bipolar cells are the secondary neural cells, which their dendrites synapse with cone or rod cells and their axons synapses with the ganglion cells. The ganglion cells are the third type of the neural cells, and their axons are connected to the optic nerve. Millions of optic nerve fibers connect the ganglion cells to the inferior poles of the optic disk.

3 THE INTERACTION OF THE LIGHT AND THE EYE

Two different interaction mechanisms of the light and the eye is going to be explained in the section 3. The first mechanism is the optical interactions, which will be detailed as optical properties of the eye. The second mechanism will be detailed as the material properties of the eye. It is very important to understand the difference between these two mechanisms. In order to have the perfect vision or in other words perfect retinal image quality, having the perfect refraction for focusing the light on the retina is as important as having transparent optics and clear optical way.

3.1 THE OPTICAL PROPERTIES OF THE EYE

In order to understand how the eye functions, the eye can be compared with a camera. The cornea and the lens together would be equivalent to the optics (lens), the iris would be equivalent to the diaphragm, and the retina will be the sensor or the film. For creating a better understanding of the optics of the eye, this section will be focusing on the refraction, diffraction, and aberrations.

3.1.1 THE REFRACTION

The eye consists different refractive factors such as cornea (with refractive indice of 1.37), the aqueous humour (1,34), the crystalline lens (1,42) and the vitreous humour (1,33). The total refractive power of the eye (in the Gauss model) is approximately +58D, which is +43D from cornea and +15D from the crystalline lens [1].

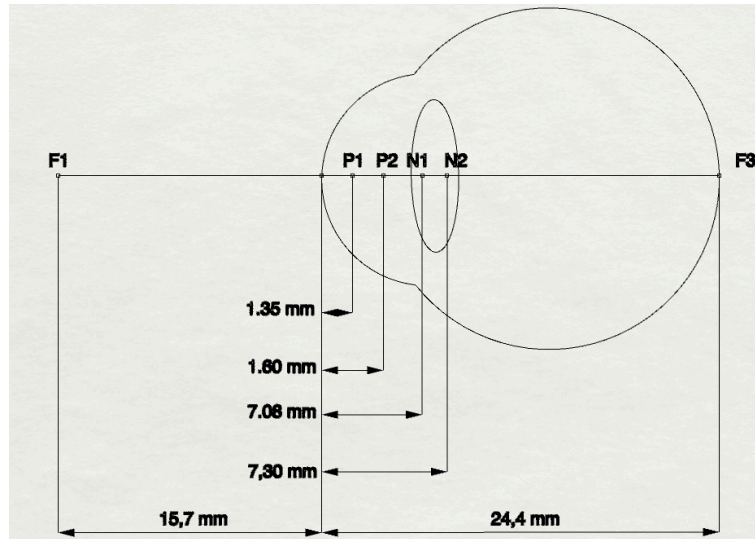


Figure 6 Gauss' eye model

When the eye is analyzed as an optical system (Gauss), three pairs of cardinal points exist; two principal foci, two principal points, and two nodal points. The two principal foci (F1, F2) are located at 15,7 mm in front of and 24,4 mm behind the cornea. The two principal points (P1, P2) is located in the anterior chamber 1,35 mm and 1,60 mm behind the anterior surface of the cornea. Moreover, the two nodal points (N1, N2) are located in the posterior part of the lens 7,08 mm and 7,33 mm behind the anterior surface of the cornea [1].

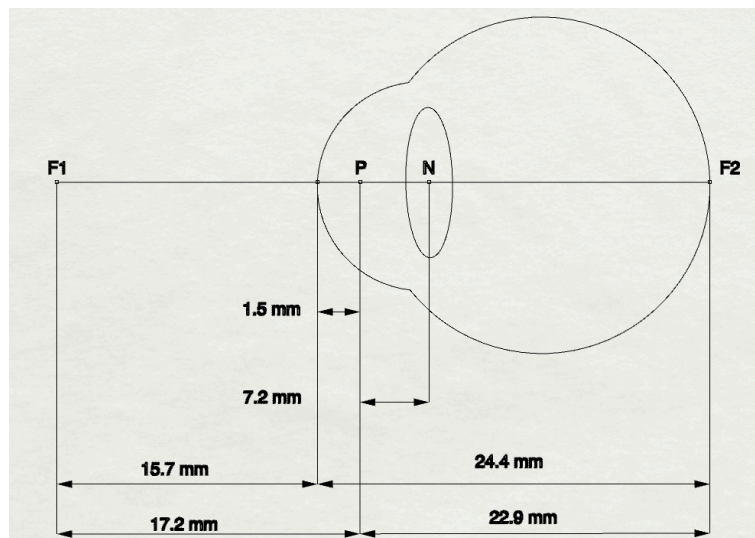


Figure 7 Listing's reduced eye model

Furthermore, there is also reduced eye model described by the Listing. This reduced eye model is simplified by selecting a single principal point and two nodal points. The total refractive power of the Listing's model is +60D. The principal point (P) is located at 1,5 mm

behind the anterior surface of the cornea. The nodal point (N) is located at 7,2 mm behind the anterior surface of the cornea. The anterior focal point is located at 15,7 mm in front of the anterior surface of the cornea. The posterior focal point (on the retina) is located at 24,4 mm behind the anterior surface of the cornea. The anterior focal length is situated as 17,2 mm ($15,7 \pm 1,5$) and the posterior focal length is 22,9 ($24,4 \pm 1,5$) [1], [10].

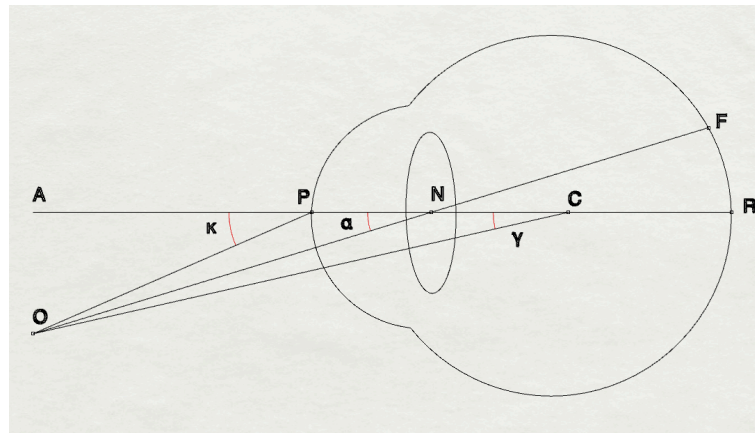


Figure 8 The axes and the angles of the eye

In the eye, three axes, and three visual angles exist. The optical axis passes from the center of the cornea (P) and the center of the lens (N) and ends in the nasal side the fovea, which is on the retina (R) on. The visual axis is starting from fixation point (O) passes from the nodal point (N) and ends in the fovea (F). The last axis of the eye is the fixation axis, which starts with fixation point and finishes at the center of the rotation (C). The three angles are as following; angle alpha (ONA) is between the optical axis and visual axis at the nodal point. Angle gamma (OCA) is between the optical axis and fixation axis at the center of rotation of eyeball. Angle kappa (OPA) is between visual axis and center of the pupil. However, within these three angles, only the angle kappa has clinical significance [1], [10].

3.1.2 DIFFRACTION

Diffraction is the phenomenon that bending of a wave around an obstacle or spreading through an opening. This phenomenon occurs in the eye with light through the pupil and on the projection of the image plane, which is retina. The effect of this phenomenon is

dependent on the size of the opening and the wavelength and the distance of the image plane. Accordingly, more diffraction is observed for smaller openings and smaller wavelengths.

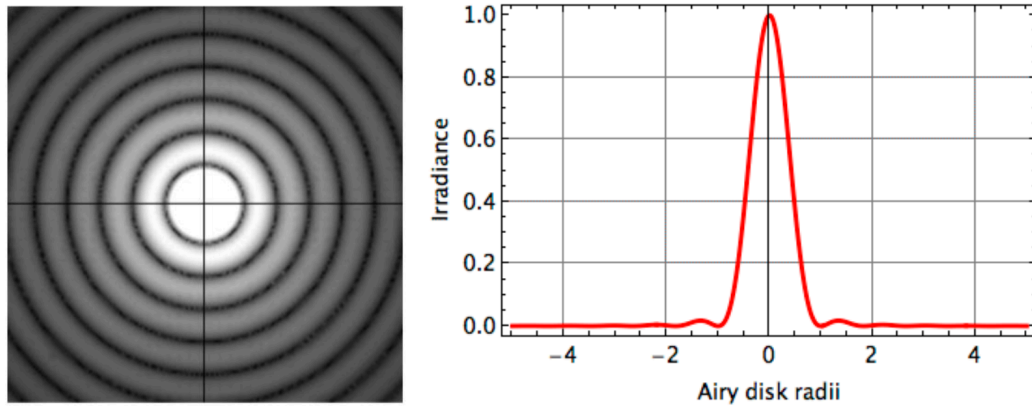


Figure 9 Airy disk pattern and profile

With perfect optics and a circular aperture, the diffraction phenomenon is observed as the Airy pattern or the Airy Disk. The intensity of the Airy pattern with an aperture of radius r can be calculated with the Fraunhofer (far-field) approximation for a diffraction limited system is presented with the following formula (1);

$$(1) \quad \theta = \frac{1.22 \lambda}{2 r}$$

Human iris can contract and dilate between 1 to 7 mm. When the diffraction is calculated the effective diffraction is between 1-3 minutes of arc on the human eye.

3.1.3 ABERRATIONS

Aberration in optics refers to a defect in a lens such that light is not focused to a point, but is spread out over some region of space [11]. Depending on the type of aberration the image formed in the human eye by the lens and cornea aberration is blurred or distorted on the retina. Although the perfect optical system is free from aberrations and only limited by the diffraction, it is not possible to consider the human eye as a perfect optical system. Thus, the aberrations in the human eye could be described under two main topics, which are the monochromatic aberrations and chromatic aberrations.

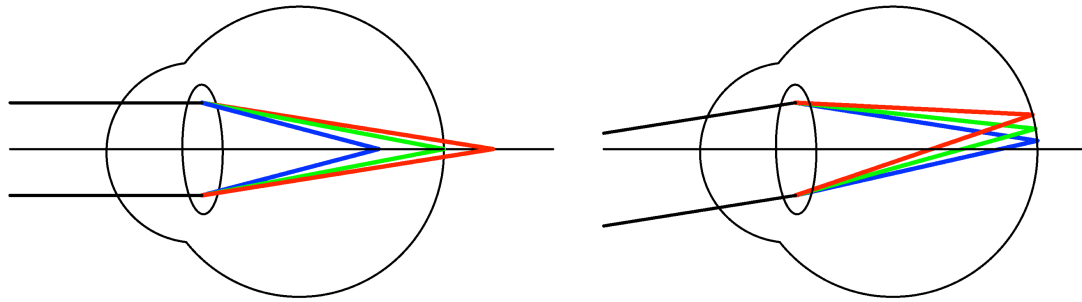


Figure 10 The LCA (LEFT) AND TCA (RIGHT)

Chromatic Aberrations

The chromatic aberration occurs when a lens in an optical system is unable to focus the different wavelengths of the light in the same point due to dispersion [12] and manifests itself as "fringes" of color along boundaries that separate dark and bright parts of the image [13]. The difference on the focal length of the lens index changes amount of the chromatic aberration observed [14]. In humans, chromatic aberrations can be classified as the longitudinal chromatic aberration (LCA) [12] and transverse chromatic aberrations (TCA) [15]. In existence of straight incidence light, LCA occurs in such system when the optics focus the different wavelengths in the different longitudinal position during the optical axis Figure 10 (LEFT). In existence of obliquely incident light, TCA occurs in such system when the optics focus the different wavelengths in the same plane but the foci are not placed along the optical axis Figure 10 (RIGHT).

Monochromatic Aberrations

Unlike chromatic aberrations, there are outnumbered monochromatic aberrations. Due to defects or deformation such as curvature, deformation of the optics can cause monochromatic aberrations. The most common monochromatic aberrations are tilt, defocus, spherical, coma, astigmatism, field curvature, distortion. In any optical system, one or more of these monochromatic aberrations could be observed. Due to the existence of the high number of aberrations and different variations, these aberrations usually are presented as Zernike polynomials or Wavefronts.

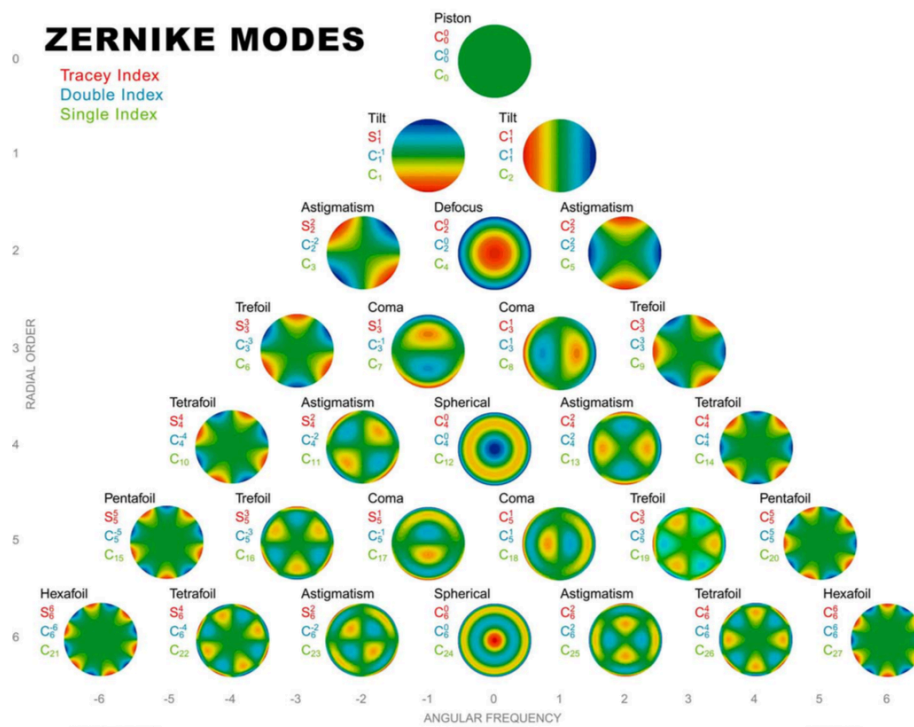


Figure 11 Aberrations represented as Zernike functions

It is important to remember that the aberrations are dependent on the pupil diameter. The aberrations can also be categorized as low order ($n < 3$) and high order ($n \geq 3$) aberrations. These aberrations are generally measured by ray tracing and Wavefront analysis.

The Hartmann-Shack Aberrometer

The Harman-Shack aberrometers are commonly used in the clinical routine for evaluating aberrations in the eye. The Hartman-Shack aberrometers consist an array of the laser source (SLD) is projected as a small dot on the retina. A CCD camera is focused the image plane through an array of microlenses. These microlenses are used to separate different light rays exiting the eye. Aberrations cause tilts on these exiting rays and any aberration can be approximated as a wavefront by calculating tilts of this array of lenslets.

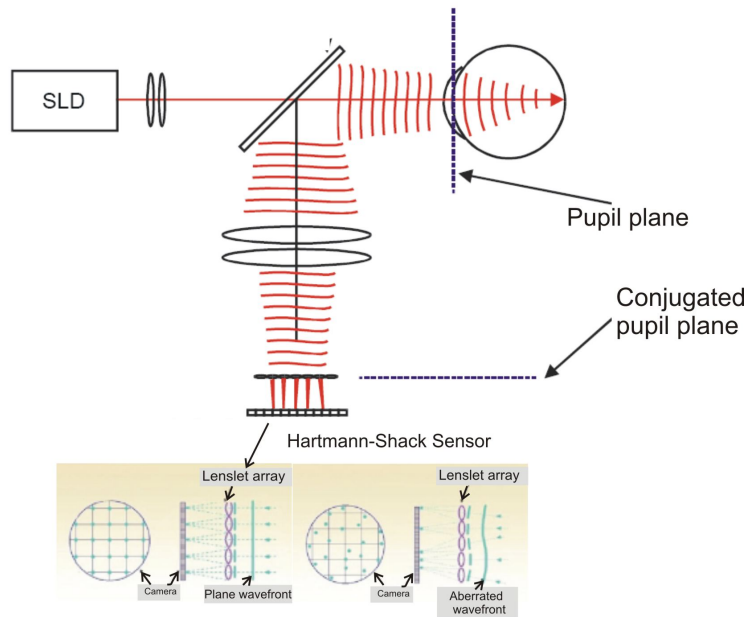


Figure 12 The Schematic of Hartmann-Shack Aberrometer

Ray Tracing Aberrometer

The ray tracing aberrometers are the second type for measuring the high and low order aberrations. Ray tracing uses a parallel laser beam sent through the pupil and measuring the exact location where the laser reaches the retina. The linear X, Y sensors measure the reflected light. The aberrations cause shifts in the retina. This measurement is repeated for different locations of the pupil and each shift for each position is recorded. The algorithm uses this information and calculates and reconstructs the real wavefront error [16].

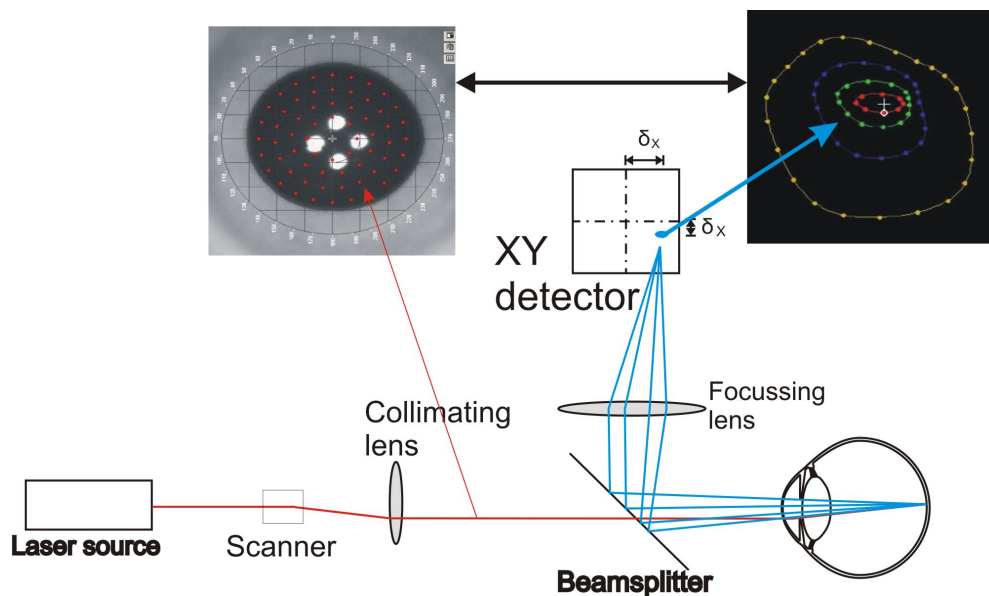


Figure 13 Schematic of Ray Tracing Aberrometer

3.1.4 THE POINT SPREAD FUNCTION

It is not only important to understanding the optics for professions who produce ophthalmic and/or medical device. It is also important for professions who use and analyze the patient data. The image formation on the image plane is the first step in the vision process and it has similarities between different platforms such as eyes, cameras, telescopes. The conventional optical laws are valid for all these systems. However, Atchison states that there are some interesting differences because of the eye's biological basis [17].

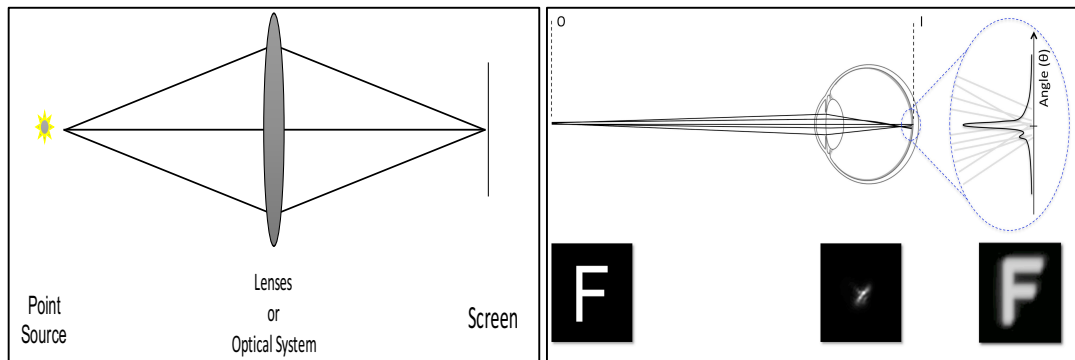


Figure 14 The point spread function on optical systems and human eye

The point spread function (PSF) is an important metric for the evaluation of the quality of the optical systems. PSF is the distribution of a light source on the image plane (Figure 14) and it is used for developing telescopes or camera systems frequently. If a small light source introduced a perfect optical system, a small point on the image plane is observed. However, aberrations and light scattering causes the broadening of the PSF and reduce the retinal image quality. The PSF (Figure 14) contains various information related either to optical properties and material properties of the human eye. Thus, more and more scientist began to focus and try to understand the effects of the PSF on the vision.

Different areas of PSF reveals distinctive information of the human eye. The central part of the PSF comprises information related the optics, blur, aberrations, and resolution. The peripheral part (more than 1 degree) of the PSF is mostly related to conditional loss of contrast, scattering and glare [18].

The glare specific part of the PSF in the human eye (2) for angles ranging from 3 to about 30 degrees can be approximated by the Stiles-Holladay formula [19]–[21].

$$(2) \quad PSF(\theta) = \frac{S}{\theta^2}$$

Furthermore, obtaining the PSF and the straylight the wavelength of the light source had significant importance. The study [22] showed the wavelength of the light source effects the central part of the PSF. Furthermore, it also mentioned that the peripheral part of PSF which is more related with the straylight and glare is not dependent on the wavelength and the 550 nm is defined as the optimum wavelength for measurement of both central and the peripheral PSF.

3.2 MATERIAL PROPERTIES OF THE EYE

In the eye, the light interacts with structures with different refractive indexes. Although, the refractive power is obtained from the cornea and the lens, the straylight can be introduced by several factors such as the tear film, the cornea, the lens, the aqueous humor, the iris, the sclera and the vitreous. The irregularities and defects are the important factors on the transparency of these structures.

The three non-refractive elements can induce intraocular scattering due to the insufficient and low-quality production. Especially, the tear film shapes the outermost surface of the cornea and the first interaction of the light is with the tear film. Thus, the production in quantity and quality of the tear-film can induce scattered light. Secondly, it is reported that vitreous loses the gel-like structure with age and becomes more liquid. Furthermore, due to floaters in the vitreous, patients can observe scattering. The pigmentation of the iris can also effect the amount of straylight. The highly pigmented irises block more light than the low pigmented eyes. Thus, the eyes with light colors observe more straylight from the iris.

Although several factors can be described as the source of the intraocular scattering. The cornea and the lens are the most significant scatterers in the eye.

The transparency of the cornea, relatively the intraocular scattering is affected, from the types and distribution of the collagen fibers, the diameter and density of the fibrils, refractive index difference within the structures of the cornea, stromal thickness and spatial ordering of fibrillary array [23], [24].

Additionally, the outcomes of the study state important changes in the corneal morphology after refractive treatments [25]. Measurements of confocal microscopy showed highly reflective corneal surfaces at postoperative measurements. The study pointed out that refractive surgery and healing process affects the transparency of the corneal structures which are the important factors for the intraocular scattering.

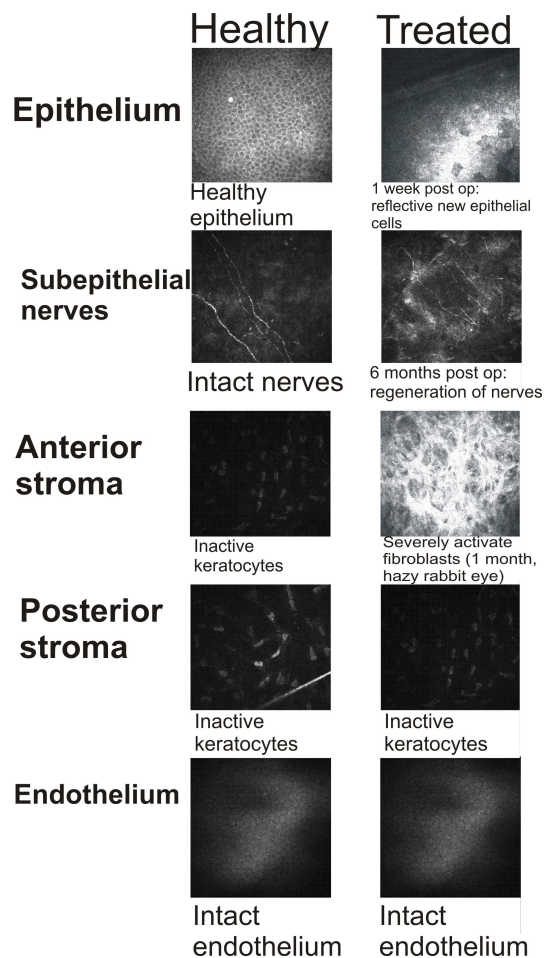


Figure 15 Representative images of the different corneal layers before (left) and after (right) refractive surgery as seen in in vivo confocal microscopy. [26]

The second significant source of the intraocular scattering is the crystalline lens. The loss of transparency and induced intraocular scattering can occur with the embryonic or pediatric defect, metabolic effects, trauma or aging.

Mittendorf dot, epicapsular star, Peters anomaly and congenital cataracts are some examples of the embryonic or the pediatric defects which affect the lens and cause loss of transparency.

Traumas are the second type of defects which can affect the transparency of the crystalline lens. Perforating or penetrating injury, foreign bodies, radiation, chemical injuries can cause the transparency loss depending on the severity of the trauma.

The human body is a well-designed machine which performs several vital functions for long years and regenerates itself. However, due to some metabolic diseases can affect the crystalline lens. Diabetes mellitus, Wilson disease, galactosemia, myotonic dystrophy, hypocalcemia are some examples.

There are several causes of affects described above which can cause the loss of transparency in the lens and induce more scattering in the eye. However, none of these effects are as common as the age-related cataracts. With aging, the lens undergoes chemical, biomechanical and optical changes. After 40 years the lens starts losing the ability to accommodate and after 60 years the chemical change of the proteins of the lens starts inducing pigmentations which can lead the patient to the visual impairment which is called cataract.

Although, all these effects exist for ages the knowledge and understanding of the intraocular scattering is not as good as the understanding of the refraction or aberrations. We believe that the analysis of visual performance will be incomplete without analyzing the intraocular straylight. The following chapters will focus on several studies which worked on measuring, quantifying and understanding of the straylight phenomenon.

4 INTRAOCULAR SCATTERING & STRAYLIGHT

Intraocular light scattering is the phenomenon that part of the light reaching the retina does not partake in normal image formation. Rays originating from a certain point in space are converged by the refracting surfaces of the eye to the focal area in the eye [27]. The human ocular media is not perfect due to reasons which are mentioned in the previous section. The Light interacts several tissues, with different refractive indexes. All of these different elements such as cornea, lens, vitreous and fundus induce scattering and any abnormalities (See 3.2) in any of these elements such as the cataract in the lens or the haze on cornea, will create a significant increase in the intraocular scattering. The increase on outer skirt of PSF which is related with intraocular scattering causes veiling luminance over the whole retina that adds to the retinal projection of the visual scene, thereby reducing the contrast of the retinal image [28].

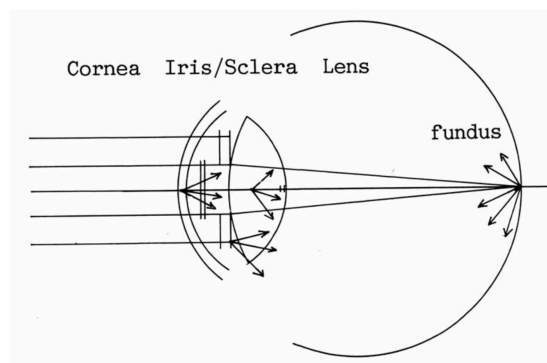


Figure 16 The sources of intraocular scattering[29]

The severity of this contrast loss depends on the illuminance ratio between background and image. The extreme situation is represented by the classical glare condition: strong light somewhere in the visual field while a weakly lit object has to be observed. Depending on the distance between glare source and object this situation can lead to complete blinding. The

typical situation is blinding by oncoming traffic at night [27]. As an example, the Figure 17 demonstrates the effect of straylight. In order to understand the effect a scenery needs to be existent which contains bright sources and dark area. The light sources on the top are six times magnitude higher than the dark areas. When the higher numbers of straylight existed system the detail and contrast lost around the light sources can be observed (down). Depending the amount of straylight the detail and contrast loss increases relatively.

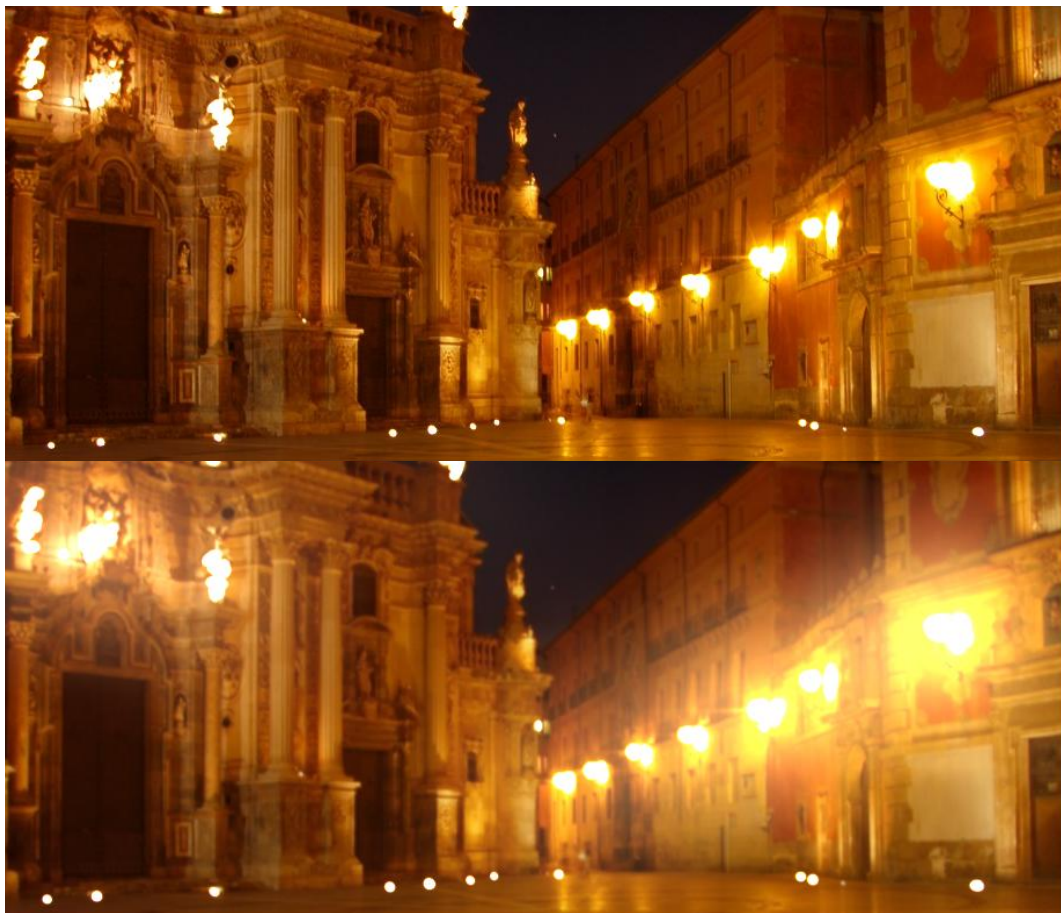


Figure 17 The effect of the straylight

The scattered light can be categorized as the backscattered and forwardscattered light. If the scattered light is more than 90 degrees, this type of scattering is called as the backscattered light. The backscattered light is commonly used in the clinical routines for evaluating the corneal haze or grading the cataract. Especially, the cataract grading systems [30]–[33] such as LOCS III are using the backscattering light for quantifying the amount of cataract. However, our and several other studies (Sections 4.1, 4.2, 5.2.4, 5.2.5) showed that the

backscattered light does not always necessarily to give information for the patient's visual performance. Thus, following chapters will focus several methods and devices on advancement of the intraocular straylight measurements for the forward light scattering.

4.1 PSYCHOPHYSICAL MEASUREMENT OF THE STRAYLIGHT

Luuk et. al. stated in that there was no instrument or method existed that is generally accepted for routine clinical assessment of (functional) retinal straylight [28] until early 80s when van den Berg introduced “compensation comparison method for assessment of retinal straylight”, developed the psychophysical device and presented on the effects of intraocular straylight which influenced several scientists to focus and measure the intraocular straylight on humans [28].

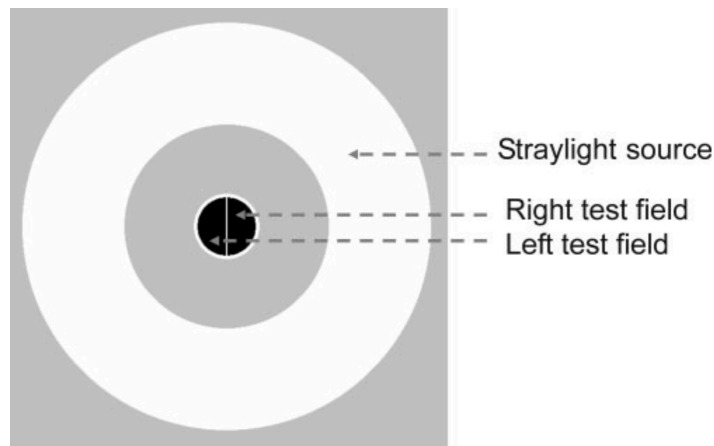


Figure 18 Test screen of psychophysical straylight meter (C-Quant) [28]

The straylight meter consists a test screen (Figure 18) [28] and two push buttons. The test screen contains two circles. The first is the inner circle is in the middle and which is divided vertically into two parts and the second is the bigger circle which is used as the straylight source. In one of two halves semi circles the compensation light is presented randomly and the second half receives no compensation light. Due to the scattered light from the big circle, light is also observed in the second half which has no compensation light. The compensation light and the peripheral circle, which is the source of scattering, are modulated in counter phase. Thus, two different flickering is observed in the two halves. The first half is the

straylight only (field S) and the second half is the straylight and compensation (field C) light combined. During the measurement, it is asked the subjects to select the stronger flickering half and give the response in limited time with two buttons which represent the semi halves.

During the test, different amount of compensation light is introduced. If the amount of compensation light is higher than the straylight the field C looks stronger for the subjects and as the difference gets higher the probability of selecting field C gets closer to 1. When the straylight is higher than the compensation light the field S looks stronger for the subject and as the difference gets higher the probability of selecting field S gets closer to 1. During the measurement, a psychophysical function fit is applied to the subjects' responses. Moreover, the amount of compensation light is equal to the straylight in the system where the probability of the psychophysical fit is equal to 1/2 [28].

The outcomes of the first large population study revealed the function (3) which revealed the relation of the straylight with the age. Increase in straylight (S) was observed as an outcome of the study [34].

$$(3) S(\theta) = 10 * \left[1 + \left(\frac{AGE}{70} \right)^4 \right]$$

A large study [35] was conducted between 2422 European Drivers. The outcomes, of the study supported the increase the straylight with the age (Figure 19). Interestingly, the results also showed high straylight values can exist in young age population.

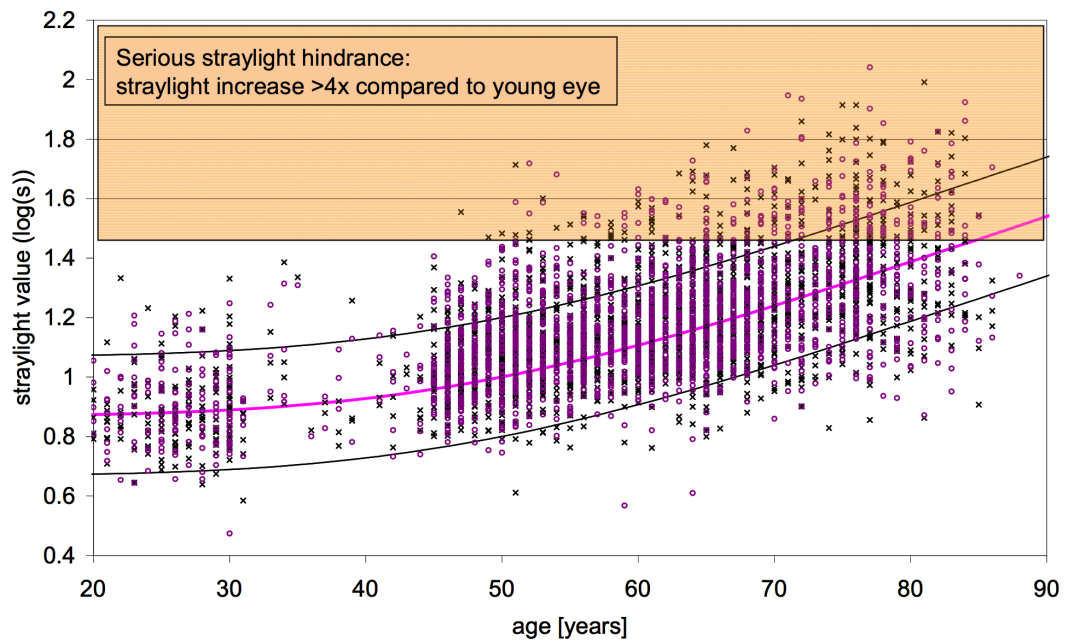


Figure 19 Log(s) values as a function of age for a population of European drivers [29], [35]

A proposal was made to the Commission International de l'Eclairage (CIE) Standard Glare Observer for with the outcomes of several studies explained above. The application was accepted in 1999. This report was accepted as the standard for the intraocular straylight [36].

4.2 OPTICAL MEASUREMENT OF THE STRAYLIGHT

The challenge on the optical measurement of the straylight was the central part of the PSF is six orders of magnitude [20] brighter than the peripheral part of the PSF. For this reason, the amount of reflected light from the peripheral part of the PSF was below the threshold and noise level even for most sensitive equipment and was the challenge. Thus, relative information to the intraocular scattering could not be extracted optically. Although the study [37] evaluated the intraocular straylight on single pass method in cadaver eyes, there was no optical/objective technique or technology existed back that time for clinical measurements.

There were several systems developed for measuring the intraocular scattering based on either single (SP) or double (DP) pass principle. Unlike SP systems, DP systems did not require feedback from subjects. The double pass principle bases on projecting the light source on the retina and sensing the reflected light by a camera or a detector.

4.2.1 OPTICAL QUALITY ANALYSIS SYSTEM (OQAS) II - DP OPTICAL SYSTEM FOR MEASURING CATARACTS

Pablo et.al. proposed in 2011 a new DP optical method [38] for measuring intraocular scattering. QOAS II system was used for capturing the DP images. The schematic representation is presented in the Figure 20. In the setup, an infrared laser diode is used. The generated laser light was projected on to retina after passing collimator (CL) and annular aperture (P1) through 2mm of entrance in the pupil plane. The exit measurement area is set to 4mm in the pupil plane. After being reflected from a beam splitter and exit aperture (P2) the reflected light is sensed by a camera. The system is capable of correcting the refractive error sphere and astigmatism included.

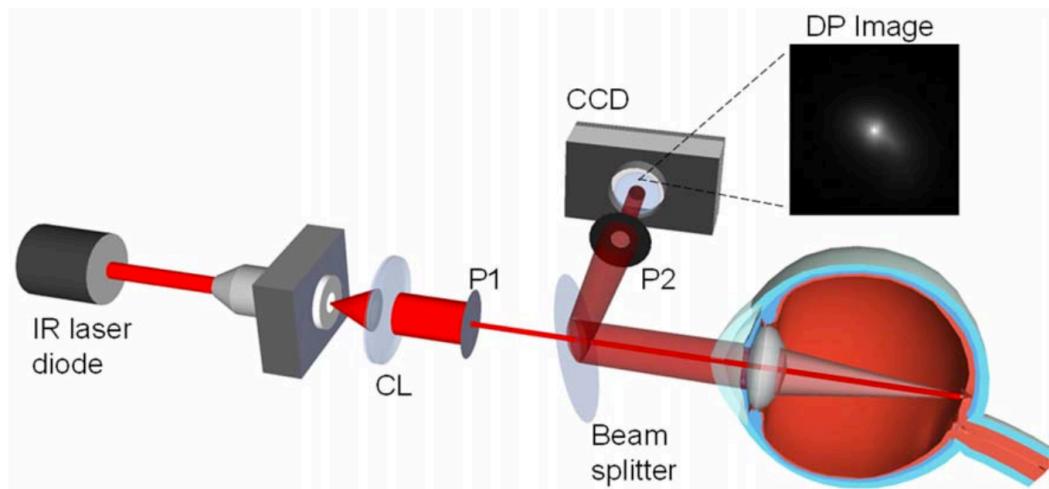


Figure 20 Schematic representation of DP system for optical measurement of the straylight[38]

Series of retinal images, which is above the intensity level of 200, were captured as well as the background images. Average intensity and background contribution is calculated. The final value is obtained by subtracting the background from the measured intensity.

An optical index was defined, which is called objective scatter index (OSI), for quantifying the amount of the intraocular straylight. The calculation was based evaluating the ratio between the amount of light in central peak (circle of 1 mins of arc) and the light in the periphery (12 and 20 mins of arc). The values OSI of ranged from 0 to 25, where values below 1 were considered as normal and eyes over 5 were considered as eyes with induced

scattering. The retinal images of a normal eye (image A) and eye with higher straylight are presented at the Figure 21.

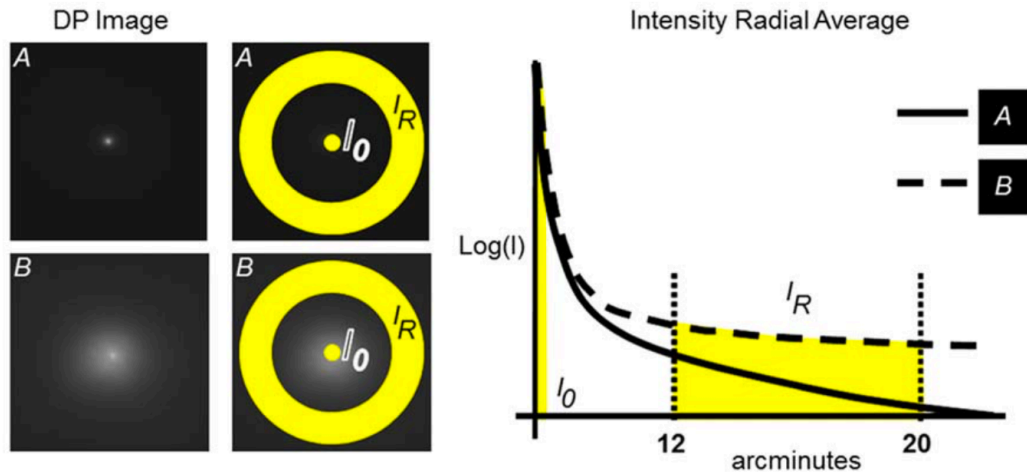


Figure 21 Example of the selection of the zone in the double-pass image used to define the objective scatter index (OSI)[38]

A correlation study was performed between the DP system developed and the LOCS III subjective grading system between a healthy control group and eyes with cataract.

Cataract Group	Control	NO2	NO3	NO4
OSI	$0,7 \pm 0,3$	$3,0 \pm 1,0$	$6,0 \pm 2,0$	$9,0 \pm 2,0$

Table 1 The average OSI values with respect to grading groups

The OSI measurement outcomes with subjective LOCS III grading are presented in the Figure 22 (LEFT). The average OSI values with respect to grading groups is given in the Table 1 and presented in the Figure 22 (RIGHT).

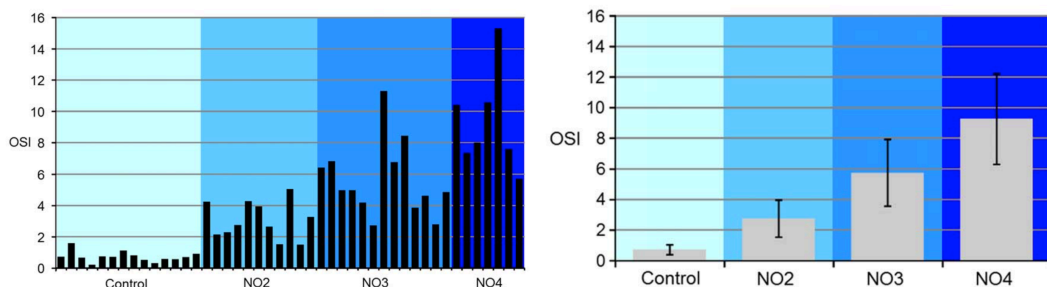


Figure 22 The OSI values with respect to grading groups (LEFT) and the average OSI values with respect to grading groups (RIGHT)[38]

The study results concluded that the developed system was capable of differentiating the OSI values of the cataract patients graded with LOCS III system.

4.2.2 DP OPTICAL METHOD FOR RECONSTRUCTING THE WIDE-ANGLE PSF OF THE HUMAN EYE

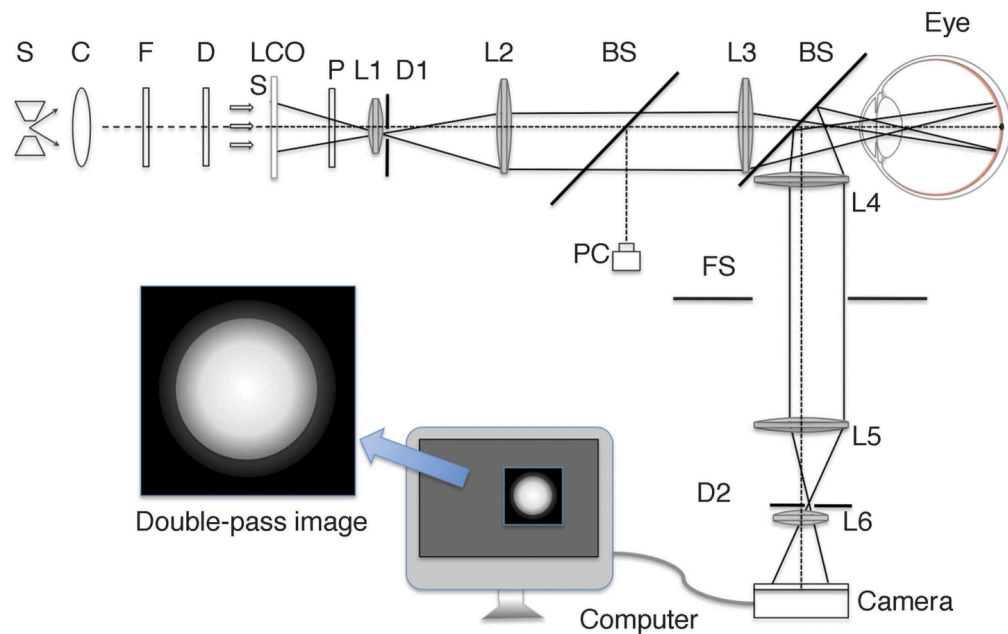


Figure 23 Optical setup for reconstruction the wide-angle PSF of the human eye[39]

Ginis et.al. introduced the system [39] (Figure 23) for reconstruction the wide-angle PSF by projecting extended light source to the retina. As the light source, a Xenon lamp with LCOS 2002 liquid crystal modulator (LCM) in front, is used in the system. In the system, light passes through a collimator, green filter (530 ± 30 nm) and diffuser and reach the LCM which is conjugated to the retina plane. Disks with different sizes were projected after passing a diaphragm and several optics on the retina. The reflected light from the eye is sensed through a multiplying CCD camera after passing a beam splitter, several optics and a diaphragm. The diaphragm which is conjugated to the pupil plane and limits the light entering the eye is equal to 2 mm diameter. Additionally, the second diaphragm, which is also conjugated to the pupil plane, controls and limits the exiting reflected light is equal to 4 mm in diameter. Both centers of the diaphragms do not overlap in order to avoid the crosstalk of the signals or reflections.

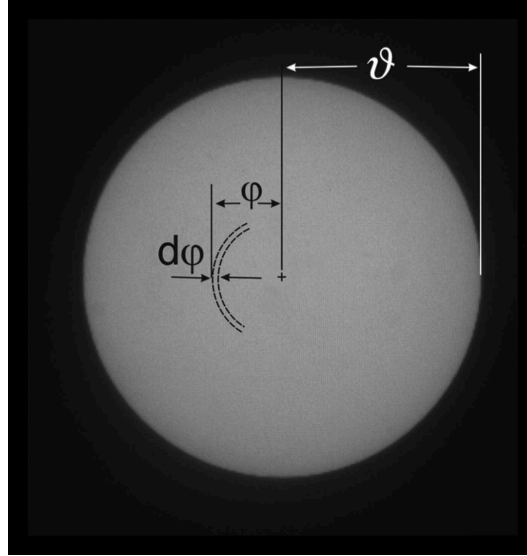


Figure 24 Uniform disk which is projected to retina and the dimensions which are used for calculation of the PSF[39]

The intensity of center of each projected disk (with averaging of 3 X 3 pixels) were recorded. The central intensity the biggest available disk was used for normalization. By using the model of PSF in human eye formula (4) the PSF was calculated for angles of 1,25 and 5,25 degrees (Figure 24).

$$(4) I_c(\vartheta) = \int_0^{\vartheta} 2\pi\phi PSF_{dp}(\phi)d\phi$$

Subject were stabilized with a mouth piece to the system and the alignments were performed with a pupil camera and there-axis stage. The eyes were fixated in such position for avoiding the center of disks from the blood vessels on the retina. Fifty disks with various diameters which changes between 0,18 and 8,1 degrees were exposed to the retina for 300 ms.

The comparison tests were performed with two types of previously documented [40], [41] lenses for measuring intraocular scattering. The first type is the Black Promist 2 lenses produced by the Tiffen company. This lens has an additional effect on the straylight parameter of 0,88 log units. The second type is rigid gas-permeable contact lenses produced by Menicon company. These hard contact lenses have no refractive power and induce 0 to 0,6 log units of addition to the straylight [28].

In order to test the consistency and validate the device several measurements were performed. The first comparison was performed between two healthy subjects. The outcomes (Figure 25) showed that the system was capable of detecting straylight difference even between young healthy subjects.

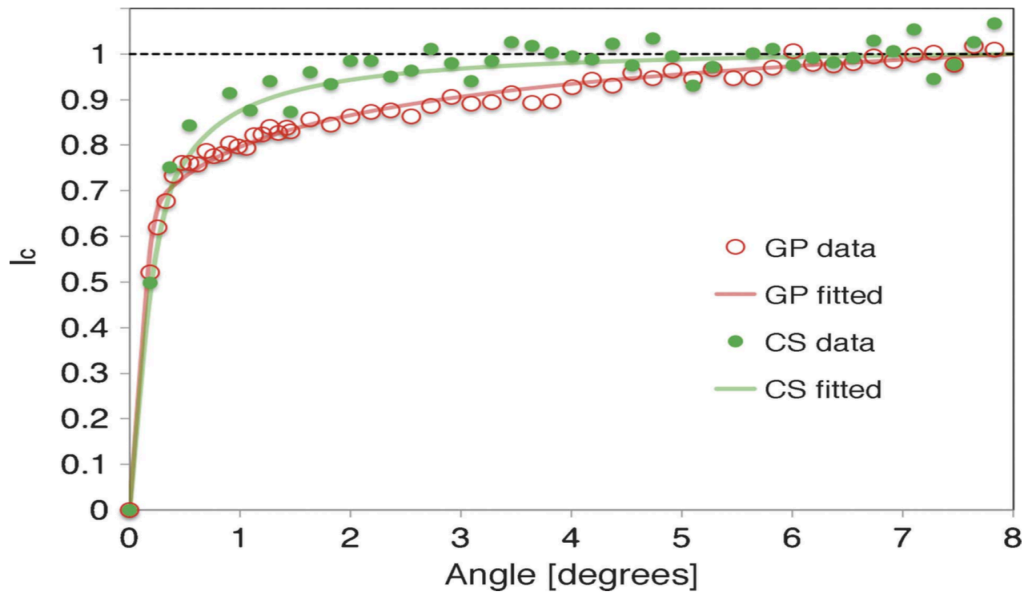


Figure 25 Experimental data acquired from two healthy subjects [39]

The second validation (Figure 26) study was made between artificial eye, artificial eye and promist filter, healthy subject GP, healthy subject GP + Menicon lens grade 3, healthy subject GP + Menicon lens grade 5 and healthy subject JB.

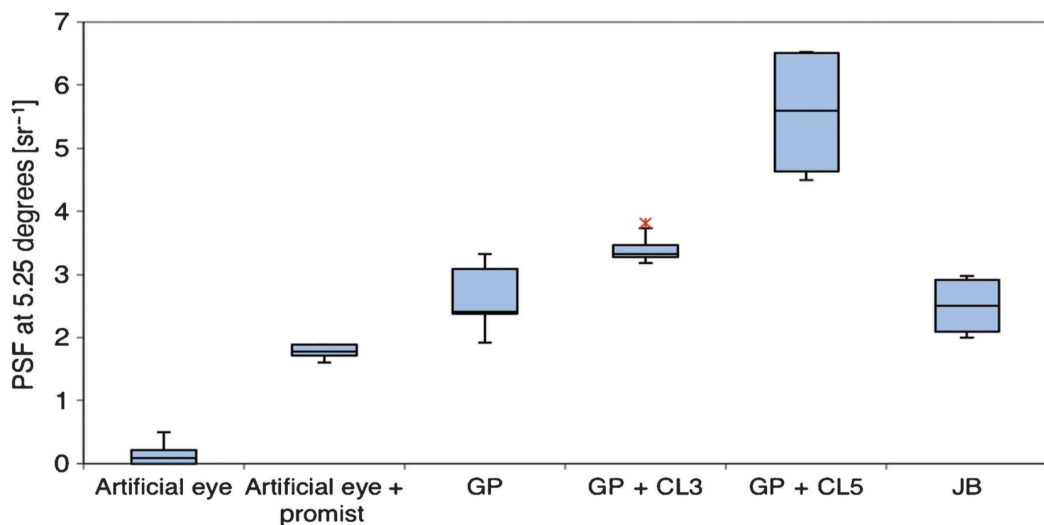


Figure 26 Experimental data between artificial eye, two healthy subjects and additional scatterers [39]

The authors stated that “A new, accurate, and objective optical method to reconstruct for the first time the wide-angle PSF in the human eye has been developed and demonstrated” [39]. Thus, the first system which is capable of optically detecting the intraocular straylight difference even between young patients were developed.

5 FAST OPTICAL MEASUREMENTS OF THE STRAYLIGHT

There are three systems described in the previous sections that outcomes of these studies showed that those systems were capable of quantification of the intraocular scattering in human eyes. However, each system has its own deficiencies in the process of measuring intraocular straylight.

The psychophysical method (described in 4.1) was commercialized with a device which is called C-Quant by Oculus. The device became a trademark and studies with a high number of subjects were enrolled for measurement of the intraocular scattering. C-Quant's outcomes of come to an initial point that creates a new definition of the international standard in the intraocular straylight research area. Although, there were big numbers of patients were examined in Europe with this device, C-Quant has two deficiencies.

The first one, C-Quant examination time is the biggest problem for implementing the psychophysical straylight measurements to the clinical routine. As described in the relevant chapter measurement requires patient responses and with informing the patients required approximately 4 to 5 mins for a patient. The second problem is that the device requires feedback of the patients by pressing two push buttons. If it is considered that the main source for scattering is the cataract, the age of prospective patients starts with 60. As the age increases the patients who could not be measured with the C-Quant increased relatively [42], [43].

In the section 4.2.1 OQAS II system and the its results were described. Although OQAS II is commercialized and is capable of measuring optically. The system could never achieve the success of the psychophysical measurement due to sensitivity to the low order aberrations

and narrow angle acquisition of the PSF. Furthermore, the system was stated as not practical [39].

In the section 4.2.2 the first DP system which can optically quantify the intraocular scattering difference even between young health eyes are described [39]. This system has disadvantages which are similar to the previous devices. The long time is required for the measurements. More importantly, the system is impractical due to the bulky system design and a requiring special mouth piece for measurement of the patients. This makes the system impossible to use in the clinical routine.

		C-Quant	OQAS	DP System for Wide-Angle PSF
Practicality	Fast Measurements	X	X	X
	Do not Require Feedback	X	✓	✓
	Compact Design	✓	✓	X
	Do not Require Dilation	✓	✓	X
Robustness	Measure Wide-Angle PSF	✓	X	✓
	Sensitive Measurements	✓	X	✓

Table 2 Advantages and disadvantages of previous systems for measuring intraocular scattering

We analyzed the advantages and the disadvantages (Table 1) of the current systems and we aimed to design such system which might be able to overcome all disadvantages that previous systems had.

5.1 INSTRUMENT SPECIFICATIONS

In this chapter, we are going to describe a new compact device for measuring intraocular scattering, which is developed in the Institute of Vision Optics, the University of Crete. The section consists details of hardware, electronics, theory and analysis and validation and

correlation studies which are either published or presented in congresses (3 papers and 3 ARVO contributions with poster presentation) [42]–[47].

5.1.1 THE HARDWARE

The optical setup (Figure 28) of the system consists a specially designed light source, 4 lenses, 3 diaphragms, 2 pupil cameras, 1 D shaped mirror, and silicon photomultiplier device as the detector.

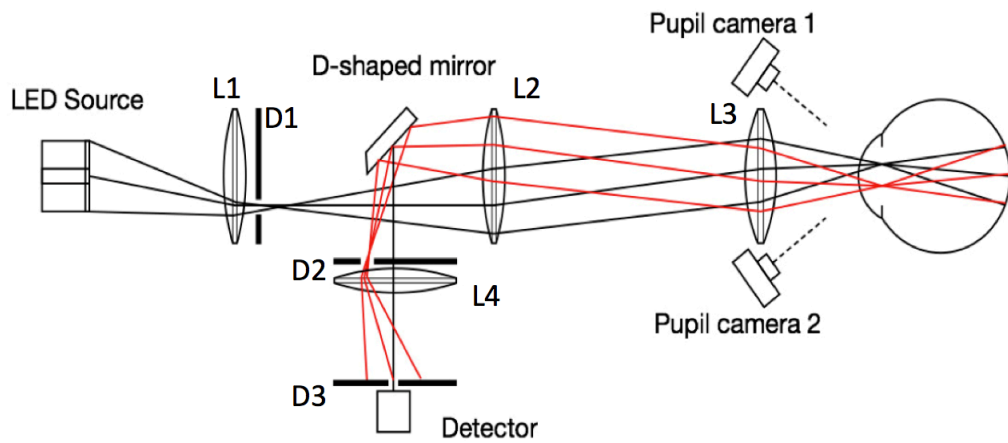


Figure 27 Schematic of the optical setup

The system uses a specially designed light source (Figure 28) which 8 LEDs formed into two different zones. The first zone is the central disk which contains a single green LED (528 ± 10 nm). The second zone is the annulus which contains an array of 7 green LEDs. The light source contains light shaping diffusers for creating a homogenous light distribution.

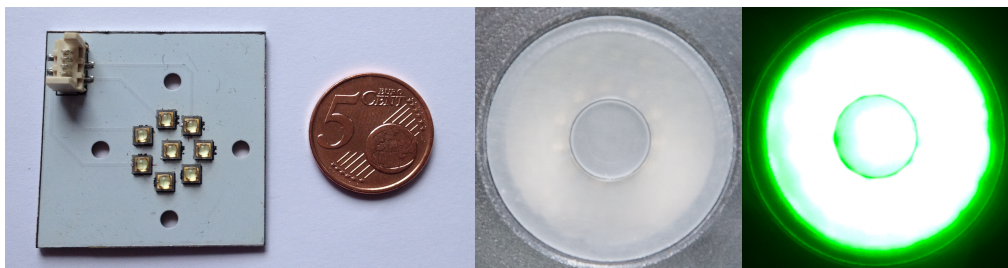


Figure 28 The light source

The previous study [22] stated that the optimum wavelength for straylight measurements is 550 nm. Depending on these results, we selected the green LEDs were the closest wavelength with required luminance.

Each zone was modulated with a square-wave with different frequencies. The central disk, which corresponds to 3 deg of visual angle on the retina, was modulated with 483 Hz. The annulus, which corresponds to 3 to 8 degrees of visual angle on the retina, was modulated with 769 Hz.

The illumination path is formed as following; the modulated light, which is created and diffused (Retina Plane) in the LED source, crosses from the Lens 1 (Crystalline Lens Plane), limited by the Diaphragm 1 (Pupil Plane – Superior), then crosses from Lens 2 and 3 and projected to the retina.

The reflected light is separated by the Diaphragm 2 (Pupil plane – Inferior) after crossing from Lens 3, 2 and 4. Then the Diaphragm 3, which is a pinhole, selects the central part of the projected image and the reflected light is measured by the detector.

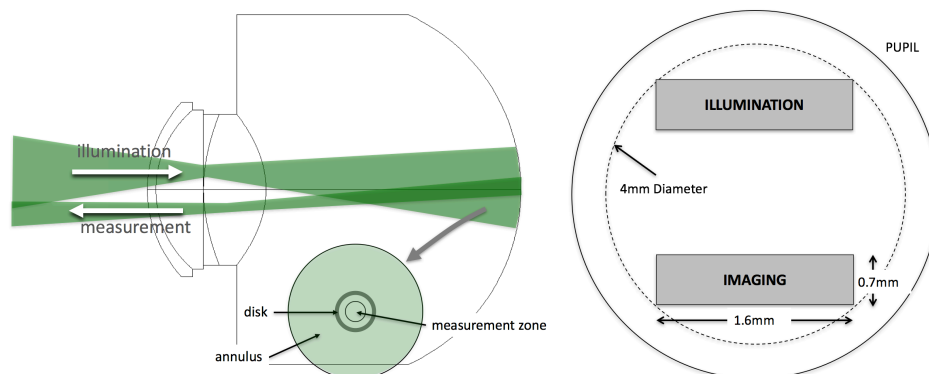


Figure 29 The separation of the illumination and imaging path via Diaphragm 1 and 2 on the pupil plane

Each diaphragm has significance in the illumination and imaging process. The diaphragm 1 and 2 separate the illumination and imaging paths. Thus, the measurements do not contain any backscattered light or reflected light.



Figure 30 Actual image of the projected LED source on the fundus.

The diaphragm 3, which is a pinhole, selects only the central part of the projected image on the fundus (Figure 30). Additionally, this pinhole reacts as a diffraction limited system and regardless the refraction error creates aberration free measurements (See 5.2.2).

The separation of these two paths was strongly dependent on the horizontal, vertical and especially axial alignment. In order to precisely control the alignment, two pupil cameras are used.

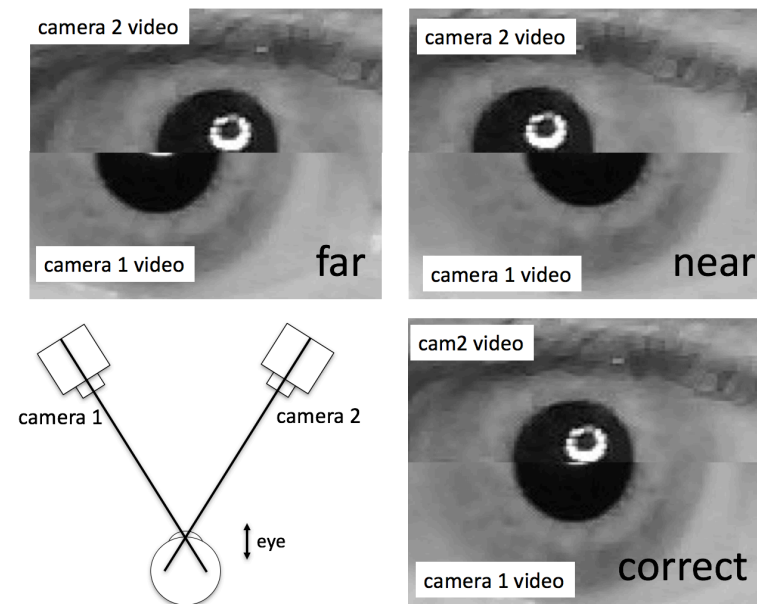


Figure 31 The use of the pupil cameras for alignment

Calibrated images of two pupil cameras are presented as a single image in the measurement screen (Figure 31). The transverse and axial alignment is performed by adjusting and matching the size of the upper and lower image of the pupil.

The data acquisition is made with a sampling frequency of 48 KHz from an analog port of USB6009 interface produced by the National Instruments.

As hardware system also contains a switch mode power supply, control board. The design and optimization of the control board also completed at the University of Crete. The control board contains a microcontroller and current limiters. This board synchronizes the press of the measurement button and the data acquisition interface. Thus, provides the safety limitation for the LED source while modulating two zones in different frequencies.

5.1.2 THE SOFTWARE

A graphical user interface (GUI) was developed on MATLAB platform. The software is capable of performing several tasks such as; image processing (for alignment), data analysis and calculation, patient management (keeping the patient database and measurements) and calibrations. All these abilities were programmed by us and have easy, separate GUI for the final user (8A4.1.1).

The measurement, data acquisition and analysis routines are performed as following; User clicks the measurement button on the main GUI. Patient GUI opens and the user enters the patient name and relative information. After completion of the patient details, the measurement GUI opens. The user clicks the start measurement button and image processing starts acquiring images from the pupil camera. The user aligns the system and presses the measurement button. The control board recognizes the input, starts the modulation of the LED source and data acquisition simultaneously for 300 ms. The GUI records the data signal. The recorded signal is an analog composition of the central ring and the peripheral annulus (Figure 33 – UP). The algorithm applies the Fast Fourier transform (FFT) for separating the magnitudes of two different signals.

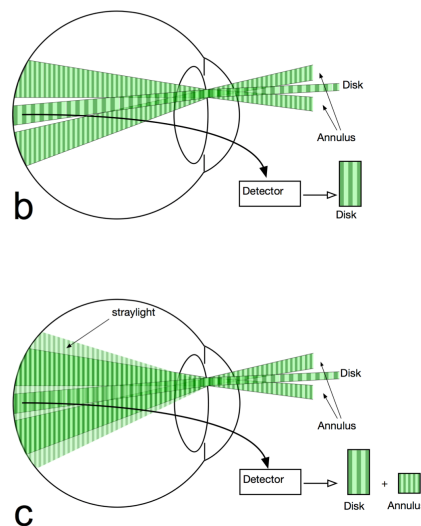


Figure 32 The effect of the scatter on measuring the central part of the fundus image

It is important to emphasize the effect of the scattering at this point. It is mentioned several times that the measurements are performed by the only central part of the fundus image. If

the measured system were a perfect optical system the FFT transform would reveal only one intensity which would belong to the central disk (Figure 32 - UP). However, the eye is not perfect optical system regarding the quality of the optical media the light scatters from the periphery to the center (Figure 32 - DOWN). Thus, when the FFT is applied to the measurement system, two peak points are observed on the relevant frequencies (Figure 33 – Down).

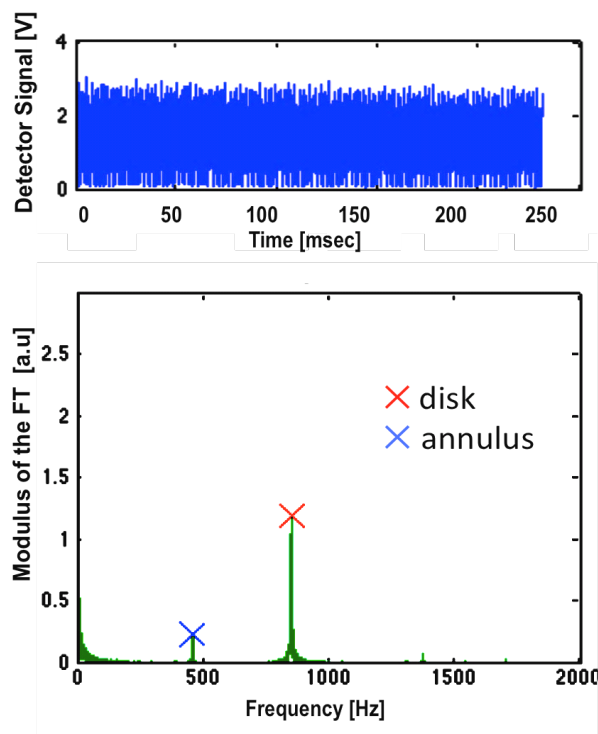


Figure 33 The analog signal (UP) and the signal after FFT is applied (DOWN)

The intensity of the central disk is used for determining the reflectance of the relative fundus and the intensity relation between the disk and fundus reveals the induced straylight in the measured eye. After the calculation is complete the calculated PSF value is presented in the system and the measurement is recorded in the database of the patient.

5.1.3 THE ANALYSIS

In the previous section, obtaining the measurement signal was described. For the calculation of the PSF, the FFT transform is applied to the signal which is detected form central part of the projected image at the fundus. The FFT transform separates the amplitudes of the signal,

which is the contribution of the disk and annulus and reveals the amplitude of the signals both disk (I_d) and the annulus (I_a) separately. If the central disk is considered as circularly symmetrical, the contribution of the central disk is given by;

$$(5) \quad I_d = I_o \int_0^{\theta_1} 2\pi\theta \text{PSF}(\theta) d\theta$$

Accordingly, the contribution of the scattered light from the annulus is as follows;

$$(6) \quad I_a = I_o \int_{\theta_1}^{\theta_2} 2\pi\theta \text{PSF}(\theta) d\theta$$

θ_1 Presents the diameter of the central disk and θ_2 present the maximum diameter of the annulus.

The calculation of the double pass PSF of an angular range contribution of an annulus, which was described in previous study [39], is as follows;

$$(7) \quad \text{PSF}_{dp} = \frac{1}{2\pi\theta_s} \frac{1}{\theta_2 - \theta_1} \frac{I_a}{I_a + I_d}$$

where $\theta_s = (\theta_2 - \theta_1)/2$.

The straylight is presented as follows;

$$(8) \quad S_{dp} = \theta_s^2 \text{PSF}_{dp}$$

The estimated straylight from double pass straylight parameter is presented as;

$$(9) \quad S = \frac{S_{dp}}{2}$$

The equation (7) normalize the measured intensities of the annulus and the disk. The calculation of the PSF depends on the relative contribution of the geometry of the source. Thus, intensities which are calculated from the disk and annulus can directly be used.

This methodology of PSF calculation of the contribution of the annulus increases the dynamic range and the measured signals become the same order of the magnitude [43] at an

angle of 5,5 degrees. Beside the theoretical calculations described above, the measurements are not performed from an infinitesimally small area. Furthermore, calculation of finite differences in eq (7) requires derivative approximation for the exact calculation of the PSF. Instead of processing calculation and approximations in every measurement, a lookup table is created which reveals the PSF by using the relation between the magnitude of signals which are I_a and I_d .

An artificial eye with a glass lens, which is assumed to has no straylight, is used to perform the calibration. Any background signals and straylight existed in the system is removed from the measurements of the human eye.

5.2 THE PROOF OF CONCEPT AND PUBLICATIONS

The system had 3 versions during the production and optimization period (8). The repeatability, consistency, and functionality were tested under several conditions. Furthermore, correlation studies were also performed with previously accepted methods. We made three publications of the system. The first paper was published in “Biomedical optics express” with the title “Compact optical integration instrument to measure intraocular straylight” [43]. The second paper was published in “SPIE BiOS. International Society for Optics and Photonics” with the title “Fast optical measurement of intraocular straylight” [44]. The third paper was published in “Journal of Refractive Surgery” with the title “Optical measurement of straylight in eyes with cataract” [42]. Furthermore, outcomes of the project were also presented at three ARVO meetings in the poster sections [45]–[47]. This section will give detailed information and results for the publications mentioned above.

5.2.1 STUDY I - ARTIFICIAL EYE AND LENSES WITH MICROSPHERES

The first study on the proof and concept and constancy evaluations were performed on an artificial eye (Figure 34 - LEFT). The artificial eye consisted of an artificial cornea (Figure 34 – MIDDLE, from a glass lens) and artificial retina (Figure 34 - LEFT).

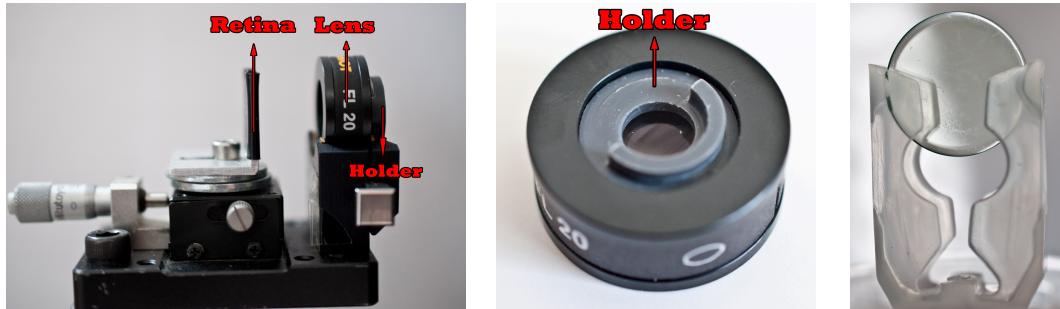


Figure 34 Artificial eye (LEFT) the artificial eye (MIDDLE) and special lens with microspheres (RIGHT)

Menicon developed hard contact lenses which contain microspheres for inducing additional straylight. There are 5 different version of the Menicon lenses which contain microspheres with different size and density. The induces straylight is induced from 1 to 5 where the 5 induce highest straylight into the system. These lenses were previously documented in previous studies for measurement of straylight [28], [39].

The measurements were performed with the 1st generation of the system (8A1). In this version, the light source of the system contained 4 different zones which corresponded to 0.42, 1.83, 4.23 and 9.65 degrees of visual angle on the retina. First measurements were made only with the artificial eye. The second set were performed with the artificial eye and the Lens 3 which was placed in a holder in front of the cornea. The last set of measurements were performed on the artificial eye and the Lens 5.

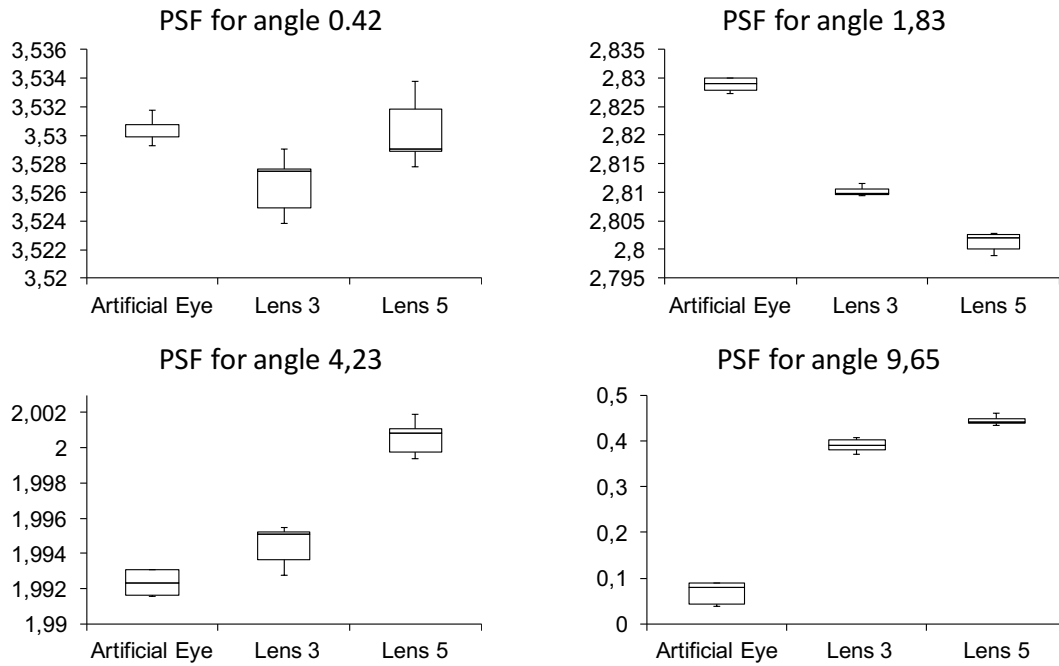


Figure 35 Straylight measurements of artificial eye and lenses with microspheres for different angles

The measurement revealed that the system was capable of detection of 0.1 log units of the straylight parameter for any visual angle (Figure 35). With this study, the first proof of concept was completed with an artificial eye. Moreover, outcomes of this study were presented as a poster presentation in the Association for Research in Vision and Ophthalmology (ARVO) annual meeting 2012, Fort Lauderdale, USA. Furthermore, indexed in Investigative Ophthalmology & Visual Science (IOVS) [45].

5.2.2 STUDY II – EFFECT OF THE DEFOCUS ON THE ARTIFICIAL EYE AND THE PILOT MEASUREMENTS OF AN HUMAN EYE

In the section 5.1.1 we stated that the design of diaphragms allows the system to minimize the influence of the defocus on the straylight measurements. For this purpose, we prepared the optical system and for testing the effect of the defocus the artificial eye was used. The artificial eye was fixed in front of the system, which eliminated the effect of alignment, and measurements were collected by changing the position of the retina. This was corresponding inducing myopia or hyperopia. Additionally, the repeatability and the effect of axial alignment of the pupil camera was tested by taking 10 measurements from the different axial positions from an eye of a subject.

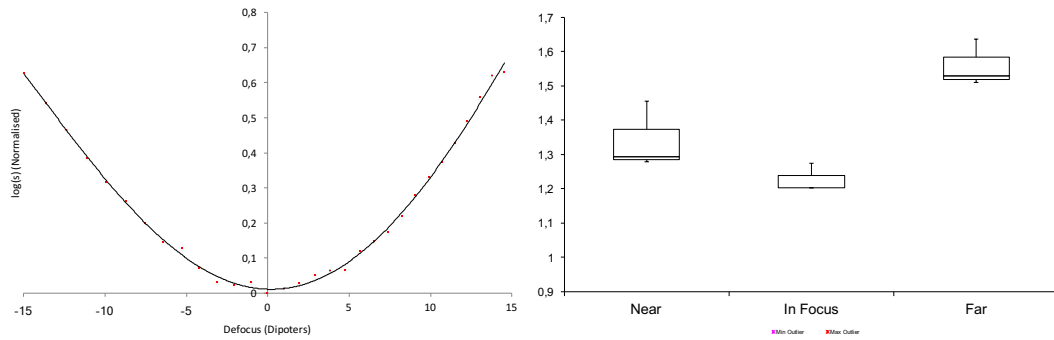


Figure 36 The defocus curve (LEFT) and straylight measurements of a healthy eye with different alignments (RIGHT)

The outcomes showed that the effect of Refractive errors which were lower than $\pm 5D$ were negligible (Figure 36 - LEFT).

Furthermore, the pilot measurements on human eyes revealed the importance of the alignment. The significant measurement error observed for in the measurement for both near and far. Consecutive measurements were taken from a healthy eye which was axially aligned in far, focus and near (Figure 36 – RIGHT). The importance and necessity of the dual camera system was demonstrated on human eyes. This study was presented as a poster presentation at the ARVO annual meeting 2013, Seattle, USA. Furthermore, indexed in IOVS [46].

5.2.3 STUDY III – HEALTHY HUMAN EYES AND DIFFUSERS

The previous study presented in section 5.2.2 tested the repeatability of measurements of the human eye. The purpose of this study was evaluating the change on the scattering difference by adding previously documented [40] diffusing filters which are produced by Tiffen company. Thus, the sensitivity and accuracy is aimed to be tested.

Four different filters, which induce different amounts of scattering in the system is placed as close as possible to the eye of subjects, for the simulation of the cataract. 10 eyes of 10 young healthy subjects, which has no pathology, were measured.

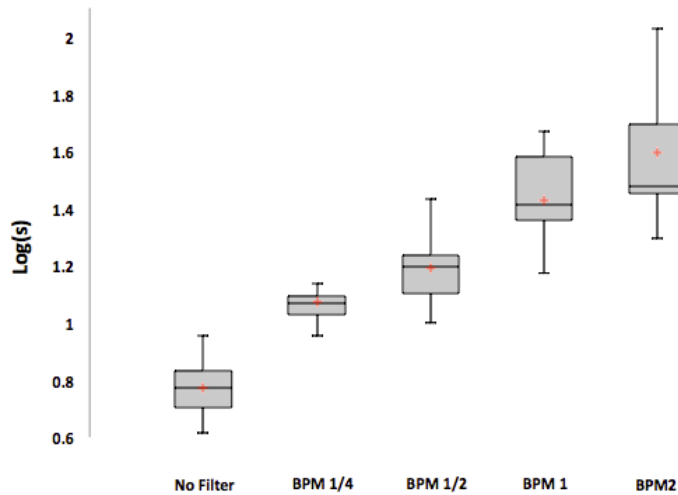


Figure 37 Straylight measurement with human eyes and diffusing filters

Outcomes of these study showed the clear difference between different amount of straylight between different scatterers. The results showed that the system is capable of detecting different amounts of straylight on human eyes. Thus, we proved that the new method is suitable for clinical practice for evaluating the patients with induced straylight. The work was published in Biomedical Optics Express, 2014 [43].

5.2.4 STUDY IV - OPTICAL AND PSYCHOPHYSICAL MEASUREMENTS COMPARISON CLINICAL STUDY I

Previous studies proved that the developed system is sensitive, repeatable and ready for clinical trials within the patient groups. The first clinical study was enrolled with institutional board approval in University Hospital of Heraklion, Crete. The aim of the study was evaluating the straylight measurements with prospective cataract patients.

This study enrolled 64 eyes of 39 patients. The crystalline lens of 13 eyes were already replaced with IOLs. The measurement routine consisted 3 steps; the first is subjective grading of patients' cataract according to the LOCS III system by an ophthalmic surgeon. In the secondary step, psychophysical measurement of straylight was performed. Finally, the straylight measurements of patients were obtained with the developed optical device.

	Healthy Subjects		Cataract Patients		IOL			
	Psychophysical	Optical	Psychophysical	Optical	Psychophysical	Optical		
Min	0,63	0,51	Min	1,00	0,64	Min	0,70	0,53
Max	1,40	1,12	Max	2,25	2,36	Max	1,82	1,57
Mean	0,89	0,71	Mean	1,52	1,39	Mean	1,27	0,85
Std	0,19	0,16	Std	0,28	0,42	Std	0,40	0,27

*Units of log(s)

Figure 38 Outcomes of the optical and psychophysical measurements of the study

The outcomes (Table 2) showed an average value of log(S) 0.88 for healthy and 1.52 for cataract for psychophysical measurements. Relatively an average of log(s) 0.70 for healthy and 1.39 for cataract patients were measured from the optical measurements.

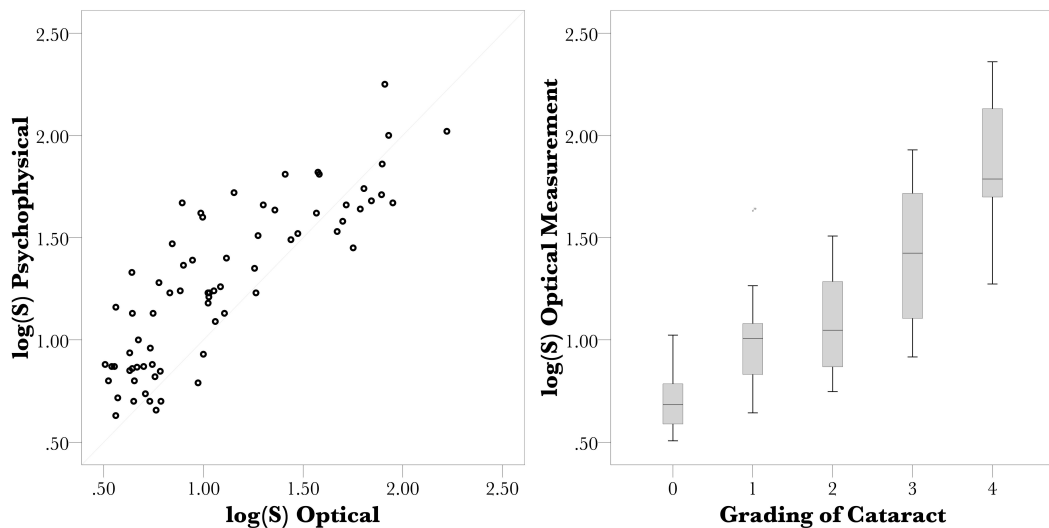


Figure 39 Correlation between psychophysical and optical measurements (LEFT) and Straylight measurements with LOCS III gradings of cataract (RIGHT)

The measurements of the optical measurements showed a low variance coefficient of 0,015. The statistical analysis revealed that the correlation between psychophysical and optical measurement was %84,4 (Pearson's $r = 0.844$ with significance level 0.01 "2-tailed",

Figure 39 – LEFT).

One of the significant outcomes of this study is presented in the Figure 39 – RIGHT. Although the optical measurement showed high correlation with the optical measurement, LOCS III gradings of the cataract patients showed high distribution. As mentioned in the previous chapters, the LOCS III grading is performed by the backscattered light. Thus, these

outcomes state that the backscattered light does not always correlate with the forward scatter. Furthermore, this subjective grading has much less sensitivity than the developed device.

It is important to state that; the optical measurement of the patients and the subjects were performed in all eyes. However, 16 patients could not cooperate and finish the psychophysical measurements (%41). This is presented as an important outcome of this study.

The study was presented as a poster presentation and was also presented in the exhibition in the ARVO annual meeting 2014 (indexed in IOVS) [47]. The study was published in SPIE BiOS, 2015 [44].

5.2.5 STUDY IV - OPTICAL AND PSYCHOPHYSICAL MEASUREMENTS COMPARISON CLINICAL STUDY II

The second clinical study was enrolled with institutional board approval in Hospital Virgen de la Arrixaca of Murcia. The aim of the study was evaluating the straylight measurements with prospective cataract patients in another clinical setting and validate the previous studies. In addition to the first comparison study, dilated measurements were also taken from the patients for observing any difference between.

	AGE		
	min	mean	max
<u>Healthy Subjects (9)</u>	28	34.6	45
<u>Cataract Patients (44)</u>	55	62.9	72

Table 3 Age distribution of the healthy subjects and the cataract patients

44 randomly recruited cataract patients and 9 young healthy subjects were enrolled in this study (Table 3). Only one eye of the subject and patients were used although, the measurements were performed for both eyes.

The measurement routine consisted 4 steps; subjective grading of patients' cataract according to the LOCS III system by an ophthalmic surgeon. In the secondary step, psychophysical measurement of straylight was performed. In the third step, the straylight

measurements of patients were obtained with the developed optical device. In the final step, patients and subjects were dilated and optical and psychophysical measurements were repeated.

The mean value for the straylight parameter was $1,34 \pm 0,29$ for the non-dilated eyes and $1,28 \pm 0,27$ for the dilated eyes. The optical measurement between dilated and non-dilated eyes showed a significant difference of $0.061 \log(S)$ ($P=0,004$) and correlation of two measurement set was $\%87,9$ ($P<0,001$). Although the difference was statistically significant, the difference was not clinically significant. Thus, thus further analyses were performed with non-dilated optical measurements.

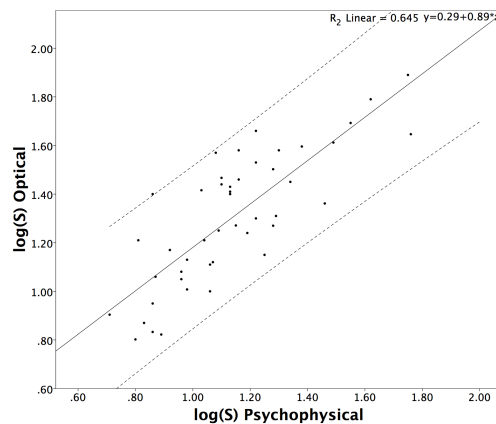


Figure 40 Correlation graph of optical and psychophysical measurements

The measurement sets of the optical and psychophysical measurements showed $\%80,3$ ($p<0,001$) correlation (Figure 40). Furthermore, the psychophysical measurement (mean: $1,14 \pm 0,240$) and optical measurement (mean: $1,30 \pm 0,27$) showed $0,17 \pm 0,16 \log(s)$ statistical significant difference ($P<0,001$). In addition to this outcome, Bland-Altman analysis also confirmed that the bias was significant (Figure 41).

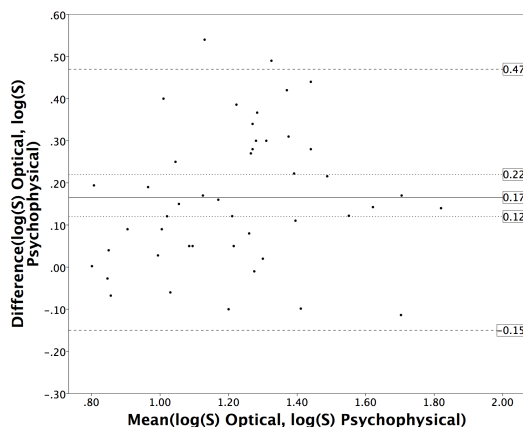


Figure 41 Bland-Altman plot

The final analysis of optical measurements was performed between different groups of cataract gradings. The Bonferroni correction revealed significant differences between all groups ($P < 0.004$).

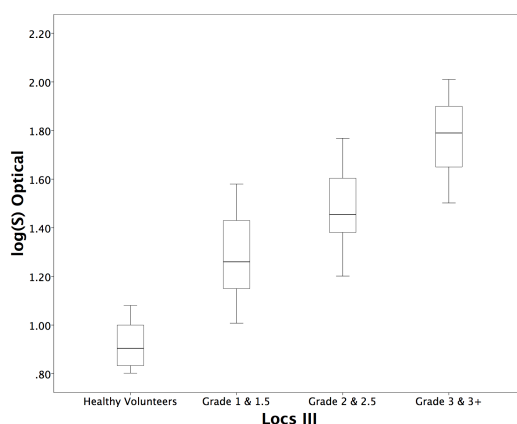


Figure 42 Straylight parameter values within different cataract groups and healthy subjects

The outcomes of both clinical studies showed parallel results. In addition to the first clinical study, 2 patients with a pupil diameter < 4 mm, could not be measured with optical method and the number was 5 for the psychophysical measurements.

Furthermore, for the significant difference between two straylight measurements, we stated that “it is possible that the optical measurement overestimates the severity of straylight when compared to other measurements involving wider pupils, such as the psychophysical measurement that was performed in a generally wider natural pupil. Moreover, it must be kept in mind that although the two instruments report the same quantity (the straylight

parameter), they arrive at its value using different methods and assumptions. The Sigma instrument analyses scattering in the optics of the eye to estimate the straylight parameter, whereas the C-Quant straylight meter uses a psychophysical task to estimate a visual value”.

The study was published in Journal of Refractive Surgery, 2016 [42].

6 CONCLUSION

In this thesis, a novel optical device for measuring forward intraocular scattering with double pass method is developed and results are shown.

		C-Quant	OQAS	DP System for Wide-Angle PSF	Sigma
Practicality	Fast Measurements	X	X	X	✓
	Do not Require Feedback	X	✓	✓	✓
	Compact Design	✓	✓	X	✓
	Do not Require Dilation	✓	✓	X	✓
Robustness	Measure Wide-Angle PSF	✓	X	✓	✓
	Sensitive Measurements	✓	X	✓	✓

Figure 43 Advantages and disadvantages of previous systems for measuring intraocular scattering and Sigma

Currently the most accepted method of measurement of the intraocular straylight is the psychophysical method. However, as explained before the psychophysical measurement has two important disadvantages; the requirement of the feedback of the patients (an elderly population) and the measurement time. The motivation for creating a method of optical measurement for straylight is eliminate the dependency on the patient feedback. Here, Sigma and other optical methods described can meet this purpose. On the other hand, OQAS was not capable of the wide-angle measurements of the PSF and the system was very sensitive of the effect of defocus and aberrations.

The DP system for measuring the wide angle PSF can overcome disadvantages of previous systems (Figure 43). It did not require patients' responses and could measure the wide-angle PSF. However, it was bulky, time demanding, requiring mouth piece for alignment and

pupils of the patients were needed to be dilated for the measurements. Here, our proposed prototype is deficiency-free unlike previous systems. With our novel methodology, Sigma device has following advantages;

- Measurements are performed quickly (300 ms)
- Measurements do not require any feedback from the patients.
- Measurements do not require dilation of pupils (for pupils > 4 mm)
- Measurements are not affected by defocus
- Measurements give relative information of wide-angle PSF
- Higher sensitivity which is capable of detecting difference even young subjects
- Compact design.

Besides advantages describe above, the Sigma has some limitations as well. For example, Sigma is not capable of measuring patients with pupil size which is smaller than 4 mm. Sigma's illumination and measurement path on the cornea plane is only designed for the best dimension and performance ratio practices. To do that, different diaphragm dimensions and designs were tested optimum one is chosen. Since 4mm design parameter is used, smaller dimensions are considered as limitation for the system.

Another important limitation is the measurements of the patients whose cataracts have non-uniform distribution of transparency, may not contain the exact straylight parameter.

At this point it is important to state that, neither Sigma nor previous systems are capable of defining the exact source of the induced straylight in the human eye. All systems give a cumulative value for the measurement of intraocular straylight. Measurements of the intraocular straylight will create a broader knowledge. Thus, Clinicians will approach patients with more caution for patients with induced straylight.

In this thesis, we concluded that 4mm in diameter of pupil size is optimum. Thus, it must be preserved for the future versions to provide consistency and repeatability of Sigma. As future

work, Sigma can be improved for measuring the straylight for non-uniform cataract types. The improvement includes two circular motors attached to the diaphragms which controls the areas to be measured on the pupil plane. So that, patients can be measured more than one time (number of measurements X 300 ms) and an average, the min and the max amount of straylight can be calculated. For cataract types such as nuclear cataract, the outcomes of the measurements will be identical with the current system. However, the measurements will create more relevant information for cataract types which do not have uniform distribution.

The development of Sigma has an impact on cataract and refractive clinical routines and related scientific works. This system can achieve a stable platform for evaluation of the straylight. For an example, the induced halos around the car lights after refractive surgery is one of the most common complains postoperatively. We are aiming to enroll studies for comparison of pre/postoperative straylight values for different refractive surgeries. Moreover, we also aim to evaluate and identify reasons for the complains of induced straylight for such patients.

Cataract clinic is another pin point of this research theme. Our methodology has promising results to sensitively measure the straylight. This will give the opportunity for the clinicians to evaluate early cataracts which are not possible to observe with the slitlamp. Furthermore, we are expecting to replace the subjective grading systems and become a clinical routine, such as biometry, for the cataract patients who will undergo the cataract surgery.

In final words, the development of such device gives advancement for the clinical routine beyond the aberrations and reflections. Besides the subjective methods of grading cataract, this method gives fast, relevant, sensitive and significant information for the optical effects of the cataract. This device could be a step forward in the clinical routine and helps clinicians for the objective evolution of the material properties of the eye.



Figure 44 The developed compact system for optical measurements of forward scattering

We published three papers and we made three contributions to the ARVO congress. In addition to that, we also presented the compact device as an “exhibitor” in the annular ARVO 2014 meeting.

The device shows a high correlation with the previously accepted methods. The proof of concept, repeatability, functionality was tested either in test or clinical conditions, with various studies mentioned in the sections.

During three years several versions of the device developed in different sizes and technologies. The final version, shaped as a compact and user-friendly device. Furthermore, the device has been tested under clinical conditions of two different hospitals in two different countries. Currently, two systems are actively used. These devices are suitable for clinical routine and several other studies are being performed for understanding different effects of the straylight on the vision.

This work was supported by ITN OpAL (PITN-GA-2010-264605) and by European Research Council Advanced Grant ERC-2013-AdG-339228 (SEECAT) to P. Artal.

7 BIBLIOGRAPHY

- [1] A. K. Khurana, *Comprehensive ophthalmology*. New Age International, 2007.
- [2] J. V. Forrester, A. D. (Andrew D. Dick, P. G. McMenemy, F. (Pathologist) Roberts, and E. Pearlman, *The eye : basic sciences in practice*. 2005.
- [3] AAO, *Fundamentals and Principles of Ophthalmology*. American Academy of Ophthalmology, 2014.
- [4] P. Riordan-Eva, J. Whitcher, D. Vaughan, and T. Asbury, *Vaughan & Asbury's general ophthalmology*. Lange Medical Books/McGraw-Hill Medical Pub. Division, 2008.
- [5] A. K. O. Denniston and P. I. Murray, *Oxford handbook of ophthalmology*. 2014.
- [6] M. J. Hogan, J. A. Alvarado, and J. E. Wedell, *Histology of the Human Eye*. 1971.
- [7] D. B. Goldberg, "Computer-animated model of accommodation and theory of reciprocal zonular action.," *Clin. Ophthalmol.*, vol. 5, no. 1, pp. 1559–66, 2011.
- [8] R. G. Kessel and R. H. Kardon, *Tissues and organs : a text-atlas of scanning electron microscopy*. W.H. Freeman, 1979.
- [9] D. J. D'Amico, "Diseases of the Retina," *N. Engl. J. Med.*, vol. 331, no. 2, pp. 95–106, Jul. 1994.
- [10] M. Bass and Optical Society of America., *Handbook of optics II*. McGraw-Hill, 1995.
- [11] L. D. Kirkpatrick and G. F. Wheeler, *Physics : a world view*. Saunders College Pub, 1992.

- [12] D. H. Marimont and B. A. Wandell, “Matching color images: the effects of axial chromatic aberration,” *J. Opt. Soc. Am. A*, vol. 11, no. 12, p. 3113, 1994.
- [13] B. Kruger and R. Aggarwala, “Chromatic Aberration Fincham Revisited and Ocular Focus ;,” vol. 33, 1993.
- [14] H. HARTRIDGE, “The chromatic aberration of the human eye and its physiological correction.,” *Experientia*, vol. 6, no. 1, pp. 1–10, Jan. 1950.
- [15] S. Winter, R. Sabesan, P. Tiruveedhula, C. Privitera, P. Unsbo, L. Lundström, and A. Roorda, “Transverse chromatic aberration across the visual field of the human eye.,” *J. Vis.*, vol. 16, no. 14, p. 9, 2016.
- [16] A. C. Gómez, A. Verdejo, C. P. Bautista, A. E. Ferrándiz, D. C. González, and S. C. Burgos, “Principles and Clinical Applications of Ray-Tracing aberrometry (Part I),” *J. Emmetropia*, vol. 3, no. Part I, pp. 96–110, 2012.
- [17] D. Atchison and G. Smith, *Optics of the Human Eye*. Butterworth-Heinemann, 2000.
- [18] T. J. van den Berg, “Analysis of intraocular straylight, especially in relation to age.,” *Optom. Vis. Sci.*, vol. 72, no. 2, pp. 52–9, Feb. 1995.
- [19] L. Holladay, “Action of a light-source in the field of view in lowering visibility,” *JOSA*, vol. 14, pp. 1–15, 1927.
- [20] J. J. Vos, “Reflections on glare,” *Light. Res. Technol.*, vol. 35, no. 2, pp. 163–176, Jun. 2003.
- [21] W. S. Stiles, “The Effect of Glare on the Brightness Difference Threshold,” *Proc. R. Soc. London B Biol. Sci.*, vol. 104, no. 731, 1929.
- [22] H. S. Ginis, G. M. Perez, J. M. Bueno, A. Pennos, and P. Artal, “Wavelength dependence of the ocular straylight.,” *Invest. Ophthalmol. Vis. Sci.*, vol. 54, no. 5, pp. 3702–8, May 2013.

- [23] L. Spadea, G. Maraone, F. Verboschi, E. M. Vingolo, and D. Tognetto, “Effect of corneal light scatter on vision: a review of the literature.,” *Int. J. Ophthalmol.*, vol. 9, no. 3, pp. 459–64, 2016.
- [24] J. V Jester, T. Moller-Pedersen, J. Huang, C. M. Sax, W. T. Kays, H. D. Cavanagh, W. M. Petroll, and J. Piatigorsky, “The cellular basis of corneal transparency: evidence for ‘corneal crystallins,’” *J. Cell Sci.*, vol. 112 (Pt 5, pp. 613–622, 1999.
- [25] D. De Brouwere, H. Ginis, G. Kymionis, I. Naoumidi, and I. Pallikaris, “Forward scattering properties of corneal haze.,” *Optom. Vis. Sci.*, vol. 85, no. 9, pp. 843–8, Sep. 2008.
- [26] D. De Brouwere, H. Ginis, G. Kymionis, I. Naoumidi, and I. Pallikaris, “Forward scattering properties of corneal haze.,” *Optom. Vis. Sci.*, vol. 85, no. 9, pp. 843–8, Sep. 2008.
- [27] T. J. van den Berg, “Importance of pathological intraocular light scatter for visual disability.,” *Doc. Ophthalmol.*, vol. 61, no. 3–4, pp. 327–33, Jan. 1986.
- [28] L. Franssen, J. E. Coppens, and T. J. T. P. van den Berg, “Compensation comparison method for assessment of retinal straylight.,” *Invest. Ophthalmol. Vis. Sci.*, vol. 47, no. 2, pp. 768–76, Feb. 2006.
- [29] L. Franssen and J. E. Coppens, “Straylight at the retina: scattered papers,” University of Amsterdam, 2007.
- [30] N. A. Sparrow, N. A. Frost, E. P. Pantelides, and D. A. Laidlaw, “Decimalization of The Oxford Clinical Cataract Classification and Grading System.,” *Ophthalmic Epidemiol.*, vol. 7, no. 1, pp. 49–60, Mar. 2000.
- [31] a B. Hall, J. R. Thompson, J. S. Deane, and a R. Rosenthal, “LOCS III versus the Oxford Clinical Cataract Classification and Grading System for the assessment of nuclear, cortical and posterior subcapsular cataract.,” *Ophthalmic Epidemiol.*, vol. 4,

- no. 4, pp. 179–94, Dec. 1997.
- [32] B. Thylefors, L. T. Chylack, K. Konyama, K. Sasaki, R. Sperduto, H. R. Taylor, S. West, and WHO Cataract Grading Group, “A simplified cataract grading system.,” *Ophthalmic Epidemiol.*, vol. 9, no. 2, pp. 83–95, Apr. 2002.
- [33] H. R. Taylor and S. K. West, “The clinical grading of lens opacities.,” *Aust. N. Z. J. Ophthalmol.*, vol. 17, no. 1, pp. 81–6, Feb. 1989.
- [34] J. K. Ijspeert, P. W. de Waard, T. J. van den Berg, and P. T. de Jong, “The intraocular straylight function in 129 healthy volunteers; dependence on angle, age and pigmentation.,” *Vision Res.*, vol. 30, no. 5, pp. 699–707, Jan. 1990.
- [35] T. J. T. P. van den Berg and L. J. van Rijn, “Relevance of Glare Sensitivity and Impairment of Visual Function Among European Drivers,” 2005.
- [36] J. J. Vos and T. van den Berg, “Disability glare a state of the art report,” 1999.
- [37] T. J. Van den Berg and J. K. Ijspeert, “Light scattering in donor lenses.,” *Vision Res.*, vol. 35, no. 1, pp. 169–77, Jan. 1995.
- [38] P. Artal, A. Benito, G. M. Pérez, E. Alcón, A. De Casas, J. Pujol, and J. M. Marín, “An objective scatter index based on double-pass retinal images of a point source to classify cataracts.,” *PLoS One*, vol. 6, no. 2, p. e16823, Jan. 2011.
- [39] H. Ginis, G. M. Pérez, J. M. Bueno, and P. Artal, “The wide-angle point spread function of the human eye reconstructed by a new optical method.,” *J. Vis.*, vol. 12, no. 3, pp. 1–10, Jan. 2012.
- [40] G. C. de Wit, L. Franssen, J. E. Coppens, and T. J. T. P. van den Berg, “Simulating the straylight effects of cataracts.,” *J. Cataract Refract. Surg.*, vol. 32, no. 2, pp. 294–300, Feb. 2006.
- [41] J. M. Bueno, D. De Brouwere, H. Ginis, I. Sgouros, and P. Artal, “Purkinje imaging

- system to measure anterior segment scattering in the human eye.,” *Opt. Lett.*, vol. 32, no. 23, pp. 3447–9, Dec. 2007.
- [42] O. Sahin, A. Pennos, H. Ginis, L. Hervella, E. A. Villegas, B. Cañizares, J. M. Marin, I. Pallikaris, and P. Artal, “Optical Measurement of Straylight in Eyes With Cataract,” *J. Refract. Surg.*, vol. 32, no. 12, pp. 846–850, Dec. 2016.
- [43] H. Ginis, O. Sahin, A. Pennos, and P. Artal, “Compact optical integration instrument to measure intraocular straylight.,” *Biomed. Opt. Express*, vol. 5, no. 9, pp. 3036–41, Sep. 2014.
- [44] H. Ginis, O. Sahin, and P. Artal, “Fast optical measurement of intraocular straylight.,” in *SPIE BiOS. International Society for Optics and Photonics*, 2015, vol. 9307, p. 93070R–93070R.
- [45] O. Sahin, H. S. Ginis, G. M. Perez, J. M. Bueno, and P. Artal, “Measuring Intraocular Scattering With Spatio-temporally Modulated Light,” *Invest. Ophthalmol. Vis. Sci.*, vol. 53, no. 14, pp. 3054–3054, 2012.
- [46] O. Sahin, H. Ginis, G. Perez, J. Bueno, and P. Artal, “A novel compact optical instrument for the clinical measurement of intraocular light scattering,” *Invest. Ophthalmol. Vis. Sci.*, vol. 54, no. 15, pp. 5545–5545, 2013.
- [47] O. Sahin, H. S. Ginis, M. K. Tsilimbaris, and P. Artal, “Clinical instrument for the optical measurement of straylight in the human eye,” *Invest. Ophthalmol. Vis. Sci.*, vol. 55, no. 13, pp. 2116–2116, 2014.

8 APPENDIX

A1 SYSTEM 1ST GENERATION

The first system was setup on an optical table. The measurements were performed with an algorithm which was developed in Labview. On the other hand, the data analysis and calculations were performed on MATLAB.

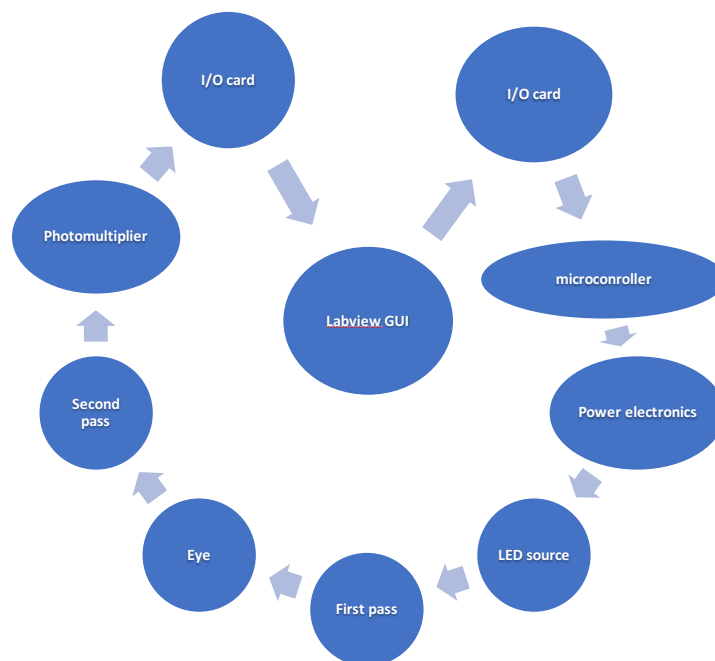


Figure 45 Measurement process

The measurement routine was as following (Figure 45); the user aligns the eye and press start button on Labview GUI. When the start button is pressed, Labview sends a digital output to PIC microprocessor via DAQ-USB6009 (data acquisition and measurement card). When PIC gets this digital input, shutter opens and a square wave at main frequency (1538 Hz) is created for 150 ms. When this simultaneous flickering finishes microprocessor creates

four frequencies (483 Hz, 769 Hz, 1077 Hz, 1791 Hz) for 150 ms. These outputs are used to drive FETs (16) to drive LED source. (This FETs and LEDs are protected by Limiter Circuits). The light passes through optics and reaches the eye. The backscattering also travels through the same optics and reaches to photomultiplier. The light is converted to electric signal and captured by DAQ card. Labview saves signal data to system.

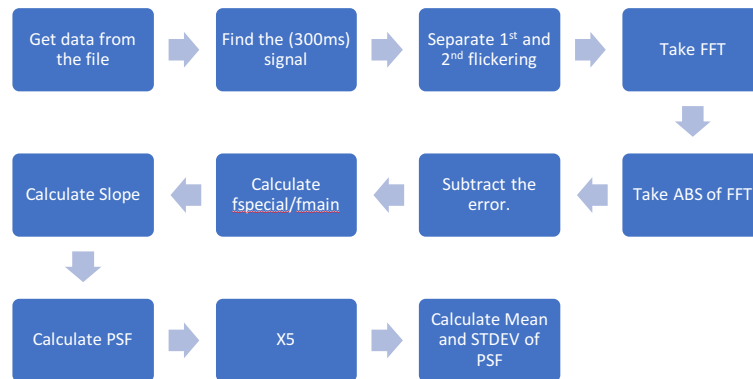


Figure 46 Analyzing process

For analyzing PSF (Figure 46) a MATLAB script is developed. The developed algorithm takes signal data, which labview saved before, from the file and finds 300ms signal. Separates it into two segments. After taking FFT of each signal algorithm subtracts error and calculates relative magnitude by making f_x/f_{main} . Then system calculates slope and then the PSF. Depending on user's preference algorithm can make this calculation for different measurements of same subject and calculate the mean and stdev of PSF.

A1.1 HARDWARE

A1.1.1 LIGHT SOURCE

Philips Lumiled LXML-PM01 1W LEDs (Figure 47) were used¹ for the light source. These LEDs are high power LEDs, which require 1A 3.4V and create up to 160lm light luminance. As a designing criterion it was decided to create LED sets. Each set has 8 LEDs (some sets have 7). In total there were 70 LEDs, which required 14A in 50V.

¹ <http://www.philipslumileds.com/products/luxeon-rebel/luxeon-rebel-color>

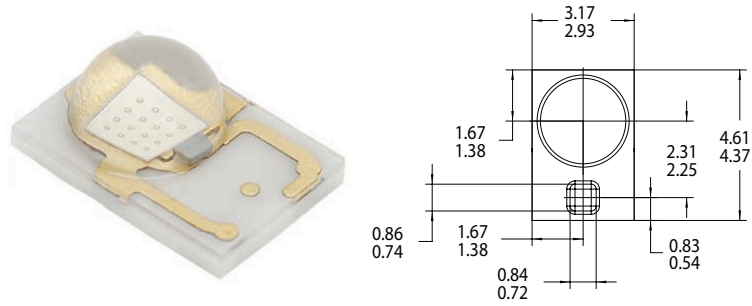


Figure 47 Used LEDs and Dimensions (mm/inch)

The light source contained 6 RINGS (Figure 48) divided into 4 different zones (Figure 49) by internal walls.

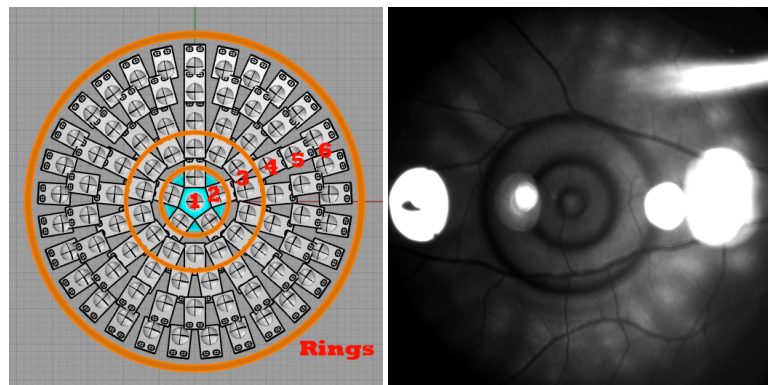


Figure 48 Rings

In Table 4 numbers of LEDs for each RING are presented.

	RING1	RING2	RING3	RING4	RING5	RING6
LEDs	1	5	14	16	23	30

Table 4 Number of LEDs on RINGS

The light source was separated into four zones, which represented different angles on retina. Each zone was flickering in different frequencies (Table 5). The aim was using the Fourier Transform and analyze and separate each signal.

	ZONE1	ZONE2	ZONE3	ZONE4
Diameter	3	10	20	50
Angle cor. on Retina	0.85°	0.85°-2.81°	2.81°-5.65°	5.65°-13.65°
Flickering Frequency	483 Hz	769Hz	1077Hz	1791Hz

Table 5 Detailed information of each zone in light source



Figure 49 Zones of the light source of the first generation

A1.1.2 OPTICS

The optical system (Figure 50) were consisted of two diaphragms, a 45-degree mirror two lenses for focusing the LED light source on the retina. And a photomultiplier with a pinhole were conjugated on the retina plane.

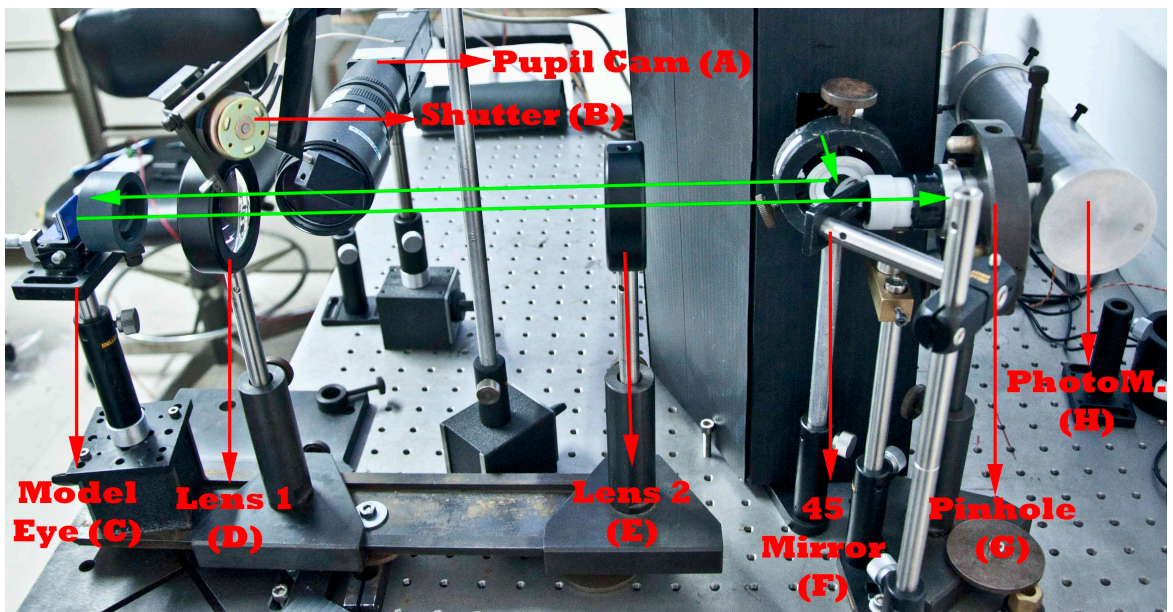


Figure 50 Optical System

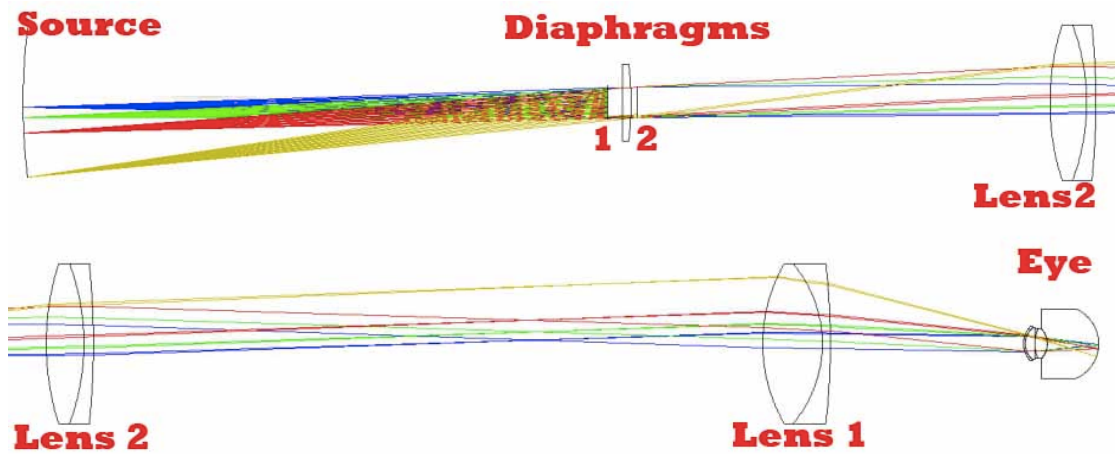


Figure 51 Optical System Zemax Simulation

The light which was created from LED source, passes through two diaphragms (Figure 52). It is reflected by a 45-degree mirror and passes from Lens1² and Lens2³ and projected on to the retina.

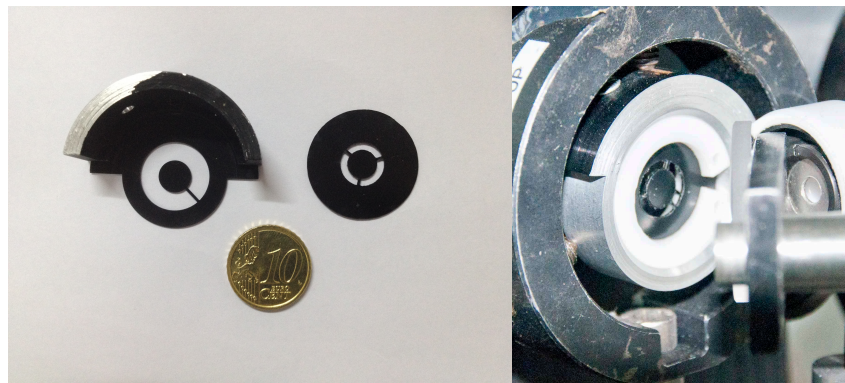


Figure 52 Diaphragms

The reflected light from retina passes from lens1 and lens2 and reaches to 45-degree mirror (Figure 53). This mirror has a hole in the center that enables system to carry back reflected light to the pinhole.

² <http://www.thorlabs.de/thorProduct.cfm?partNumber=AC508-075-C>

³ <http://www.thorlabs.de/thorproduct.cfm?partnumber=AC508-150-A>

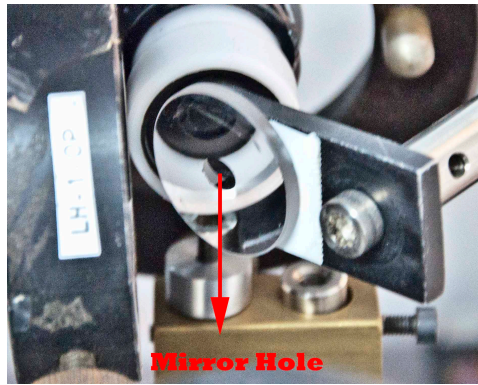


Figure 53 Mirror

A1.1.3 PHOTOMULTIPLIER

An Hamamatsu R928 photomultiplier⁴ (Figure 54) tube was used to measure backlight scattering in the system. The photomultiplier tube was placed in lightproof case and a pinhole (Figure 50 G), which was conjugated to the retinal plane, was located at the entrance of this case.



Figure 54 Photomultiplier Tube

A1.1.4 NI DAQ-6009 DATA ACQUISITION CARD

After conversion of the light signals into the electrical signals by the photomultiplier. A DAQ6009⁵ (Figure 55) National Instruments Data Acquisition card was used for capturing these analog signals. This card has 48kS/s maximum sampling rate. For our system, the sampling rate of this card was suitable for acquiring the signals, which were modulated between 0,5-1,5 KHz.

⁴ http://sales.hamamatsu.com/assets/pdf/parts_R/R928_R955_TPMS1001E07.pdf

⁵ <http://sine.ni.com/nips/cds/view/p/lang/en/nid/201987>



Figure 55 DataQ-6009 Data Acquisition Card

A1.2 ELECTRONICS

This system required many electronic components for driving LEDs safely. The system demanded a light with high currents with the voltage regulation. Normal day use limiters were not acceptable this project, due to inability to drive the system in regulated mode with required frequencies. Thus, a power source, a control board, a limiter board, an Illumination source and a microprocessor board is designed.

A1.2.1 POWER BOX

The system required 14A of current in max power. The first system had 4 signals for driving LED zones. Thus, 4 different transformers used for each zone in order to avoid crosstalk between the zones. The manufactured power box was capable of generating 16A-50V outputs with avoiding the crosstalk.

A1.2.2 CONTROL BOARD

There were many safety points was designed in order to avoid any dangerous effects of high current and voltage. A control board (Figure 56 fuse circuit) was designed to control any overflow current in case of any limiter boards malfunction.

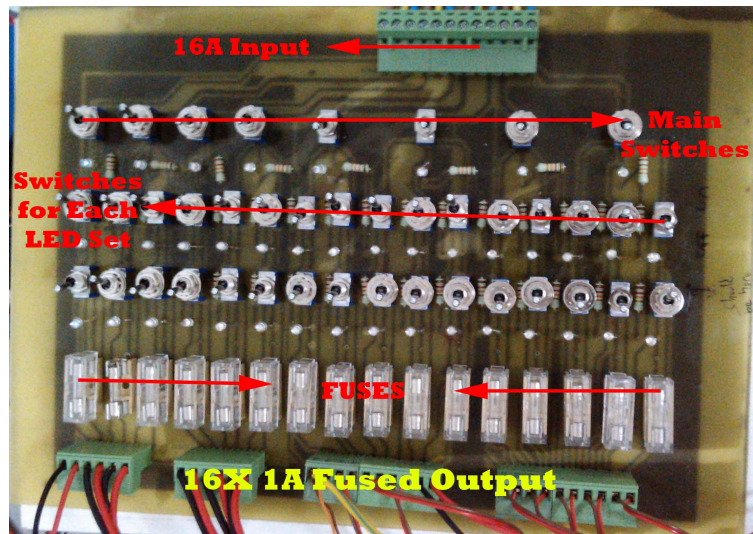


Figure 56 Control Board (Fuse Circuit)

This circuit created the ability of controlling each LED set. Each set could be switched on or off. Moreover, each set was fused (1A) for the control of the current.

A1.2.3 LIMITER CIRCUITS

Limiter circuits (Figure 57) had significant importance on controlling brightness and protection of LEDs. Each circuit consisted of 4 transistors, a sensing resistor and a potentiometer for adjusting the desired current.

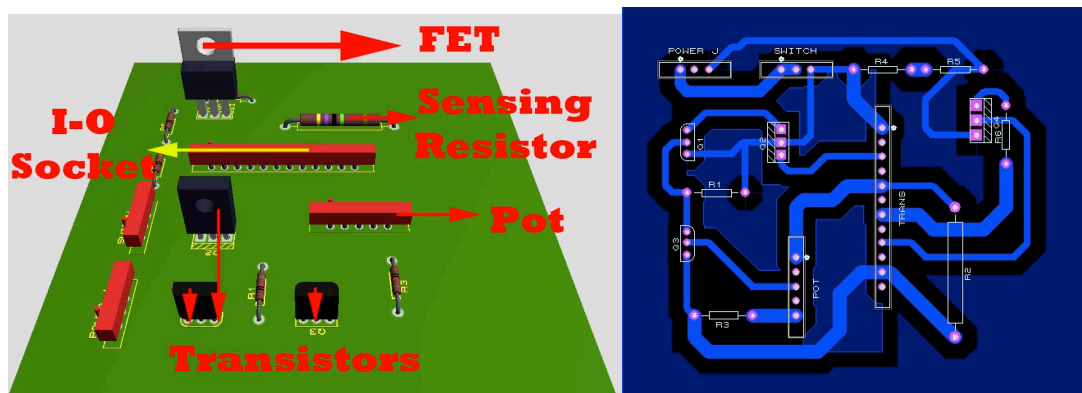


Figure 57 Limiter Circuit

There were 15 limiter circuit on the system, 14 were used to limit LED source and 1 were used for controlling IR illumination LEDs. The power was connected to limiter circuits and output of limiter was connected to LEDs. Anode of LED was connected to Power FET's Source. Signal is connected to FET's Gate and Drain is connected to ground. By this way the

system could create the modulation with the desired brightness and multiple protection mechanisms.

A1.2.4 PIC MICROPROCESSOR

In the system, a 16F877A⁶ microprocessor was used for creating 4 different for driving the LED source. The 16f877A has 20MHz clock frequency. When user aligns system, user presses the measurement button. This generates a digital output from NI DAQ card. When PIC gets this input, pic opens shutter with a digital out. Then it creates a main frequency for all 4-output ports, which drives each LED ZONE. (for 150ms). When first flickering is completed PIC generates the specific frequencies for each ZONE for 150ms. After this process completed PIC closes the shutter and waits for another input.

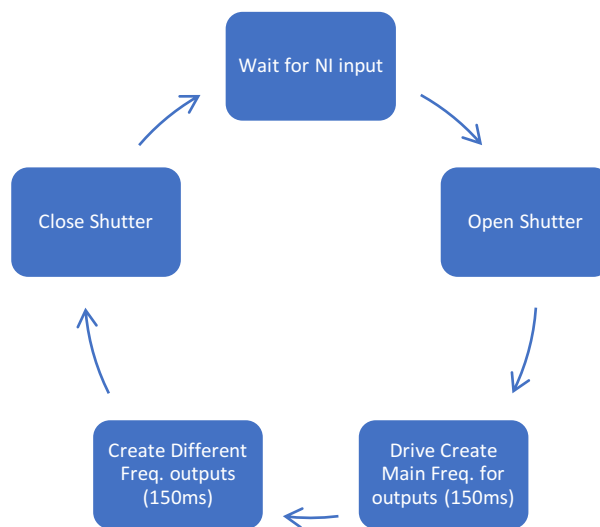


Figure 58 Working Flow of PIC Microprocessor

A1.3 SOFTWARE

The system required NI-Labview software for measurement, MatLab software for analyzing data. The future versions were built on MatLab.

⁶ <http://ww1.microchip.com/downloads/en/devicedoc/39582b.pdf>

A1.3.1 LABVIEW

For the measurement, a Labview GUI system was designed. Alignment can easily made by a pupil camera. User could define measurement details and take a measurement by pressing a button. Furthermore, user could immediately see the measured signal on the interface.

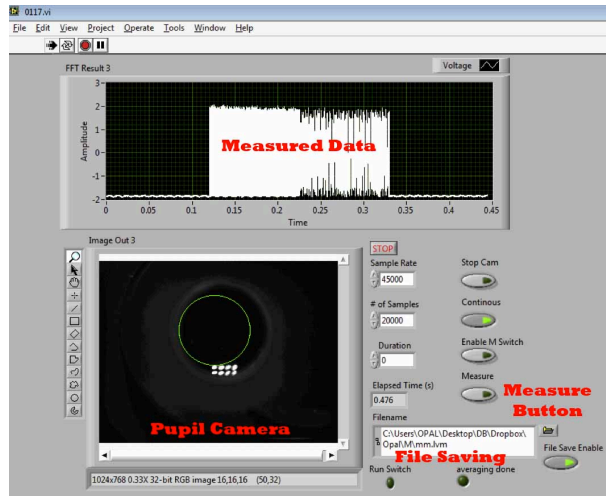


Figure 59 Labview GUI

A1.3.2 MATLAB

MatLab was used for analyzing the signal that was measured. The matlab script collects the measurement signal. Then an algorithm detects measurement signal. When the signal is detected, the algorithm separates first and second flickering (Figure 60).

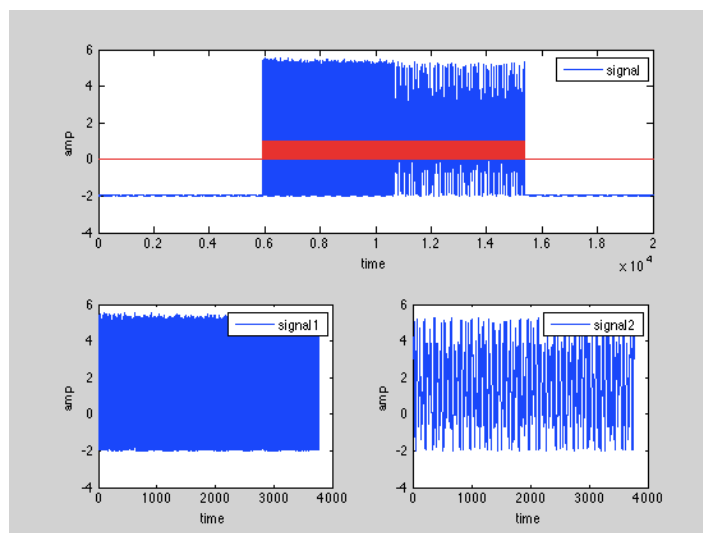


Figure 60 Signal Detection Output

Then FFT of each signal is applied. When the absolute of FFT results calculated, the script shows FFT results (Figure 61).

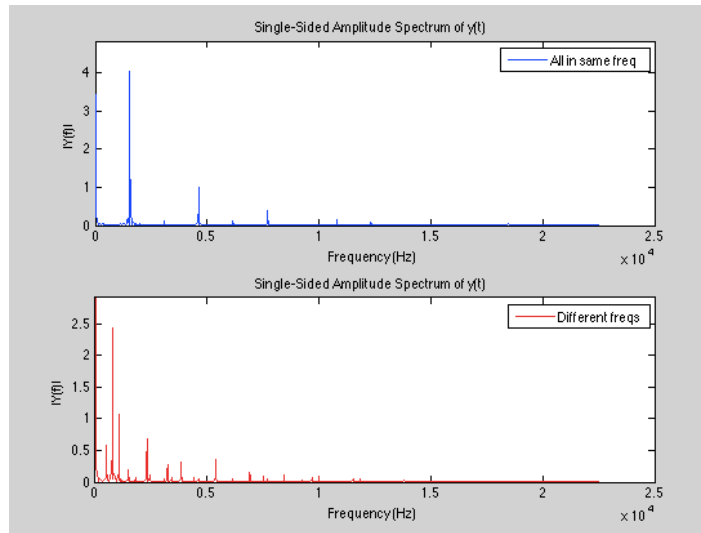


Figure 61 FFT Results Output

The PSF is calculated by analyzing these FFT results. The algorithm makes normalization by making by using the simultaneous flickering information and by calculating slope algorithm calculates PSF. The results are saved to a file. If there is more than one measurement were made, script can repeat itself and writes additional results to the file. The algorithm also calculates mean data and standard deviation for multiple measurements and plots results.

A2 SYSTEM 2ND GENERATION

The second generation of the system was designed on an optical breadboard as compact optical setup. The light source and electronics were replaced. Furthermore, dependency of Labview was eliminated and all functions were performed on the MATLAB platform.

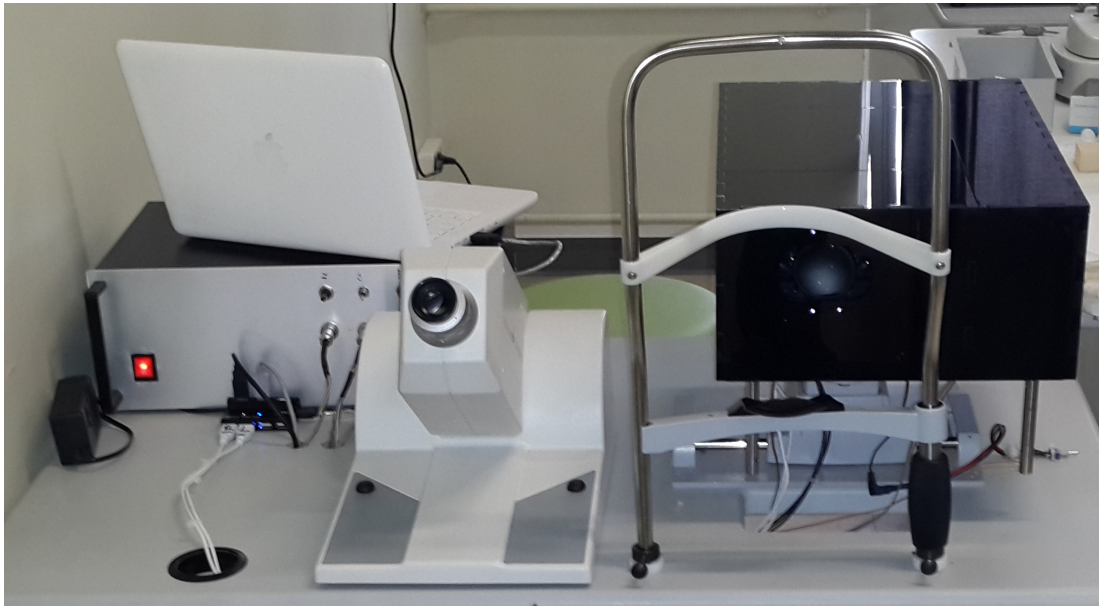


Figure 62 Clinical setup for psychophysical and optical measurements of intraocular straylight

A2.1 HARDWARE

A2.1.1 LIGHT SOURCE

The necessity of the big source was evaluated with the first system. It was decided to create a new source with two zones which contains 4 led in the central ring and 27 in periphery.

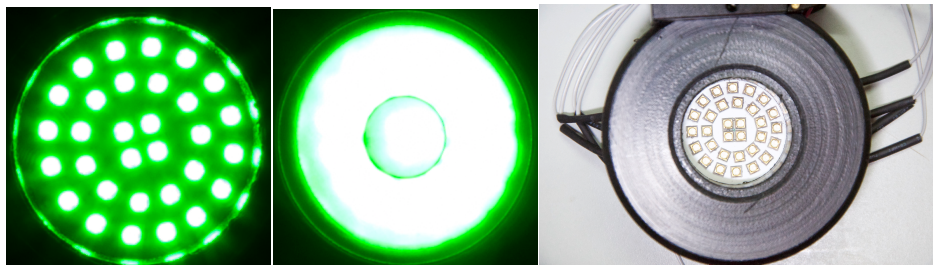


Figure 63 The light source of the 2nd generation system

A2.1.2 OPTICS

The although the optical path was the same, several additional optical elements were used for obtaining compact system.

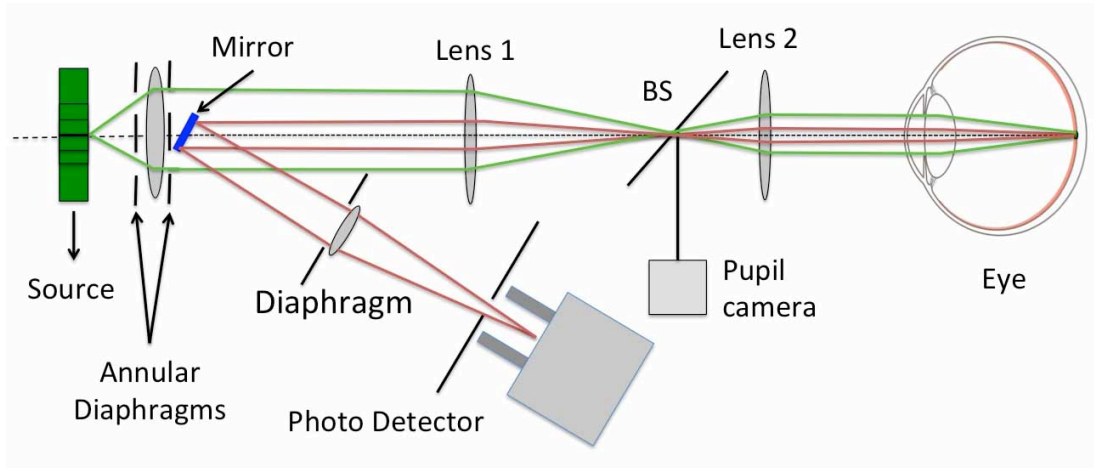


Figure 64 Schematic of the optical of the 2nd generation system

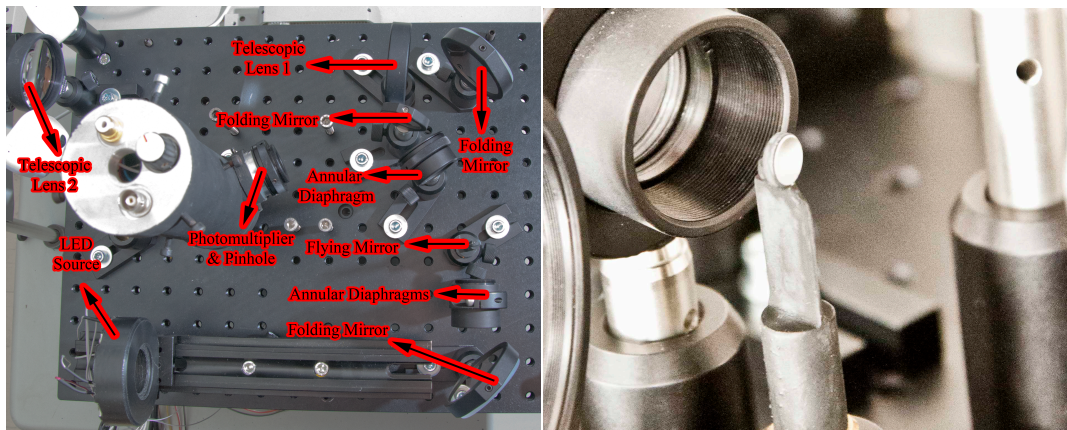


Figure 65 Optical setup of the 2nd generation system (LEFT) and the flying mirror (RIGHT)

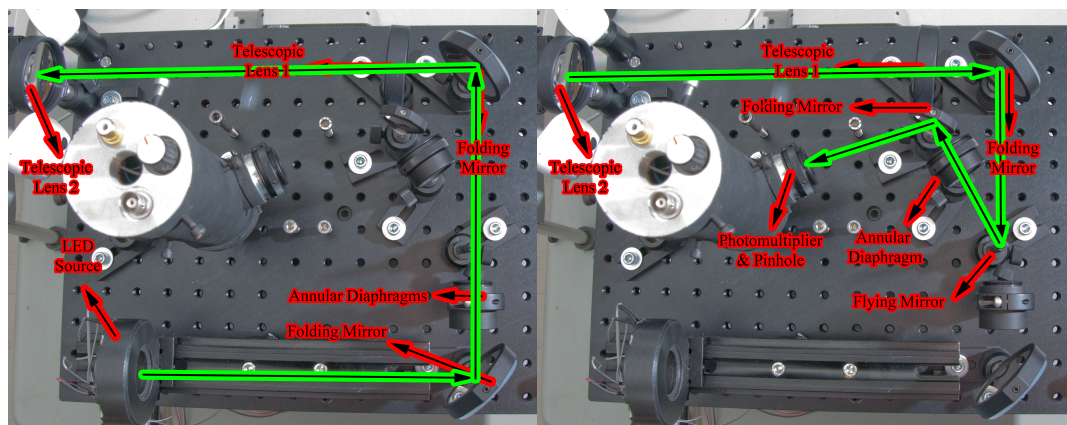


Figure 66 Illumination (LEFT) and measurement paths (RIGHT)

A2.2 ELECTRONICS

The power box and limiter were designed in a compact size due to lower dependency of the smaller light source. Thus, bulky transformers were replaced with SMPS and relatively, due to less number LED sets, less number of limiters were used.

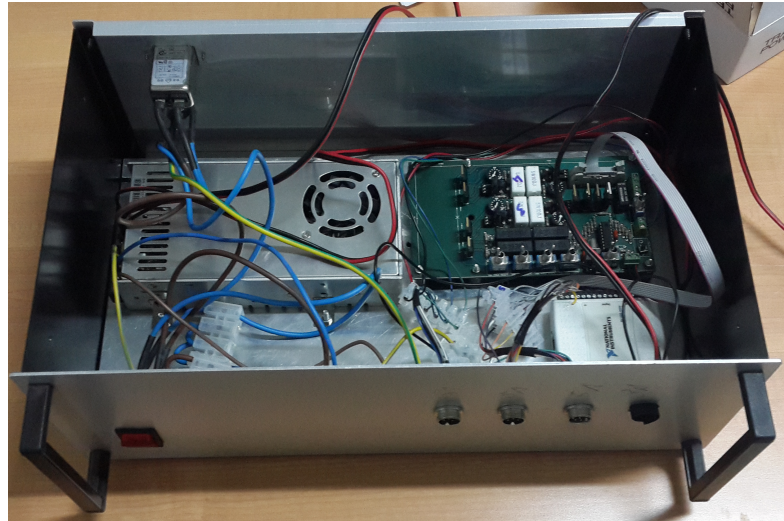


Figure 67 Electronic box of the 2nd generation system

A3 SYSTEM 3RD GENERATION (SIGMA)



Figure 68 The developed compact system for optical measurements of forward scattering

A3.1 HARDWARE

A3.1.1 OPTICS

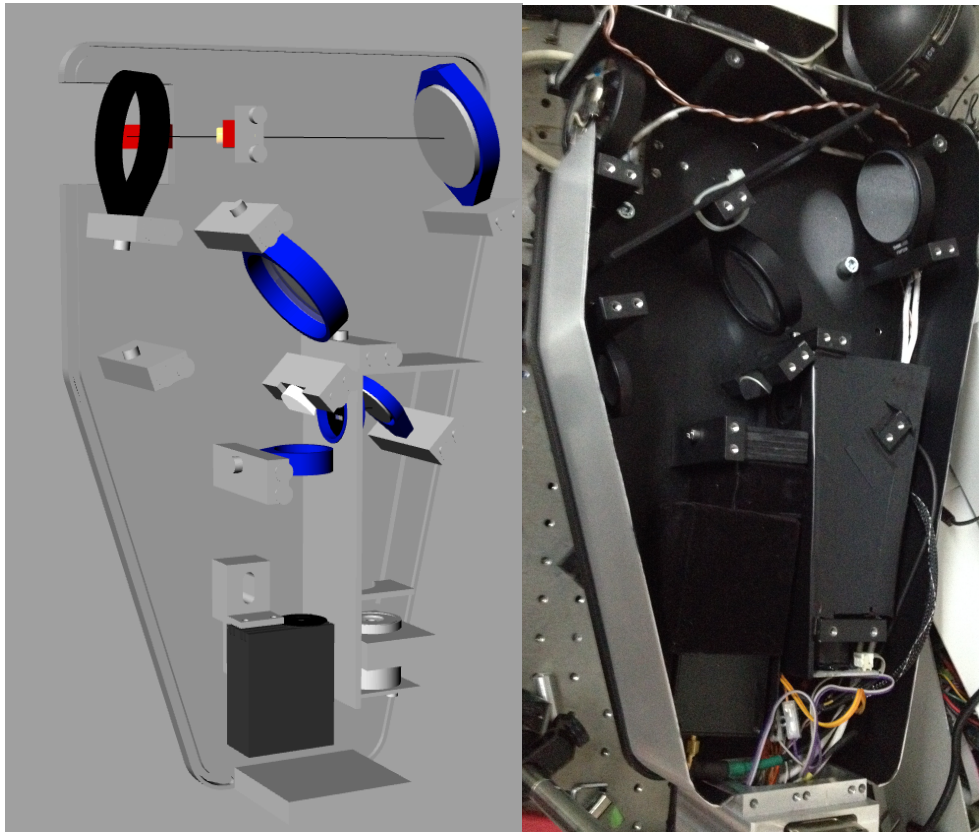


Figure 69 Optics of the Sigma

A3.2 ELECTRONICS

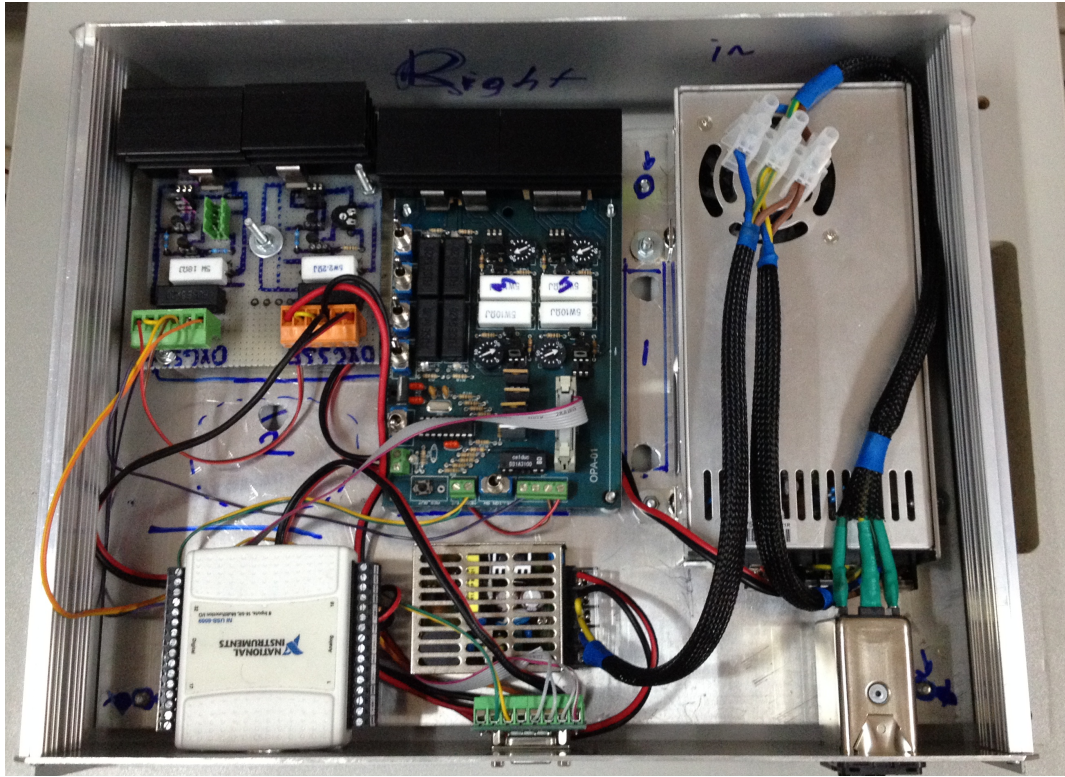


Figure 70 Hardware box of the Sigma

A4 FINAL CODES

A4.1 MATLAB

A4.1.1 GUI SCREENS

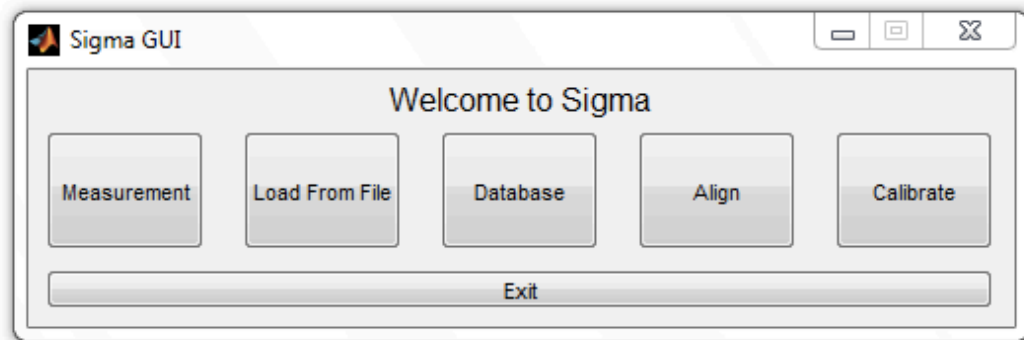


Figure 71 Main GUI of the Sigma

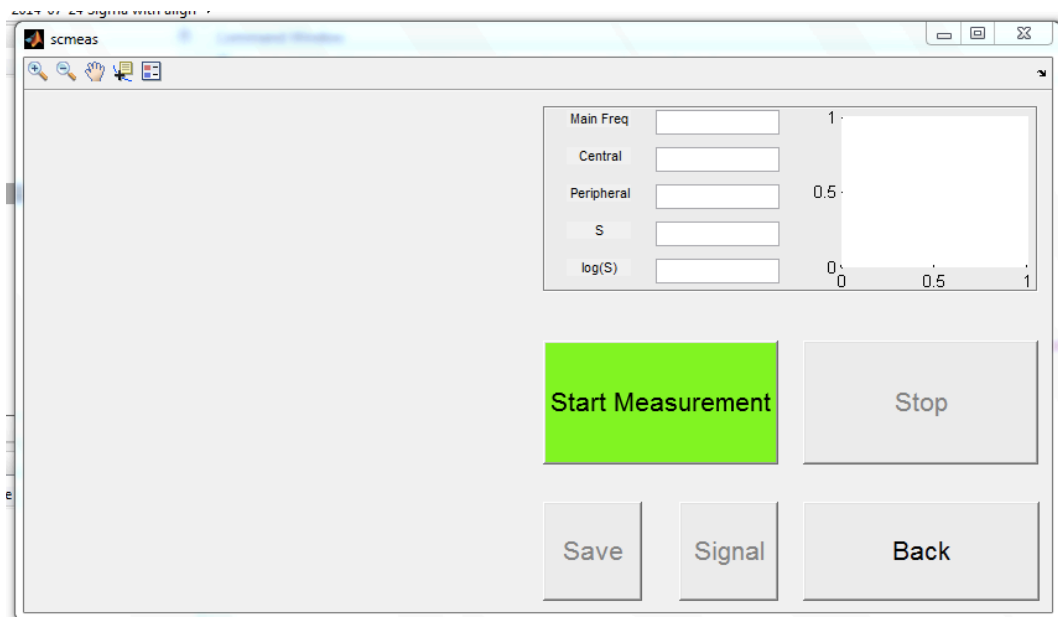


Figure 72 Measurement GUI of the Sigma

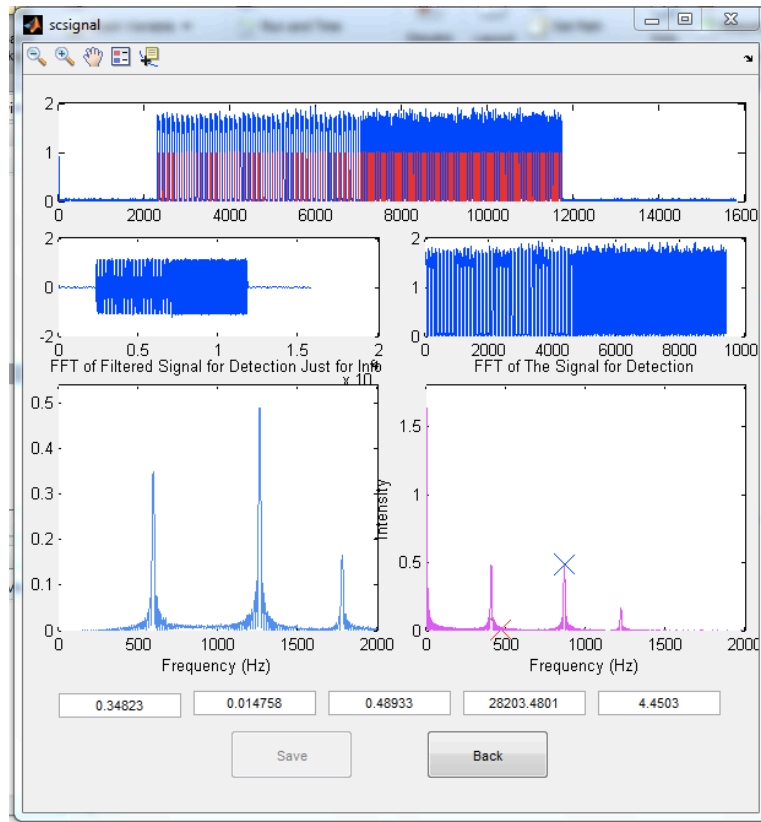


Figure 73 PSF calculation GUI of the Sigma

The 'scdata' GUI contains the following sections:

- Management:** 'New Patient', 'Edit Patient', 'Del Patient', and 'Del Meas' buttons.
- Patient Data:** Fields for Name (eye), Surname (fundusrtwo), Year of Birth (1999), and Gender (male).
- OD (Right Eye) Refraction:** Sphere (0), Cylinder (0), and Axis (0).
- OS (Left Eye) Refraction:** Sphere (0), Cylinder (0), and Axis (0).
- OD and OS Cataract:** Dropdown menus for Nuclear, Cortex, P. Subcapsular, and A. Subcapsular, all set to 0.
- C-Quant:** Fields for OD (0) and OS (0).
- Buttons:** 'Save DB', 'Backup Database', and 'Cancel'.
- Comments:** A text area for patient notes.

Figure 74 Database GUI of the Sigma

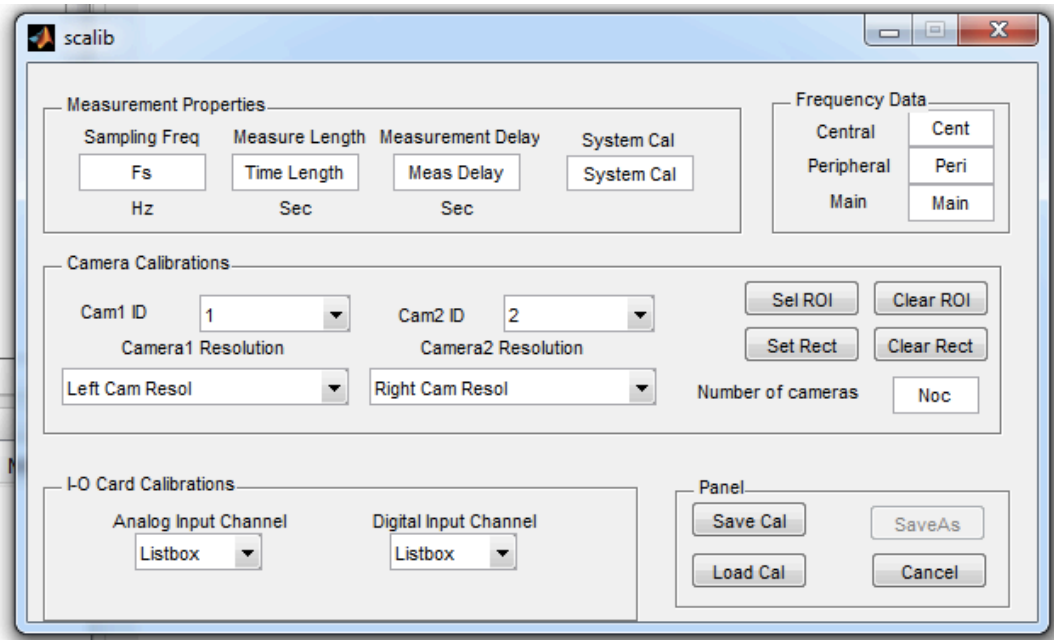


Figure 75 Calibration GUI of the sigma

A4.1.2 CODE OF MAIN GUI



Main

```

function varargout = main(varargin)

gui_Singleton = 1;
gui_State = struct('gui_Name',       mfilename, ...
                  'gui_Singleton',  gui_Singleton, ...
                  'gui_OpeningFcn', @main_OpeningFcn, ...
                  'gui_OutputFcn',  @main_OutputFcn, ...
                  'gui_LayoutFcn',   [], ...
                  'gui_Callback',    []);

if nargin && ischar(varargin{1})
    gui_State.gui_Callback = str2func(varargin{1});
end

if nargin
    [varargout{1:nargout}] = gui_mainfcn(gui_State, varargin{:});
else
    gui_mainfcn(gui_State, varargin{:});
end

function main_OpeningFcn(hObject, eventdata, handles, varargin)
global g;
global gp;
global gd;
% clear g;
errflag=0;

try
gp.pathname=[pwd '/'];
gd=load([gp.pathname '00sigma_database.mat ']);
gp.dbname = '00sigma_database.mat';
catch
errflag=1;
h=msgbox('There is no Database
file!!!','Info','error','modal');
waitfor(h);
closereq;
error('No Database File');
end

try
if(gp.firststrun==4)
end
catch
gp.firststrun=1;
end

if(errflag==0 && gp.firststrun==1)
gp.firststrun=0;
str={'Heraklion' ; 'Murcia' ; 'Other'};
clear s4 v4;
[s4,v4] = listdlg('PromptString','Which System?',...
                 'SelectionMode','single',...
                 'ListString',str);

pause(0.1)
if(v4==1)
if(s4==1)
gp.systmm=1;

elseif(s4==2)
gp.systmm=2;

elseif(s4==3)
gp.systmm=3;
end
else
closereq;
clear all;
end
% gp.mainflag=1;
clear s4 v4;
g=0;
% global g;

scdef

scdef

if(errflag==0)
gp.merror=0;
else
gp.merror=1;
end

end

handles.output = hObject;
guidata(hObject, handles);
try
movegui('center');
end

function varargout = main_OutputFcn(hObject, eventdata, handles)
varargout{1} = handles.output;

function bmeas_Callback(hObject, eventdata, handles)
global gp;
global g;

if(gp.merror==0)
set(handles.mainfig, 'Visible', 'off');
gp.measflag=1;
  
```

```

scmeas();

end

function bload_Callback(hObject, eventdata, handles)
global gp;
global g;
errflag=0;
gp.measflag=0;

% scdef;

% scfilt;

warning off
delete('temp.txt');
warning on

if(errflag==0)

str={'From Current DB','From File', 'Other DB', 'All DB'};

[s1,v1] = listdlg('PromptString','Select a file:',...
                 'SelectionMode','single',...
                 'ListString',str);

% v=1;
% s=2;
if(v1==1)
if(s1==2)
scanly;
end
if(s1==1)
tempx=1;
scanlydb;
end
if(s1==3)
tempx=2;
scanlydb;
end
if(s1==4)
scalldb;
end
else
errflag=1;
end

end

if(errflag==0)
scsigpro;
end
if(errflag==0)
scsignal();
end

function bdata_Callback(hObject, eventdata, handles)
warning off
delete('temp.txt')
scdata();

function balign_Callback(hObject, eventdata, handles)
set(handles.mainfig, 'Visible', 'off');
scalign();

function bcal_Callback(hObject, eventdata, handles)
global gp;
set(handles.mainfig, 'Visible', 'off');
scalib();

function bexit_Callback(hObject, eventdata, handles)
closereq;
clear all;

function mainfig_CloseRequestFcn(hObject, eventdata, handles)
scstopsc;
delete(hObject);
clear all;

Scdef

gp.pathname=[pwd '/'];
%% Prepare Video
if(errflag==0)
try
% Get a handle to each cam
try
gp.Lvid = videoinput('winvideo', g.camlid,
g.resolL);
gp.Rvid = videoinput('winvideo', g.cam2id,
g.resolR);
catch
h = msgbox('ERROR: Video. In Calibration
Select Cameras and Resolutions', 'Info','error','modal');
waitfor(h);
end

gp.Lsrc = getselectedsource(gp.Lvid);
gp.Rsrc = getselectedsource(gp.Rvid);

set(gp.Lvid,'TriggerRepeat',Inf);
set(gp.Rvid,'TriggerRepeat',Inf);

triggerconfig(gp.Lvid, 'Manual');
triggerconfig(gp.Rvid, 'Manual');
  
```


A4.1.3 CODE OF MEASUREMENT GUI



Scmeas

```

set(gp.Lvid, 'FramesPerTrigger', 1);
set(gp.Rvid, 'FramesPerTrigger', 1);

set(gp.Lvid, 'ReturnedColorSpace', 'grayscale');
set(gp.Rvid, 'ReturnedColorSpace', 'grayscale');
roires=textscan(g.resolL, '%5*c %3d %1*c %3d ');
try
gp.Lvid.ROIPosition = g.LROIPosition;
gp.Rvid.ROIPosition = g.RROIPosition;

catch
gp.Lvid.ROIPosition = [0 0 roires{1} roires{2}];
gp.Rvid.ROIPosition = [0 0 roires{1} roires{2}];
end

catch err
errflag=1;
disp(['Error video: ' err.message]);
h = msgbox(['ERROR: Video. ' err.message], 'Info', 'error', 'modal');
waitfor(h);
end

%% Prepare IO Device
%% Clean Previous Analog I-O

try
stop(gp.ai);
delete(gp.ai);
disp('INFO: Stopped and deleted old analog device handle')
catch
disp('INFO: No old analog I-O to clean up.')
end
%% Clean Previous Digital I-O
try
stop(gp.dio);
delete(gp.dio);
disp('INFO: topped and deleted old Digital device handle')
catch
disp('INFO: No old digital I-O to clean up.')
end

%% Set I-O Channels

if(errflag==0)
try
daqregister('nidaq');
disp('INFO: USB-6009 is registered!')
catch
errflag=1;
h = msgbox('No Devices Registered', 'Info', 'error', 'modal');
disp('INFO: USB-6009 is NOT!!! registered!')
end

if(errflag==0)
try
sdev=daq.getDevices;
devID= sdev.ID;

gp.dqas=daq.createSession('ni');
gp.dqas.addAnalogInputChannel(devID,g.anainp, 'Voltage');
gp.dqas.Rate=g.Fs;
gp.dqas.DurationInSeconds= g.tlength;
gp.dqas.addTriggerConnection('external', [devID '/PF10'], 'StartTrigger');
gp.dqas.ExternalTriggerTimeout= inf;
gp.lh= gp.dqas.addlistener('DataAvailable', @trgg);

catch err
errflag=1;
display(['ERROR: IO Card. ' err.message]);
h = msgbox(['ERROR: IO Card. ' err.message], 'Info', 'error', 'modal');
waitfor(h);
end

%%Image Processing Defs
gp.whitecircle = vision.ShapeInserter('Shape', 'Circles', 'BorderColor', 'Custom', 'CustomBorderColor', 250);
gp.black = vision.ShapeInserter('Shape', 'Circles', 'BorderColor', 'Custom', 'CustomBorderColor', 1);
gp.whiteline = vision.ShapeInserter('Shape', 'Lines', 'BorderColor', 'Custom', 'CustomBorderColor', 250);
gp.whiterectangle = vision.ShapeInserter('Shape', 'Rectangles', 'BorderColor', 'Custom', 'CustomBorderColor', 250);

gp.stst=0;
gp.aopen=5000;
gp.bvw=0.15;
gp.radd=100;

scfilt;
  
```

```

function varargout = scmeas(varargin)

gui_Singleton = 1;
gui_State = struct('gui_Name', mfilename, ...
'gui_Singleton', gui_Singleton, ...
'gui_OpeningFcn', @scmeas_OpeningFcn, ...
'gui_OutputFcn', @scmeas_OutputFcn, ...
'gui_LayoutFcn', [], ...
'gui_Callback', []);

if nargin && ischar(varargin{1})
gui_State.gui_Callback = str2func(varargin{1});
end

if nargout
[Varargout{1:nargout}] = gui_mainfcn(gui_State, varargin{:});
else
gui_mainfcn(gui_State, varargin{:});
end

function scmeas_OpeningFcn(hObject, eventdata, handles, varargin)
handles.output = hObject;
guidata(hObject, handles);
movegui('center');

global g; %Calibration Variables
global gp; %P

gp.pathname=[pwd '/'];
gd=load([gp.pathname '00sigma_database.mat' ]);

a=whos('-file', '00sigma_database.mat');
str = {a.name};
[s,v] = listdlg('PromptString', 'Select a Patient:', ...
'SelectionMode', 'single', ...
'ListString', str);
h = msgbox('Pass 1', 'Info', 'error', 'modal');
pause(0.1);

if(v==1)
gp.newname=a(s).name;
disp(['INFO: Selected patient ' gp.newname]);

else
closereq;
main();
scdata();
h = msgbox('Please Select or Create a patient', 'Info', 'error', 'modal');
end

function varargout = scmeas_OutputFcn(hObject, eventdata, handles)
try
varargout{1} = handles.output;
end
scstopsc;

function bstart_Callback(hObject, eventdata, handles)
set(hObject, 'BackgroundColor', [0.9 0.9 0.9]);
set(hObject, 'Enable', 'off');
set(handles.bsave, 'Enable', 'off');
set(handles.bsignal, 'Enable', 'off');
set(handles.bstop, 'Enable', 'on');
set(handles.bstop, 'BackgroundColor', [1 0 0]);
warning off
delete('temp.txt')
warning on

global g; %Calibration Variables
global gp; %Program Variables
global gd; % Patient Database
% clear gd;
gp.stopflag=0;

gd=load([gp.pathname '00sigma_database.mat' ]);

gd.temp=gd.(gp.newname);

% eval(['gd.temp =gd.' gp.newname '']);

errflag=0;

gp.ceye = listdlg('PromptString', 'Which Eye?', ...
'SelectionMode', 'single', ...
'ListString', {'OD', 'OS'});

%Run I-O Scrtipt
scio

if(errflag==0 && gp.stopflag==0)
set(handles.bsave, 'Enable', 'on');
set(handles.bsignal, 'Enable', 'on');

%Calculating signal
  
```

```

scsigpro
end

% GUI callbacks
if(errflag==0 && gp.stopflag==0)
    set(handles.tspair, 'String', num2str(gp.S));
    set(handles.tlogspair, 'String', num2str(gp.logss));
    set(handles.tfmain, 'String', num2str(gp.plotmaxx));
    set(handles.tfcemt, 'String', num2str(gp.tempcemt));
    set(handles.tfper, 'String', num2str(gp.tempper));

    %Plot FFT

    plot(handles.afft, gp.tfft2, gp.vfft2, 'color', t2)
    title(handles.afft, 'FFT of Flickering Rings at Different
Freq')
xlabel(handles.afft, 'Frequency (Hz)')
ylabel(handles.afft, 'Intensity')
axis(handles.afft, [300 1000 0 max(gp.vfft2)*1.1])

    set(handles.afft, 'NextPlot', 'add');
    plot(handles.afft, gp.tfft2(g.freqcent), gp.tempcemt,
'x', 'color', 'r', 'MarkerSize', 18);
    plot(handles.afft, gp.tfft2(g.freqper), gp.tempper,
'x', 'color', 'b', 'MarkerSize', 18);
    set(handles.afft, 'NextPlot', 'replace');

    disp('DONE: FFT Calculations')
end

bstop_Callback(handles.bstop, eventdata, handles);

function bsave_Callback(hObject, eventdata, handles)

global g; %Calibration Variables
global gp; %Program Variables
global gd;% Patient Database

set(hObject, 'Enable', 'off');
scsavedata;

function bstop_Callback(hObject, eventdata, handles)
try
set(hObject, 'BackgroundColor', [0.9 0.9 0.9]);
set(hObject, 'Enable', 'off');
set(handles.bstart, 'Enable', 'on');
set(handles.bstart, 'BackgroundColor', [0 1 0]);
end

global g; %Calibration Variables
global gp; %Program Variables

gp.stopflag=1;
scstops;

function bsignal_Callback(hObject, eventdata, handles)

a=1;
scsignal();

function bback_Callback(hObject, eventdata, handles)
scstops;
pause(1);
closereq;
main();

function tfmain_Callback(hObject, eventdata, handles)

function tfmain_CreateFcn(hObject, eventdata, handles)
if ispc && isequal(get(hObject, 'BackgroundColor'),
get(0, 'defaultUicontrolBackgroundColor'))
set(hObject, 'BackgroundColor', 'white');
end

function tfcent_Callback(hObject, eventdata, handles)

function tfcent_CreateFcn(hObject, eventdata, handles)
if ispc && isequal(get(hObject, 'BackgroundColor'),
get(0, 'defaultUicontrolBackgroundColor'))
set(hObject, 'BackgroundColor', 'white');
end

function tfper_Callback(hObject, eventdata, handles)

function tfper_CreateFcn(hObject, eventdata, handles)
if ispc && isequal(get(hObject, 'BackgroundColor'),
get(0, 'defaultUicontrolBackgroundColor'))
set(hObject, 'BackgroundColor', 'white');
end

function tspair_Callback(hObject, eventdata, handles)

function tspair_CreateFcn(hObject, eventdata, handles)
if ispc && isequal(get(hObject, 'BackgroundColor'),
get(0, 'defaultUicontrolBackgroundColor'))
set(hObject, 'BackgroundColor', 'white');
end

function tlogspair_Callback(hObject, eventdata, handles)

function tlogspair_CreateFcn(hObject, eventdata, handles)
if ispc && isequal(get(hObject, 'BackgroundColor'),

```

```

get(0, 'defaultUicontrolBackgroundColor'))
set(hObject, 'BackgroundColor', 'white');
end

Scio

warning off;

% Start Video & Wait for User Measurement Button
try
start(gp.Lvid);
start(gp.Rvid);
% start(gp.ai);
gp.dags.startBackground();
picloop=1;
try
close(222);
end
try
close(223);
end

while(1)

if (~gp.dags.IsRunning)
% % % Collect Data
leftallcell=(leftall(1:end));
gp.leftallarr=cell2mat(leftallcell);
figure(222)
imshow(gp.leftallarr)

rightallcell=(rightall(1:end));
gp.rightallarr=cell2mat(rightallcell);
figure(223)
imshow(gp.rightallarr)

clear leftall rightall;

break
end

trigger(gp.Lvid);
trigger(gp.Rvid);

left = getdata(gp.Lvid);
right = getdata(gp.Rvid);

% left = 1;
% right = 1;
left = imresize(left, [200 200]);
right = imresize(right, [200 200]);
% left = getsnapshot(gp.Lvid);%h
% right = getsnapshot(gp.Rvid);%h

lsize=size(left);
rsize=size(right);

if (lsize~=rsize)
error('ERROR: Resolutions are not same!!!');
break
end

% Image processing
% scimgproc;

frame(1:(lsize(1)/2), 1:lsize(2)) =
left(1:(lsize(1)/2), 1:lsize(2));
frame((lsize(1)/2):lsize(1), 1:lsize(2)) =
right((lsize(1)/2):lsize(1), 1:lsize(2));

frame=step(gp.whitcircle, frame, int32((lsize(1)/2
lsize(2)/2 gp.rad/4));
frame=step(gp.whiteline, frame,
int32([0, lsize(2)/2, lsize(1), lsize(2)/2]));
frame=step(gp.whiteline, frame,
int32([lsize(1)/2, 0, lsize(1)/2, lsize(2)]));
try
frame=step(gp.whiterectangle, frame, int32(g.rect1));
frame=step(gp.whiterectangle, frame, int32(g.rect2));
end

imshow(frame, 'Parent', handles.avid);
gp.lframe=frame;

leftall(picloop)=left;
rightall(picloop)=right;
picloop=picloop+1;
if picloop>20
leftall=(leftall(end-19:end));
rightall=(rightall(end-19:end));
picloop=1;
end

flushdata(gp.Lvid);
flushdata(gp.Rvid);

end

catch err
display(['Error: IO. ' err.message])
bstop_Callback(handles.bstop, eventdata, handles);
errflag=1;
end

try

if strcmp('on', get(handles.bstop, 'Enable'))

% Detection of measurement press
disp('INFO: Measurement button is pressed')

try
stop(gp.Lvid);
end
try
stop(gp.Rvid);
end

```

```

end
catch err
display([err.message])
bstop_Callback(handles.bstop,eventdata, handles);
errflag=1;
end

```

Scsigpro

```

if(errflag==0)
try
% CALCULATIONS
disp('ON PROGRESS: getfile')
[gp.vb,gp.tb,fn]=getfile('temp.txt',gp.pathname,1);
disp('DONE: getfile')
filename=fn;
catch err
disp(['CHECK: No Temp Found. OK if loading database '
err.message])
end
try
% FIND SIGNAL
disp('ON PROGRESS: fsignal')
warning off
[gp.sig1,gp.sig2,gp.Inrange,gp.sl] =
fsignal(gp.vb,gp.filt);
disp('DONE: fsignal')
catch err
disp(['ERROR: Bad Signal. ' err.message])
h = msgbox(['ERROR: Bad Signal. '
err.message],'Info','error','modal')
errflag=1;
end
warning on

if(errflag==0)
try
%% FFT CALCULATIONS
disp('ON PROGRESS: FFT Calculations')
% try
[gp.vfft1,gp.tfft1,gp.NFFT1] =
takefft(gp.sig1,g.Fs,gp.sl);
[gp.vfft2,gp.tfft2,gp.NFFT2] =
takefft(gp.sig2,g.Fs,gp.sl);

gp.vfft1=2*abs(gp.vfft1(1:gp.NFFT1/2+1));
gp.vfft2=2*abs(gp.vfft2(1:gp.NFFT2/2+1));

gp.sizz=size(gp.tfft2);

disp('DONE: FFT')

t=rand(1,3); %creating random colors
t2=rand(1,3);

gp.tempcnt=gp.vfft2(g.freqcent);
gp.tempper=gp.vfft2(g.freqper);

gp.plotmaxx=gp.vfft1(g.freqmain);

gp.r=gp.tempper/gp.tempcnt;

sclogscal

scsave
scsave

scsave
disp('INFO: Measurement saved into log file');
catch err
disp(['ERROR: Signal Processing. ' err.message])
h = msgbox(['ERROR: Signal Processing. '
err.message],'Info','error','modal')
errflag=1;
end
end

```

Sclogscal

```

disp('ON PROGRESS: LogS cal')
% if(gp.system==1)
gp.S=23*(gp.r^2)+88*gp.r-0.74;
gp.logss=log10(gp.S)-g.sysscal;

gp.tt=['total' ; num2str(gp.plotmaxx) ; 'Cent' ;
num2str(gp.tempcnt) ; 'Per' ; num2str(gp.tempper) ; 'Ratio' ;
num2str(gp.r) ; 'S' ; num2str(gp.S) ; 'logS' ; num2str(gp.logss)];
disp('DONE: LogS cal')

if( gp.plotmaxx< 0.05 || gp.plotmaxx>2.95 || gp.tempcnt <
0.05 || gp.tempper < 0.02)
% h = msgbox('Consider Repeating the
measurement!!!!','Info','error','modal');
% waitfor(h);
end

try
fid = fopen('logrec.txt', 'a+');
fprintf(fid, '%s ', gp.mname);
fprintf(fid, '\t %s \t %s \t %s \t %s \t %s \t %s \t %s \t
\t %s \t %s \t %s \t %s \t %s \t %s \t %s \t %s \t %s\n',
gp.tt{1},gp.tt{2},gp.tt{3},gp.tt{4},gp.tt{5},gp.tt{6},gp.tt{7},
gp.tt{8},gp.tt{9},gp.tt{10},gp.tt{11},gp.tt{12});
fprintf(fid, '\n');
fclose(fid);
disp('DONE: Measurement written to log')
end

```

Scsavedata

```

(filename, pathname) = uigetfile(['*.mat'],'Please Select
Database');
ntime= datestr(now, 'yyyy_mm_dd_HHMMSS');

try
if(gp.ceye==2)
gp.ceye='os';
tsaveeye= ['gd.temp.m.os ' ntime];
eval([tsaveeye '=gp.vb;']);
elseif(gp.ceye==1)
gp.ceye='od';
tsaveeye= ['gd.temp.m.od ' ntime];
eval([tsaveeye '=gp.vb;']);
end

catch
gp.ceye = listdlg('PromptString','Which Eye?',...
'SelectionMode','single',...
>ListString',{'OS'; 'OD'})
if(gp.ceye==2)
gp.ceye='os';
tsaveeye= ['gd.temp.m.os ' ntime];
eval([tsaveeye '=gp.vb;']);
elseif(gp.ceye==1)
gp.ceye='od';
tsaveeye= ['gd.temp.m.od ' ntime];
eval([tsaveeye '=gp.vb;']);
end
end

try
choice = menu('You are Saving a measurement','Proceed
and save same database','Proceed and save a new
database','Cancel');

% if (choice == 1)
% gd
tsavename=[gd.temp.name '_' gd.temp.sname];
eval([tsavename '=gd.temp;']);
scdatacrltmp;
save(gp.dname , tsavename , '-append');

t=exist('meas', 'file');

if(t~=7)
mkdir('meas');
end

% end
% end
copyfile('temp.txt', ['meas\' gp.newname '_' gp.ceye '_'
ntime '.txt' ]);
imwrite(gp.lframe,['meas\' gp.newname '_' gp.ceye '_'
ntime '.tif']);
imwrite(gp.rightallarr,['meas\' gp.newname '_' gp.ceye '_'
ntime '_rightcam.tif']);
imwrite(gp.leftallarr,['meas\' gp.newname '_' gp.ceye '_'
ntime '_leftcam.tif']);

% catch
h = msgbox('Error not saved!');
% end
disp(['INFO: Measurement is saved to ' gp.newname '_'
gp.ceye '_' ntime '.txt']);
clear gp.ceye;
catch err
disp(['ERROR: Not Saved. ' err.message])
h = msgbox(['ERROR: Not Saved. '
err.message],'Info','error','modal')
errflag=1;
end
end

```

A4.1.4 CODE OF CALIBRATION GUI

```

function varargout = scalib(varargin)
gui_Singleton = 1;
gui_State = struct('gui_Name', mfilename, ...
'gui_Singleton', gui_Singleton, ...
'gui_OpeningFcn', @scalib_OpeningFcn, ...
'gui_OutputFcn', @scalib_OutputFcn, ...
'gui_LayoutFcn', [], ...
'gui_Callback', []);
if nargin && ischar(varargin{1})
gui_State.gui_Callback = str2func(varargin{1});
end

if nargout
[varargout{1:nargout}] = gui_mainfcn(gui_State,
varargin{:});
else
gui_mainfcn(gui_State, varargin{:});
end

function scalib_OpeningFcn(hObject, eventdata, handles,
varargin)
handles.output = hObject;

global g;
global gp;
% disp(gp)
try
scdeft

```

```

catch
    [filename, pathname] = uigetfile({'*.mat'}, 'No Calibration
Data Please Locate Calibration data');
    g=load([pathname filename]);
end

%Detect Second Camera
try
    out = imaghwinfo('winvideo', 2);
    out=out.SupportedFormats;
    out=[g.resolR out];
    set(handles.mresolr,'String', out);

% set(handles.mnumcam, 'String', {g.camnumb; 1;2})
catch
    set(handles.mresolr, 'Enable', 'off')
    set(handles.mresolr, 'String', 'No Second Camera')
end

scalasign

%Camera detections
t=imaghwinfo('winvideo');
t=size(t.DeviceIDs);
gp.nofcam=t(2);
set(handles.tnoc, 'String', num2str(gp.nofcam));
clear t;

tcamlid=get(handles.mcamlid, 'String');
tcam2id=get(handles.mcam2id, 'String');

for k=1:gp.nofcam

    tcamlid = [tcamlid ; num2str(k)];
    tcam2id = [tcam2id ; num2str(k)];

end

set(handles.mcamlid,'String', tcamlid);
set(handles.mcam2id,'String', tcam2id);

guidata(hObject, handles);
movegui('center');

function varargout = scalib_OutputFcn(hObject, eventdata,
handles)

varargout{1} = handles.output;
% main();

function tfs_Callback(hObject, eventdata, handles)
global g;
g.Fs= str2num(get(hObject, 'String'));

function tfs_CreateFcn(hObject, eventdata, handles)
if ispc && isequal(get(hObject,'BackgroundColor'),
get(0,'defaultUicontrolBackgroundColor'))
    set(hObject,'BackgroundColor','white');
end

function tlength_Callback(hObject, eventdata, handles)
global g;
g.tlength= str2num(get(hObject, 'String'));

function tlength_CreateFcn(hObject, eventdata, handles)
if ispc && isequal(get(hObject,'BackgroundColor'),
get(0,'defaultUicontrolBackgroundColor'))
    set(hObject,'BackgroundColor','white');
end

function tmeasdelay_Callback(hObject, eventdata, handles)
global g;
g.measdelay= str2num(get(hObject, 'String'));

function tmeasdelay_CreateFcn(hObject, eventdata, handles)
if ispc && isequal(get(hObject,'BackgroundColor'),
get(0,'defaultUicontrolBackgroundColor'))
    set(hObject,'BackgroundColor','white');
end

function mresoll_Callback(hObject, eventdata, handles)
global g;
list=get(hObject,'String');
val=get(hObject,'Value');
g.resolL=num2str(list(val));
% num2str(list(val))

function mresoll_CreateFcn(hObject, eventdata, handles)
if ispc && isequal(get(hObject,'BackgroundColor'),
get(0,'defaultUicontrolBackgroundColor'))
    set(hObject,'BackgroundColor','white');
end

function mresolr_Callback(hObject, eventdata, handles)
global g;
list=get(hObject,'String');
val=get(hObject,'Value');
g.resolR=num2str(list(val));

function mresolr_CreateFcn(hObject, eventdata, handles)
if ispc && isequal(get(hObject,'BackgroundColor'),
get(0,'defaultUicontrolBackgroundColor'))
    set(hObject,'BackgroundColor','white');
end

function manainp_Callback(hObject, eventdata, handles)
global g;
list=get(hObject,'String');
val=get(hObject,'Value');
g.anainp=str2num(list(val));

function manainp_CreateFcn(hObject, eventdata, handles)
if ispc && isequal(get(hObject,'BackgroundColor'),
get(0,'defaultUicontrolBackgroundColor'))
    set(hObject,'BackgroundColor','white');
end

function mdiginp_Callback(hObject, eventdata, handles)
global g;
list=get(hObject,'String');
val=get(hObject,'Value');
g.diginp=str2num(list(val));

function mdiginp_CreateFcn(hObject, eventdata, handles)
if ispc && isequal(get(hObject,'BackgroundColor'),
get(0,'defaultUicontrolBackgroundColor'))
    set(hObject,'BackgroundColor','white');
end

function bsave_Callback(hObject, eventdata, handles)
global gp;
save(gp.sccalfile,'-struct','g');
gp.firstrun=1;

% close(scalib)

function bsaveas_Callback(hObject, eventdata, handles)

function bload_Callback(hObject, eventdata, handles)
[filename, pathname] = uigetfile({'*.mat;*.mat'}, 'Cal Files');
global g;
g=load([pathname '/' filename]);

scalasign

function bcancel_Callback(hObject, eventdata, handles)
closereg;
main();

function tfreqcent_Callback(hObject, eventdata, handles)
global g;
g.freqcent= str2num(get(hObject, 'String'));

function tfreqcent_CreateFcn(hObject, eventdata, handles)
if ispc && isequal(get(hObject,'BackgroundColor'),
get(0,'defaultUicontrolBackgroundColor'))
    set(hObject,'BackgroundColor','white');
end

function tfreqper_Callback(hObject, eventdata, handles)
global g;
g.freqper= str2num(get(hObject, 'String'));

function tfreqper_CreateFcn(hObject, eventdata, handles)
if ispc && isequal(get(hObject,'BackgroundColor'),
get(0,'defaultUicontrolBackgroundColor'))
    set(hObject,'BackgroundColor','white');
end

function tfreqmain_Callback(hObject, eventdata, handles)
global g;
g.freqmain= str2num(get(hObject, 'String'));

function tfreqmain_CreateFcn(hObject, eventdata, handles)
if ispc && isequal(get(hObject,'BackgroundColor'),
get(0,'defaultUicontrolBackgroundColor'))
    set(hObject,'BackgroundColor','white');
end

% --- Executes on button press in broisel.
function broisel_Callback(hObject, eventdata, handles)
global gp;

gp.Lvid = videoinput('winvideo', g.camlid, g.resolL);
gp.Rvid = videoinput('winvideo', g.cam2id, g.resolR);

% Set video input object properties for this
application.
set(gp.Lvid,'TriggerRepeat',Inf);
set(gp.Rvid,'TriggerRepeat',Inf);

triggerconffig(gp.Lvid, 'Manual');
triggerconffig(gp.Rvid, 'Manual');

set(gp.Lvid, 'FramesPerTrigger', 1);
set(gp.Rvid, 'FramesPerTrigger', 1);

```

```

%         gp.Lvid.FrameGrabInterval = 1;
%         gp.Rvid.FrameGrabInterval = 1;

        set(gp.Lvid,'ReturnedColorSpace','grayscale');
        set(gp.Rvid,'ReturnedColorSpace','grayscale');

pvid=figure;

start(gp.Lvid);
start(gp.Rvid);
pause(1)
trigger(gp.Lvid);
trigger(gp.Rvid);
pause(1)

lleft = getdata(gp.Lvid,1);
rright = getdata(gp.Rvid,1);

stop(gp.Lvid);
stop(gp.Rvid);

figure(pvid)
imshow(lleft)
h = imrect;
%   gp.Lvid.ROIPosition = wait(h);
%   g.LROIPosition = wait(h);
%   gp.Lvid.ROIPosition = g.LROIPosition;

close(pvid)

pause(1)

figure(pvid)
imshow(rright)
h = imrect;
%   g.Rvid.ROIPosition = wait(h);
%   g.RROIPosition = wait(h);

flushdata(gp.Lvid);
flushdata(gp.Rvid);

save(gp.sccalfile,'-struct','g');

%   gp.xx=5;

close(pvid);

disp('INFO: ROI Selected');
gp.firstrun=1;
scstopsc;

% --- Executes on button press in broiclear.
function broiclear_Callback(hObject, eventdata, handles)
global g;

roires=textscan(g.resolL,'%5*c %3d %1*c %3d ');

g.LROIPosition = [0 0 roires{1} roires{2}];
g.RROIPosition = [0 0 roires{1} roires{2}];

disp('INFO: ROI Cleared');
% g.RROIPosition = [0 0 160 120];
% g.LROIPosition = [0 0 160 120];
% g.Lvid.ROIPosition = [0 0 640 480];
% g.Rvid.ROIPosition = [0 0 640 480];
% g.xx= [0 0];
% g.yy= [0 0];

function tsyscal_Callback(hObject, eventdata, handles)
global g;
g.syscal= str2num(get(hObject, 'String'));

function tsyscal_CreateFcn(hObject, eventdata, handles)
if ispc && isequal(get(hObject,'BackgroundColor'),
get(0,'defaultUicontrolBackgroundColor'))
    set(hObject,'BackgroundColor','white');
end

function bsetrect_Callback(hObject, eventdata, handles)
global g;

    gp.Lvid = videoinput('winvideo', g.camlid, g.resolL);
    gp.Rvid = videoinput('winvideo', g.cam2id, g.resolR);

    % Set video input object properties for this
    application.
    set(gp.Lvid,'TriggerRepeat',Inf);
    set(gp.Rvid,'TriggerRepeat',Inf);

    triggerconfig(gp.Lvid, 'Manual');
    triggerconfig(gp.Rvid, 'Manual');

    set(gp.Lvid, 'FramesPerTrigger', 1);
    set(gp.Rvid, 'FramesPerTrigger', 1);

%   gp.Lvid.FrameGrabInterval = 1;
%   gp.Rvid.FrameGrabInterval = 1;

    set(gp.Lvid,'ReturnedColorSpace','grayscale');
    set(gp.Rvid,'ReturnedColorSpace','grayscale');

%   try
%   gp.Lvid.ROIPosition = g.LROIPosition;
%   gp.Rvid.ROIPosition = g.RROIPosition;
%   end

pvid=figure;

start(gp.Lvid);
start(gp.Rvid);
pause(1)

trigger(gp.Lvid);
trigger(gp.Rvid);
pause(1)

left = getdata(gp.Lvid);
right = getdata(gp.Rvid);

stop(gp.Lvid);
stop(gp.Rvid);

left = imresize(left, [200 200]);
right = imresize(right, [200 200]);

lsize=size(left);
rsize=size(right);

if (lsize==rsize)
    error('ERROR: Resolutions are not same!!!');
end

    frame(1:(lsize(1)/2),1:lsize(2)) =
left(1:(lsize(1)/2),1:lsize(2));
    frame((lsize(1)/2):lsize(1),1:lsize(2)) =
right((lsize(1)/2):lsize(1),1:lsize(2));
%   size(frame)

figure(pvid)
imshow(frame)
h = imrect;
g.rect1 = wait(h);
hl = imrect;
g.rect2 = wait(hl);

close(pvid)

pause(1)

flushdata(gp.Lvid);
flushdata(gp.Rvid);

save(gp.sccalfile,'-struct','g');

scstopsc;
gp.firstrun=1;
disp('INFO: I-O Rectangles Selected');

% --- Executes on button press in bclrect.
function bclrect_Callback(hObject, eventdata, handles)
global g;
global gp;

g.rect1 = 0;
g.rect2 = 0;

save(gp.sccalfile,'-struct','g');

disp('INFO: I-O Rectangles Cleared');

function tnoc_Callback(hObject, eventdata, handles)

function tnoc_CreateFcn(hObject, eventdata, handles)
if ispc && isequal(get(hObject,'BackgroundColor'),
get(0,'defaultUicontrolBackgroundColor'))
    set(hObject,'BackgroundColor','white');
end

% --- Executes on selection change in mcamlid.
function mcamlid_Callback(hObject, eventdata, handles)
global g;

list=get(hObject,'String');
val=get(hObject,'Value');
g.camlid=str2num(list(val));

out = imaqhwinfo('winvideo', g.camlid);
out=out.SupportedFormats;
set(handles.mresolL,'String', out);

g.resolL=out{1};

% --- Executes during object creation, after setting all
properties.
function mcamlid_CreateFcn(hObject, eventdata, handles)
if ispc && isequal(get(hObject,'BackgroundColor'),
get(0,'defaultUicontrolBackgroundColor'))
    set(hObject,'BackgroundColor','white');
end

% --- Executes on selection change in mcam2id.
function mcam2id_Callback(hObject, eventdata, handles)
global g;

list=get(hObject,'String');
val=get(hObject,'Value');
g.cam2id=str2num(list(val));

out = imaqhwinfo('winvideo', g.cam2id);
out=out.SupportedFormats;
set(handles.mresolR,'String', out);

g.resolR=out{1};

% --- Executes during object creation, after setting all
properties.
function mcam2id_CreateFcn(hObject, eventdata, handles)
if ispc && isequal(get(hObject,'BackgroundColor'),
get(0,'defaultUicontrolBackgroundColor'))

```

```

set(hObject,'BackgroundColor','white');
end

```

A4.1.5 CODE OF DATABASE GUI

```

function varargout = scdata(varargin)
% SCDATA MATLAB code for scdata.fig

gui_Singleton = 1;
gui_State = struct('gui_Name',       mfilename, ...
                  'gui_Singleton',   gui_Singleton, ...
                  'gui_OpeningFcn', @scdata_OpeningFcn, ...
                  'gui_OutputFcn',  @scdata_OutputFcn, ...
                  'gui_LayoutFcn',  [], ...
                  'gui_Callback',    []);

if nargin && ischar(varargin{1})
    gui_State.gui_Callback = str2func(varargin{1});
end

if nargout
    [varargout{1:nargout}] = gui_mainfcn(gui_State, varargin{:});
else
    gui_mainfcn(gui_State, varargin{:});
end

function scdata_OpeningFcn(hObject, eventdata, handles, varargin)
global gd;
global gp;

% [filename, pathname] = uigetfile('*.*mat'),'Please Select Database');
gd=load([gp.pathname '00sigma_database.mat']);
gp.dbname = '00sigma_database.mat';

clear gd,temp;

handles.output = hObject;
guidata(hObject, handles);

function varargout = scdata_OutputFcn(hObject, eventdata, handles)
varargout{1} = handles.output;

function tname_Callback(hObject, eventdata, handles)
global gd;
gd.temp.name = get(hObject, 'String');

function tname_CreateFcn(hObject, eventdata, handles)
if ispc && isequal(get(hObject,'BackgroundColor'), get(0,'defaultUicontrolBackgroundColor'))
    set(hObject,'BackgroundColor','white');
end

function tname_Callback(hObject, eventdata, handles)
global gd;
gd.temp.sname = get(hObject, 'String');

function tname_CreateFcn(hObject, eventdata, handles)
if ispc && isequal(get(hObject,'BackgroundColor'), get(0,'defaultUicontrolBackgroundColor'))
    set(hObject,'BackgroundColor','white');
end

function tbirth_Callback(hObject, eventdata, handles)
global gd;
gd.temp.birth = str2num(get(hObject, 'String'));
% disp(gd.temp.birth)
tt=gd.temp.birth;

while 1
    try
        if (tt > 2100 || tt<1900)
            prompt = {'Please Enter a Correct Value'};
            dlg_title = 'Year of Birth';
            num_lines = 1;
            def = {'','hsv'};
            nfn = inputdlg(prompt,dlg_title);
            tt= str2num(nfn{1});
        else
            set(hObject, 'String', num2str(tt));
            break
        end
    catch
        prompt = {'Please Enter a Correct Value'};
        dlg_title = 'Year of Birth';
        num_lines = 1;
        def = {'','hsv'};
        nfn = inputdlg(prompt,dlg_title);
        tt= str2num(nfn{1})
    end
end
gd.temp.birth=tt;

function tbirth_CreateFcn(hObject, eventdata, handles)
if ispc && isequal(get(hObject,'BackgroundColor'), get(0,'defaultUicontrolBackgroundColor'))
    set(hObject,'BackgroundColor','white');
end

function funclear(hObject, eventdata, handles)
set(hObject, 'String', '');

function pgender_Callback(hObject, eventdata, handles)

```

```

global gd

if (get(hObject, 'Value') == 2)
    gd.temp.gender = 0;
else
    gd.temp.gender = 1;
end

function pgender_CreateFcn(hObject, eventdata, handles)
global gd;
gd.temp.gender = 1;

if ispc && isequal(get(hObject,'BackgroundColor'), get(0,'defaultUicontrolBackgroundColor'))
    set(hObject,'BackgroundColor','white');
end

function osc1_Callback(hObject, eventdata, handles)
global gd;

scdataselcat;
eval('gd.temp.osc1 = temp;');

function osc1_CreateFcn(hObject, eventdata, handles)
if ispc && isequal(get(hObject,'BackgroundColor'), get(0,'defaultUicontrolBackgroundColor'))
    set(hObject,'BackgroundColor','white');
end

function osc2_Callback(hObject, eventdata, handles)
global gd;

scdataselcat;
eval('gd.temp.osc2 = temp;');

function osc2_CreateFcn(hObject, eventdata, handles)
if ispc && isequal(get(hObject,'BackgroundColor'), get(0,'defaultUicontrolBackgroundColor'))
    set(hObject,'BackgroundColor','white');
end

function osc3_Callback(hObject, eventdata, handles)
global gd;

scdataselcat;
eval('gd.temp.osc3 = temp;');

function osc3_CreateFcn(hObject, eventdata, handles)
if ispc && isequal(get(hObject,'BackgroundColor'), get(0,'defaultUicontrolBackgroundColor'))
    set(hObject,'BackgroundColor','white');
end

% --- Executes on selection change in osc4.
function osc4_Callback(hObject, eventdata, handles)
global gd;

scdataselcat;
eval('gd.temp.osc4 = temp;');

function osc4_CreateFcn(hObject, eventdata, handles)
if ispc && isequal(get(hObject,'BackgroundColor'), get(0,'defaultUicontrolBackgroundColor'))
    set(hObject,'BackgroundColor','white');
end

function ossp_Callback(hObject, eventdata, handles)
global gd;
gd.temp.oss = str2num(get(hObject, 'String'));

tt=gd.temp.oss;

while 1
    scdatachksp
end

gd.temp.oss=tt;

function ossp_CreateFcn(hObject, eventdata, handles)
if ispc && isequal(get(hObject,'BackgroundColor'), get(0,'defaultUicontrolBackgroundColor'))
    set(hObject,'BackgroundColor','white');
end

function oscy_Callback(hObject, eventdata, handles)
global gd;

gd.temp.oscy = str2num(get(hObject, 'String'));
tt=gd.temp.oscy;

while 1
    scdatachksp
end

gd.temp.oscy=tt;

function oscy_CreateFcn(hObject, eventdata, handles)
if ispc && isequal(get(hObject,'BackgroundColor'), get(0,'defaultUicontrolBackgroundColor'))
    set(hObject,'BackgroundColor','white');
end

function osax_Callback(hObject, eventdata, handles)
global gd;

gd.temp.osax = str2num(get(hObject, 'String'));
tt=gd.temp.osax;

```

```

while 1
    scdatachkax
end

gd.temp.osax=tt;

function osax_CreateFcn(hObject, eventdata, handles)
if ispc && isequal(get(hObject,'BackgroundColor'),
get(0,'defaultUicontrolBackgroundColor'))
    set(hObject,'BackgroundColor','white');
end

function odsp_Callback(hObject, eventdata, handles)
global gd;

gd.temp.odsp = str2num(get(hObject, 'String'));
tt=gd.temp.odsp;

while 1
    scdatachksp
end

gd.temp.odsp=tt;

function odsp_CreateFcn(hObject, eventdata, handles)
if ispc && isequal(get(hObject,'BackgroundColor'),
get(0,'defaultUicontrolBackgroundColor'))
    set(hObject,'BackgroundColor','white');
end

function odcy_Callback(hObject, eventdata, handles)
global gd;

gd.temp.odcy = str2num(get(hObject, 'String'));
tt=gd.temp.odcy;

while 1
    scdatachksp
end

gd.temp.odcy=tt;

function odcy_CreateFcn(hObject, eventdata, handles)
if ispc && isequal(get(hObject,'BackgroundColor'),
get(0,'defaultUicontrolBackgroundColor'))
    set(hObject,'BackgroundColor','white');
end

function odax_Callback(hObject, eventdata, handles)
global gd;

gd.temp.odax = str2num(get(hObject, 'String'));
tt=gd.temp.odax;

while 1
    scdatachkax
end

gd.temp.odax=tt;

function odax_CreateFcn(hObject, eventdata, handles)
if ispc && isequal(get(hObject,'BackgroundColor'),
get(0,'defaultUicontrolBackgroundColor'))
    set(hObject,'BackgroundColor','white');
end

function odc1_Callback(hObject, eventdata, handles)
global gd;

scdataselcat;
eval('gd.temp.odc1 = temp;');

function odc1_CreateFcn(hObject, eventdata, handles)
if ispc && isequal(get(hObject,'BackgroundColor'),
get(0,'defaultUicontrolBackgroundColor'))
    set(hObject,'BackgroundColor','white');
end

function odc2_Callback(hObject, eventdata, handles)
global gd;

scdataselcat;
eval('gd.temp.odc2 = temp;');

function odc2_CreateFcn(hObject, eventdata, handles)
if ispc && isequal(get(hObject,'BackgroundColor'),
get(0,'defaultUicontrolBackgroundColor'))
    set(hObject,'BackgroundColor','white');
end

function odc3_Callback(hObject, eventdata, handles)
global gd;

scdataselcat;
eval('gd.temp.odc3 = temp;');

function odc3_CreateFcn(hObject, eventdata, handles)
if ispc && isequal(get(hObject,'BackgroundColor'),
get(0,'defaultUicontrolBackgroundColor'))
    set(hObject,'BackgroundColor','white');
end

function odc4_Callback(hObject, eventdata, handles)
global gd;

scdataselcat;
eval('gd.temp.odc4 = temp;');

function odc4_CreateFcn(hObject, eventdata, handles)
if ispc && isequal(get(hObject,'BackgroundColor'),
get(0,'defaultUicontrolBackgroundColor'))
    set(hObject,'BackgroundColor','white');
end

end

function tcom_Callback(hObject, eventdata, handles)
global gd;
gd.temp.com = get(hObject, 'String');

function tcom_CreateFcn(hObject, eventdata, handles)
if ispc && isequal(get(hObject,'BackgroundColor'),
get(0,'defaultUicontrolBackgroundColor'))
    set(hObject,'BackgroundColor','white');
end

function bnp_Callback(hObject, eventdata, handles)
global gd;

gd.temp.gender=1;

gd.temp.oss=0;
gd.temp.oscy=0;
gd.temp.osax=0;

gd.temp.osc1=0;
gd.temp.osc2=0;
gd.temp.osc3=0;
gd.temp.osc4=0;

gd.temp.odsp=0;
gd.temp.odcy=0;
gd.temp.odax=0;

gd.temp.odc1=0;
gd.temp.odc2=0;
gd.temp.odc3=0;
gd.temp.odc4=0;

gd.temp.cqos=0;
gd.temp.cqod=0;

gd.temp.com='';

set(handles.tname,'String','');
set(handles.tsname,'String','');
set(handles.tbirth,'String','');

set(handles.pgender, 'Value', 1);

set(handles.oss,'String','0');
set(handles.oscy,'String','0');
set(handles.osax,'String','0');

set(handles.osc1, 'Value', 1);
set(handles.osc2, 'Value', 1);
set(handles.osc3, 'Value', 1);
set(handles.osc4, 'Value', 1);

set(handles.odsp,'String','0');
set(handles.odcy,'String','0');
set(handles.odax,'String','0');

set(handles.odc1, 'Value', 1);
set(handles.odc2, 'Value', 1);
set(handles.odc3, 'Value', 1);
set(handles.odc4, 'Value', 1);

set(handles.tcom,'String','');

set(handles.tcqos,'String','0');
set(handles.tcqod,'String','0');

set(handles.ppd,'Visible','on');
set(handles.pos,'Visible','on');
set(handles.pod,'Visible','on');
set(handles.pcom,'Visible','on');
set(handles.pcq,'Visible','on');

function bep_Callback(hObject, eventdata, handles)
global gd;
global gp;

a=whos('-file',gp.dbname);
str = {a.name};
[s,v] = listdlg('PromptString','Select a file:',...
'SelectionMode','single',...
'ListString',str);

if(v==1)

set(handles.ppd,'Visible','on');
set(handles.pos,'Visible','on');
set(handles.pod,'Visible','on');
set(handles.pcom,'Visible','on');
set(handles.pcq,'Visible','on');

newname=a(s).name;
eval(['gd.temp =gd.' newname '.']);

% disp(gd.temp);

set(handles.tname,'String',gd.temp.name);
set(handles.tsname,'String',gd.temp.sname);
set(handles.tbirth,'String',num2str(gd.temp.birth));

if(gd.temp.gender == 0)
set(handles.pgender, 'Value', 2);
else
set(handles.pgender, 'Value', 1);
end

set(handles.oss,'String',num2str(gd.temp.oss));
set(handles.oscy,'String',num2str(gd.temp.oscy));
set(handles.osax,'String',num2str(gd.temp.osax));

set(handles.osc1, 'Value', gd.temp.osc1+1);
set(handles.osc2, 'Value', gd.temp.osc2+1);
set(handles.osc3, 'Value', gd.temp.osc3+1);
set(handles.osc4, 'Value', gd.temp.osc4+1);

```

```

set(handles.odsp,'String', num2str(gd.temp.odsp));
set(handles.odcy,'String', num2str(gd.temp.odcy));
set(handles.odax,'String', num2str(gd.temp.odax));

set(handles.odc1,'Value', gd.temp.odc1+1);
set(handles.odc2,'Value', gd.temp.odc2+1);
set(handles.odc3,'Value', gd.temp.odc3+1);
set(handles.odc4,'Value', gd.temp.odc4+1);

set(handles.tcom,'String', (gd.temp.com));

set(handles.tcqs,'String', (gd.temp.cqos));
set(handles.tcqod,'String', (gd.temp.cqod));

else
newname='';
end

function bdp_Callback(hObject, eventdata, handles)
global gd;
global gp;

a=whos('-file',gp.dname);
str = {a.name};
[s,v] = listdlg('PromptString','Select a file:',...
'SelectionMode','single',...
'ListString',str);

if(v==1)
cname=a(s).name;
% choice = menu('You are deleting a patient','Proceed and save
same database','Proceed and Backup the database','Cancel');
choice=1;

if (choice == 1)
gd= rmfield(gd,cname);
scdataclrtmp;
save(gp.dname ,'-struct', 'gd');

elseif( choice ==2)
gd= rmfield(gd,cname);
ndbname= datestr(now, 'yyyy_mm_dd_HHMMSS');
ndbname= ['db_' ndbname];
scdataclrtmp;
save(gp.dname ,'-struct', 'gd');
save(ndbname ,'-struct', 'gd');
gp.dname=ndbname;
end

end

function bsdb_Callback(hObject, eventdata, handles)
global gd;
global gp;

try
% disp(gd.temp);
tsavename= [gd.temp.name '_' gd.temp.sname];
eval([tsavename '=gd.temp;']);
scdataclrtmp;
save(gp.dname , tsavename , '-append');

close();
disp('INFO: Database saved');
catch
h = msgbox('Error not saved!');
end

function bsndb_Callback(hObject, eventdata, handles)
global gd;
global gp;
ndbname= datestr(now, 'yyyy_mm_dd_HHMMSS');
ndbname= ['db_' ndbname '.mat'];
% try
tsavename= [gd.temp.name '_' gd.temp.sname];
eval([tsavename '=gd.temp;']);
scdataclrtmp;
save(gp.dname , tsavename , '-append');
% end
% save(ndbname ,'-struct', 'gd');
copyfile(gp.dname,ndbname)

close();
% catch
% h = msgbox('Error not saved!');
% end

% --- Executes on button press in bcancel.
function bcancel_Callback(hObject, eventdata, handles)
close();

function tcqs_Callback(hObject, eventdata, handles)
global gd;

gd.temp.cqos = str2num(get(hObject, 'String'));
tt=gd.temp.cqos;

while 1
scdatachkcq
end

gd.temp.cqos=tt;

function tcqs_CreateFcn(hObject, eventdata, handles)
if ispc && isequal(get(hObject,'BackgroundColor'),
get(0,'defaultUicontrolBackgroundColor'))
set(hObject,'BackgroundColor','white');
end

function tcqod_Callback(hObject, eventdata, handles)
global gd;

gd.temp.cqod = str2num(get(hObject, 'String'));
tt=gd.temp.cqod;

while 1
scdatachkcq
end

gd.temp.cqod=tt;

function tcqod_CreateFcn(hObject, eventdata, handles)
if ispc && isequal(get(hObject,'BackgroundColor'),
get(0,'defaultUicontrolBackgroundColor'))
set(hObject,'BackgroundColor','white');
end

function bdm_Callback(hObject, eventdata, handles)
global gd;
global gp;

str=fieldnames(gd);

[s2,v2] = listdlg('PromptString','Select a Patient:',...
'SelectionMode','single',...
'ListString',str);

if(v2==1)
delname=str(s2);
gd.temp = gd.(delname);
end

str=fieldnames(gd.(delname).m);

[s3,v3] = listdlg('PromptString','Select a
Measurement:',...
'SelectionMode','single',...
'ListString',str);

if(v3==1)
delmeas=str(s3);

% gp.vb= gd.(tname).m.(newname{1})
end

gd.(delname).m= rmfield(gd.(delname).m,delmeas);
scdataclrtmp;
save(gp.dname ,'-struct', 'gd');

```